HAL open science

Dynamical processes on non-Markovian temporal Networks

Antoine Moinet

▶ To cite this version:

Antoine Moinet. Dynamical processes on non-Markovian temporal Networks. Statistical Mechanics [cond-mat.stat-mech]. Aix-Marseille University, 2018. English. NNT : . tel-03549485

HAL Id: tel-03549485

https://theses.hal.science/tel-03549485v1

Submitted on 31 Jan 2022

HAL is a multi-disciplinary open access archive for the deposit and dissemination of scientific research documents, whether they are published or not. The documents may come from teaching and research institutions in France or abroad, or from public or private research centers.

L'archive ouverte pluridisciplinaire **HAL**, est destinée au dépôt et à la diffusion de documents scientifiques de niveau recherche, publiés ou non, émanant des établissements d'enseignement et de recherche français ou étrangers, des laboratoires publics ou privés.

Distributed under a Creative Commons Attribution - NonCommercial - NoDerivatives 4.0 International License

Doctoral School: ED 352
Physique et Science de la Matière

A Dissertation submitted in partial fulfillment
of the requirements for the degree of
Doctor in Philosophy at Aix-Marseille University and Universitat Politècnica de Catalunya

In subject of
Theoretical and Mathematical Physics

Dynamical processes on non-Markovian temporal Networks

by Antoine Moinet

under the supervision of
Alain Barrat and Romualdo Pastor Satorras.

At the *Centre de Physique Théorique*, UMR 7332, Marseille.

Public defense scheduled in October, the 16th of 2018 in presence of the committee:

Marian BOGUÑA	Universitat de Barcelona	Referee
Renaud LAMBIOTTE	Université de Namur	Referee
Laetitia GAUVIN	ISI foundation	Examiner
Xavier LEONCINI	Université Aix-Marseille	Examiner
Clément SIRE	Université Paul Sabatier	Examiner
Alain BARRAT	Université Aix-Marseille	Supervisor
Romualdo PASTOR SATORRAS	Universitat Politècnica de Catalunya	co-Supervisor

Cette oeuvre est mise à disposition selon les termes de la Licence Creative Commons Attribution - Pas d'Utilisation Commerciale - Pas de Modification 4.0 International.

Contents

List of Figures **6**

List of Tables **11**

Introduction **13**

1 Generalities **14**
1.1 Basic concepts and formalism of static networks 16
1.1.1 Adjacency matrix 16
1.1.2 Paths and connected components 16
1.1.3 Statistical characterization of networks 17
1.2 Time-varying graphs 19
1.3 Empirical contact networks 21
1.4 Temporal network models 23
1.4.1 Activity Driven Network Model 25
1.4.2 Generalized Activity Driven networks 26
1.4.3 Reinforcement law 28
1.4.4 Attractiveness 28

2 Generalized Activity Driven Network **30**
2.1 Introduction 30
2.2 Mapping to the hidden variable formalism 31
2.3 Topological observables 34
2.3.1 Degree distribution 34
2.3.2 Moments of the degree distribution 36
2.3.3 Degree correlations of a GAD0 network 37
2.3.4 Clustering coefficient of a GAD0 network 38
2.4 GAD0 network with power-law waiting time distribution 38
2.4.1 Degree distribution 38
2.4.2 Degree correlations 41
2.5 Discussion and perspectives 43

3 Percolation **45**
3.1 Short overview of percolation theory 45

3.2 Percolation dynamics 46
3.2.1 General case 47
3.3 Summary 55

4 Temporal network poissonization and consequences on the percolation 56
4.1 Introduction 56
4.2 Definition of the procedures 58
4.2.1 Direct poissonization 58
4.2.2 Averaged direct poissonization 59
4.2.3 Reshuffling of the activation times 60
4.3 Poissonization of a network far from the threshold 61
4.3.1 Network with finite average waiting time 61
4.3.2 Waiting time distribution lacking a first moment 62
4.4 Numerical analysis 63
4.5 Conclusion 64

5 Aging Effects 67
5.1 Aging of a renewal process 67
5.2 Degree distribution of an aged PLAD0 network 70
5.2.1 Degree distribution of slightly aged networks 70
5.2.2 Degree distribution of strongly aged networks 72
5.3 Temporal percolation of aged networks 74
5.4 Poissonization of an aged network 75
5.4.1 Finite average waiting time 75
5.4.2 Infinite average waiting time 77
5.5 Conclusion 78

6 Epidemic spreading with risk perception 80
6.1 Introduction 80
6.2 Modelling epidemic spread in temporal networks 82
6.2.1 Epidemic models and epidemic threshold 82
6.2.2 Modeling risk perception 83
6.3 Epidemic spreading on synthetic networks 84
6.3.1 SIS dynamics 84
6.3.2 SIR dynamics 90
6.4 Epidemic spreading on empirical social networks 95
6.4.1 SIS dynamics 95
6.4.2 SIR 97
6.5 Conclusion 98

7 Voter-like model of opinion dynamics 101
7.1 Introduction 101
7.2 Consensus dynamics in activity driven networks with attractiveness 102

7.3 Heterogeneous mean-field analysis 103
7.3.1 Evolution equation 104
7.3.2 Conservation law 105
7.3.3 Exit probability 106
7.3.4 Average consensus time 107
7.4 Particular cases 108
7.4.1 p = 1/2 108
7.4.2 Pure voter model 109
7.4.3 Moran process 109
7.4.4 Pure Activity Driven Networks 110
7.4.5 Independent activity and attractiveness 111
7.4.6 Strongly correlated activity and attractiveness 111
7.4.7 Discussion 112
7.5 Numerical results 114
7.6 Asymptotic behaviour 114
7.7 Conclusions 115

8 Random Walks on non-Markovian temporal networks 118
8.1 Introduction 118
8.2 Random walks on non-Markovian activity driven networks 119
8.3 Random walk on a PLAD0 network 121
8.3.1 Random walk on a network with finite average individual interevent time 122
8.3.2 Network with infinite average individual interevent time 124
8.4 Conclusion 126

Conclusion 133

Bibliography 134

Appendix 153
A Tauberian theorems 153
A.1 Tauberian theorem n°1 153
A.2 Tauberian theorem n°2 153
B Taylor series expansions of the average and average square number of counted events for a renewal process with arbitrary interevent time distribution 154
B.1 Proof 155
B.2 Power-law renewal process 159
C Expansion of the steady-state infection prevalence of a SIS process with risk perception on activity driven networks 163
D Details of some computations of the voter-like model on activity driven networks with attractiveness 165

List of Figures

1.1 Time-integrated network. (c): Snapshot networks at successive times t_1, t_2 and t_3. (d): Integrated network. 15

1.2 (a): Schematic illustration of the RFID sensor system. RFID tags, shown in panel (b), are worn as badges by the individuals participating to the experiments. A face-to-face contact is detected when two persons are close and facing each other. The interaction signal is then sent to the antenna. Figure courtesy of SocioPatterns. 22

1.3 (Left): Probability distribution $\psi(\tau)$ of the gap times τ between consecutive interactions for all nodes. (Right): Probability distribution $\psi(\tau)$ of the gap times τ between consecutive interactions of the most active node in the network. On both panels we have $\psi(\tau) \sim \tau^{-1-\alpha}$ with $\alpha \simeq 0.5$. 24

2.1 (Left): Degree distribution $P_t(k)$ at time $t = 10^4$ as a function of the rescaled degree $k - \langle r \rangle_t$ from numerical simulation of the PLAD0 model with a network of size $N = 10^6$, $c_0 = 1$, and different values of α and β. The exponent $\gamma = 1 + \beta/\alpha$ is plotted in dashed line. (Right): Rescaled degree distribution $P_t(k)/(c_0 t)^\beta$ for different times t, in networks size $N = 10^6$, $c_0 = 1$, $\alpha = 0.6$, and $\beta = 1.2$. The theoretical decay exponent $\gamma = 3$ is plotted as dashed line. 42

2.2 Degree correlations of the PLAD0 network for different values of α and β. We plot the rescaled average degree of the neighbours as a function of k, $(\overline{k}^{nn}(k) - 1 - 2\langle r \rangle)/\sigma_r^2$. $c_0 = 1$, $c_{max} = 10^3$, $t = 10^3$ and network size $N = 10^6$. 43

3.1 Temporal percolation of a PLAD0 network. We plot the reduced susceptibility $\frac{\xi(t)}{2\xi_{max}}$ and the size of the largest connected component S_{GCC}/N as functions of time. $\alpha = 0.9$, $\beta = 1.1$, $c_0 = 1$, $c_{max} = 10^3$ and network size $N = 10^5$. Results are averaged over 100 iterations. 49

3.2 Percolation threshold T_p as a function of α and β. Blue dots correspond to estimations of T_p as given by the peak of the clusters' susceptibility; the surface is obtained by a numerical solution of Eq.(3.11). Network size is $N = 10^8$, $c_0 = 1$ and $c_{max} = 10^6$ (see main text). 50

3.3 Percolation threshold T_p as a function of α and β for different values of c_{max}. T_p is calculated numerically from Eq. (3.11), with $c_0 = 1$. From top surface to bottom one, values of $c_{max} = 10^3, 10^4, 10^5, 10^6$. Network size is $N = 10^8$. 51
3.4 Relative error $(T_p - T_p^0)/T_p^0$ as a function of α and β. T_p^0 is obtained by numerically solving the implicit equation ensuing from the Molloy-Reed criterion, T_p is given by the numerical solution of Eq. (3.11). Network size is $N = 10^8$, $c_0 = 1$ and $c_{max} = 10^6$. 52
3.5 Average activation number at the threshold, $\langle r \rangle_{T_p}$, as a function of α and β. Network size $N = 10^7$, $c_0 = 1$ and $c_{max} = 10^6$. 53
3.6 Percolation threshold T_p on a Lévy NoPAD network as a function of β. Three different values of the parameter c_{max} are shown. Symbols represent T_p evaluated by means of the peak of the susceptibility $\chi(s)$. Continuous lines represent T_p evaluated numerically from Eq. (3.20) and Eq. (3.11). Dashed lines represent the threshold T_p^0 given by the Molloy-Reed criterion. Triangles correspond to $c_{max} = 10^4$, circles to $c_{max} = 10^5$ and crosses to $c_{max} = 10^6$. The corresponding dashed lines follow the same downward progression. Lower bound activity $c_0 = 1$. Network size $N = 10^8$. 54

4.1 Schematic illustration of a poissonization process. (top): arbitrary sequence of activations in a time window $[0, T]$. (bottom): possible outcome of the randomization procedure. We display the percolation time of the growing network corresponding to the time-aggregation of the overall contacts sequence, and the percolation time of the activity driven network obtained through the poissonization. Note that the activation sequences do not correspond to any actual simulation or empirical data, nor do the times T_p and T_p^{AD}, but rather constitute an illustration of the general principle of the method. 57
4.2 (a) Poissonization of a PLAD0 network at $T = 10T_p$ ($T_p = 0.084$) with $\alpha = 0.9$, $\eta(c) \sim c^{-2.1}$ and $c \in [1, 10^3]$. (b): Poissonization of the same PLAD0 network at $T = T_p$. (c): Poissonization of an expAD0 network at $T = 10T_p$ ($T_p = 2.93$) with $\eta(c) \sim c^{-1.1}$ and $c \in [10^{-3}, 1]$. In each case we plot the relative size of the largest connected component S_{GCC}/N as a function of time (black circles), the function $\theta(t)$ of the original network (red circles) and the functions $\theta^{AD}(t)$ corresponding to the direct poissonization (green circles), the averaged direct poissonization (brown circles) and the reshuffling poissonization (blue circles). 61
4.3 (top): poissonization of a Weibull network (WTD ψ_1). (bottom): poissonization of a PLAD0 network (WTD ψ_2) as a function of α, for different values of T. 65

5.1 Sample realizations for three different types of renewal processes. Events are separated by waiting times, which are independently and identically distributed according to a probability density function $\psi(t)$. In black, we plot the deterministic process counting one event at each unit time step: $\psi(t) = \delta(t-1)$. In blue, we plot a realization of a Poissonian renewal with rate 1: $\psi(t) = e^{-t}$. In red, we plot the realization of a scale free process, $\psi(t) = 4.5 \times (5t+1)^{-1.9}$, the average inter-event time is infinite in this case. 68

5.2 Slightly aged degree distribution $P(k)$ for different values of α, β t_a and t. Plots (a), (b) and (c) show the non-aged distribution in black circles and the aged distribution in green squares. The behavior predicted by Eq. (5.13) (with P_0 and $\widetilde{P}_0$ previously calculated numerically) is plotted in red dashed line. Plot (d) shows the power law behavior at large k for the three aged distributions shown in the other plots: (a) squares, (b) circles, and (c) diamonds. Eq. (5.14) is plotted as a dashed line. Network size $N = 10^7$, results are averaged over 50 runs. The values of the parameters are the following. (a): $(\alpha, \beta) = (0.3, 1.2)$, $t = 10^6$ and $t_a = 10^3$. (b): $(\alpha, \beta) = (0.7, 1.8)$, $t = 500$ and $t_a = 10$. (c): $(\alpha, \beta) = (0.5, 1.8)$, $t = 5.10^3$ and $t_a = 100$. 73

5.3 Rescaled degree distribution $P_{t_a,t}(k)$ in case of strong aging. Different values of the time window t and the aging time t_a are shown. Inset: Poissonian behavior of the degree distribution $P(k)$ for small k with $t_a = 10^5$, $t = 500$. Network size $N = 10^7$. Parameters are set at $\alpha = 0.7$ and $\beta = 1.1$. 74

5.4 Percolation threshold T_p as a function of the aging time t_a. Parameters are set to $\beta = 1.5$, $c_0 = 0.001$, $c_{max} = 1$ and $\alpha = 0.3, 0.5, 0.7$ from top to bottom. Circles represent T_p evaluated numerically from (3.11). Crosses are an estimation of T_p as given by the peak of the susceptibility. The asymptotic behavior predicted by (5.20) is plotted in dashed line. Network size $N = 10^6$. 76

6.1 Effect of the strength of risk awareness on the SIS spreading on AD and ADM networks with $\Delta T = \infty$. (a): average lifetime of non-endemic runs for AD network, (b): average lifetime of non-endemic runs for ADM networks, (c): Steady state fraction of infectious for AD, (d): Steady state fraction of infectious for ADM. Vertical lines in subplots (a) and (b) indicate the position of the maximum of the average lifetime. Model parameters: $\mu = 0.015$, $\gamma = 2$, $\epsilon = 10^{-3}$, $\Delta T = \infty$ and network size $N = 10^5$. Results are averaged over 1000 realizations. 87

6.2 Analysis of finite-size effects. We plot the average lifetime of non-endemic realizations of the SIS process, for different system sizes and 2 different values of α. (a): ADM networks and $\alpha = 0$. (b): ADM networks with $\alpha = 10$. (c): AD networks. Vertical lines indicate the position of the maximum of the average lifetime. Model parameters: $\mu = 0.015$, $\gamma = 2$, $\epsilon = 10^{-3}$ and $\Delta T = \infty$. Results are averaged over 1000 realizations. 88
6.3 Finite-size scaling of the epidemic threshold of the SIS process for (a): pure AD network, (b): AD network with $\alpha = 10$, (c): ADM with $\alpha = 0$ and (d): ADM with $\alpha = 10$. 89
6.4 Effect of the local risk perception with increasing memory span ΔT for the SIS spreading on AD and ADM network. (top): AD network. (bottom): ADM network. Vertical lines indicate the position of the maximum of the average lifetime. Model parameters: $\alpha = 10$, $\mu = 0.015$, $\gamma = 2$, $\epsilon = 10^{-3}$ and network size $N = 10^4$. Results are averaged over 1000 realizations. 91
6.5 Effect of the local risk perception on the SIR spreading on AD networks and ADM networks. We plot r_∞ and σ_r/σ_r^{max} for different values of α. (a): σ_r/σ_r^{max} on AD network, (b): σ_r/σ_r^{max} on ADM network, (c): r_∞ on AD network and (d): r_∞ on ADM network. Vertical lines in subplots (a) and (b) indicate the position of the maximum of the order parameter variance. Model parameters: $\Delta T = \infty$, $\mu = 0.015$, $\gamma = 2$, $\epsilon = 10^{-3}$ and network size $N = 10^5$. Results are averaged over 1000 realizations. 93
6.6 Effect of the initial density of infectious on the SIR model on AD networks for different values of the awareness strength α and the initial density of infectious individuals ρ_0. Model parameters: $\Delta T = \infty$, $\mu = 0.015$, $\gamma = 2$, $\epsilon = 10^{-3}$ and network size $N = 10^5$. Results are averaged over 1000 realizations. 94
6.7 Finite scale effects in the SIR process on ADM. we plot σ_r for different network sizes and two values of α. Vertical lines indicate the position of the maximum of the order parameter variance. Model parameters: $\rho_0 = 1/N$, $\Delta T = \infty$, $\mu = 0.005$, $\gamma = 2$, $\epsilon = 10^{-3}$. Results are averaged over 10^5 realizations. 95
6.8 Steady state fraction of infectious for the SIS process on both empirical networks, for 2 values of α and different values of ΔT. Model parameters: $\mu = 0.001$ for Thiers and $\mu = 0.005$ for SFHH. Results are averaged over 1000 realizations. 96
6.9 Effect of the risk perception for different values of ΔT on the SIR spreading on SFHH network. (top): normalized standard deviation σ_r/σ_r^{max}. (bottom): order parameter r_∞. Model parameters: $\mu = 0.005$. $\alpha = 200$. Results are averaged over 10^4 realizations. 97

6.10 Effect of the risk perception for different values of ΔT on the SIR spreading on the Thiers network. (top): normalized standard deviation σ_r/σ_r^{max}. (bottom): order parameter r_∞. Model parameters: $\mu = 0.001$. $\alpha = 200$. Results are averaged over 10^4 realizations. 98

7.1 Characteristic consensus time τ for the dynamics on a pure activity driven network, i.e., fixed attractivity $b = b_0$, and a distribution of activities $F(a)$ given by Eq. (7.41), as a function of p and of the exponent γ of the distribution F. $\epsilon = 10^{-3}$. 111

7.2 Characteristic consensus time τ as a function of γ and p in the case $\eta(a, b) = F(a)F(b)$, with F given by Eq. (7.41) and $\epsilon = 10^{-3}$. 112

7.3 Voter-like dynamics in temporal activity driven networks with attractiveness. Reduced consensus time as a function of γ for different values of the network size N, for an activity distribution $F(a)$ given by Eq. (7.41) with $\epsilon = 10^{-3}$. (a): Voter and Moran processes (equivalent) for $\eta(a, b) = F(a)F(b)$. (b): Voter model on pure AD network ($b = 1$). (c): Moran process on pure AD network ($b = 1$). In each case, the dashed line corresponds to the analytical expression given by Eq. (7.28). 115

7.4 Voter dynamics in temporal networks with independent and equally distributed activity and attractiveness. Consensus time τ as a function of γ for activity and attractiveness distributed according to Eq. (7.41) and different values of ϵ. The analytical expression given by Eq. (7.45) is shown in dashed lines. The numerical simulations are performed with network size $N = 10^4$. 116

8.1 Directed random walk on an infinitely aged network with waiting time distribution of the form Eq. (8.12), for different values of the exponent γ of the activity distribution. Left panel: $\alpha = 1.2$. Right panel $\alpha = 1.7$. The black dashed lines correspond to the analytical result of Eq. (8.18). Number of walkers $N_1 = 5.10^6$, $t = 10^6$ and $\epsilon = 10^{-2}$. 123

8.2 Random walk dynamics on an aged network with three-valued activity and infinite average waiting time. $\eta(c) = 1/3$ and $H(c) = \delta_{c,10}$. In the panels $(\mathrm{a}_{1,2,3})$ we plot the probability of presence $P(c, t)$ as a function of time: $[P(c = 10, t) - 1/3]/2$, $1/3 - P(c = 1, t)$ and $1/3 - P(c = 0.1, t)$. (a_1): $\alpha = 0.2$. (a_2): $\alpha = 0.5$. (a_3): $\alpha = 0.7$. The behaviour predicted by Eq. (8.25) is plotted in dashed lines. Network size $N = 9.10^4$, number of walkers $N_1 = 10^6$ and aging time $t_a = 10^3$. (b): Ratios $\left[\tilde{h}_c(t_a, 0) - \tilde{h}_c(t_a, t_0)\right] / \tilde{h}_c(t_a, t_0)$ as a function of t_a, obtained from numerical simulations. The asymptotes $\alpha(t_0/t_a)^{1-\alpha}$ calculated from Eq. (8.24) are plotted in dashed lines. Reference time $t_0 = 10^3$ and $c = 1$. 128

.3 $\overline{r}_c$ and $\overline{r^2}_c$ as functions of ct for a homogeneous population with waiting time distribution $\psi_c(t) = \alpha\, c\, (ct+1)^{-1-\alpha}$ and different values of α. (a): $\alpha = 0.9$, (b): $\alpha = 0.7$, (c): $\alpha = 0.3$ and (d): $\alpha = 0.1$. The series expansions of $\overline{r}_c$ and $\overline{r^2}_c$ at order $q = 50$, given by Eqs. $(.28)$ and $(.34)$ respectively, are plotted in dashed lines, while the circles represent numerical simulations of the renewal processes defined by ψ_c. 162

List of Tables

1.1 Some properties of the SocioPatterns datasets under consideration. 23
1.2 Nomenclature of the models used in the thesis. PM stands for pairing mechanism, WTD for waiting time distribution, and PL for power law. 29

7.1 Asymptotic behaviour of the moments of the distribution $F(a)$ defined in Eq. (7.41), and resulting asymptotic behaviour of the reduced consensus time τ given by Eq. (7.45) when ϵ tends to zero, as a function of the exponent γ. For $\gamma = 0, 1, 2, 3$, logarithmic corrections are present, given in Table 7.2. 117
7.2 Asymptotic behaviour of the moments of the distribution $F(a)$ defined in Eq. (7.41), and resulting asymptotic behaviour of the reduced consensus time τ given by Eq. (7.45) when ϵ tends to zero, for the specific cases $\gamma = 0, 1, 2, 3$. 117

Introduction

Network science explores the network representations of physical, biological, technological and social systems, leading to powerful predictive models of complex phenomena. This relatively new research field is rooted at the border of all those disciplines and draws on theories and methods including graph theory from mathematics, statistical mechanics from physics, data mining from computer science, inferential modeling from statistics, and social structure from sociology. This rich theoretical grounding makes the field of network science appropriate to study the emergence of the global properties of systems as diverse as the brain or the Internet. Until recently, the network representations were constructed exclusively in terms of static graphs. However, facing the evidence that almost all real world networks evolve over time, either by adding or removing nodes or links over time, network science has been naturally extended to the emergent field of temporal or time-varying networks. Such dynamical evolution is, in particular, inherent to social networks where people make and lose friends over time, thereby creating and destroying edges, and some people become part of new social groups or leave theirs, changing the nodes in the network. The growing interest towards the temporal dimension of networks has been made possible with the gathering, over the last decades, of a tremendous amount of high resolution data from telecommunication devices, virtual social networks hosted on the internet, and all pervasive technologies in general. This data revolution not only represents valuable information allowing to directly apprehend human behaviour but also enhances advances in network science modeling. Indeed, social network science is now divided into two different research axes nourishing each other: on the first hand the collection of data allows to build real social time-varying networks which can be used as substrates for further study of collective behaviours such as information or disease spreading. On the other hand, substantial endeavour is made to identify the underlying mechanisms that lead to some kind of universality observed in the structural properties of real social networks, enabling to build models capturing some of the major aspects of real social structures. The models are in their turn used as guidelines to extract useful information from the data which would otherwise be overwhelming and sterile. Moreover, as the universality often applies beyond the borders of social systems, the models draw on and inspire theoretical developments in other fields such as biology, economy or transportation networks, leading to very

fruitful and collective improvements. Most recently, empirical evidence revealed the universality of non-Markovian temporal patterns of human dynamics, explained by underlying cognitive mechanims such as memory effects, and which affect crucially any dynamical process unfolding on such a network. My thesis lies in the core of these new exciting challenges brought forth by this promising field of social network science. This manuscript is organized as follows: In chapter 1 we introduce the time-varying networks formalism and we present empirical data sets of social dynamics, along with the different synthetic models of social dynamics extensively used in the rest of the thesis, one of which constituting a cornerstone production of my doctoral investigation. A complete analysis of the topological properties of the latter model is presented in chapter 2, generalizing the so-called Activity Driven network model to non-Markovian dynamics. Then, chapter 3 is devoted to the study of the emergence of a giant connected component in the time-integrated network constructed from our model of social dynamics, namely the temporal percolation of the network. In chapter 4, we explore the limits of the mapping that may be considered from our model to the Activity Driven model, exhibiting in particular the flaws arising in the evaluation of the percolation threshold when identifying a non-Markovian links pattern to a Poissonian dynamics. The non-Markovian nature of the interaction dynamics of our model implies in some cases a non-stationarity of the network, giving rise in its turn to aging effects visible in the topological properties of the network, whose analysis is the object of chapter 5. In the three following chapters we investigate dynamical processes running on top of the social network models and the empirical networks presented in chapter 1. In chapter 6 we evaluate the effect of risk perception on the spread of a disease in temporal networks. In chapter 7, we present a voter-like opinion dynamics model, and solve it for an underlying activity driven with attractiveness dynamics defined in chapter 1. Thirdly, we fully describe the activated random walk process running on top of our non-Markovian network model in chapter 8. A detailed summary and a discussion are reported at the end of each chapter, while conclusive remarks and perspectives for future work are discussed in Conclusion.

Most of the work presented in this thesis was published in scientific papers [114–116]. In particular, chapter 6 is similar to Ref. [114], with some minor modifications. Besides, the results of chapter 7 motivated a paper submitted to *Phys.Rev.E*, and the content of chapter 8 will soon be submitted to a scientific journal.

1. Generalities

Network science uses network representations in terms of graphs to elucidate the properties of complex systems for which such representation is possible [43, 125]. The field provides a unified framework that has been proven very effective in the understanding of the functional and structural properties of networked systems. Besides, it allows to unravel the dynamical properties of spreading and collective processes developing on top of network substrates with complex topology [17, 44]. Traditionally, network representations have been made in terms of graphs regarded as static objects, drawing an edge whenever a connection was recorded at least once between two nodes. For instance, in the actors collaboration network, two actors are linked if they have co-starred in a movie [13]. In the same manner, scientific collaboration networks connect researchers that have co-authored at least one paper [122]. Nowadays it is clear that the static representation must be regarded as a limiting case of a network evolving in time, but where the timescales ruling the link dynamics are very large compared to the observation time window. Indeed, almost all real networks exhibit dynamical structures, in which connections appear and disappear in time [70]. Many natural and artificial networks are inherently dynamic, and their temporal evolution is of particular relevance to spreading processes taking place on top of them, in particular when the dynamical process and the network itself evolve at similar timescales. In the context of social dynamics [179], the temporal evolution is particularly obvious since social relationships are based on a succession of contacts, either through physical proximity and oral communication or technological-based communication. These social contacts are inherently time-limited, but still constitute the key ingredients to the elaboration of a static network representation. In this sense, the social networks considered in previous literature [13, 102, 122] represent a projection or time-integration of the corresponding temporal networks. In this projection, a link is present as soon as it appeared at least once during the observation of the network's dynamics. An illustration of this principle is presented on Fig. 1.1.

Recently, the recording of social interactions and data in digital format has given access to data sets of unprecedented size. This so-called "data revolution" has drawn the attention of the network science community to the temporal dimension of social interactions, leading to the development of new methods and concepts that forge the rising field of time-varying networks [70]. The avail-

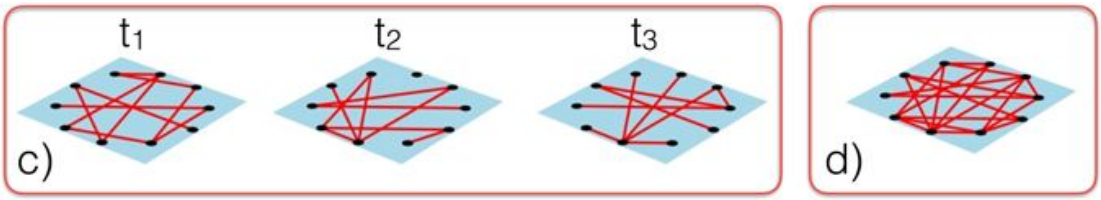

Figure 1.1.: Time-integrated network. (c): Snapshot networks at successive times t_1, t_2 and t_3. (d): Integrated network.

ability of large databases such as scientific collaboration data sets [136], and the deployment of infrastructures such as mobile phone communications [128], facilitate the real-time monitoring of social interactions in different social bodies and the reconstruction of the corresponding temporal networks [11, 34, 63, 127]. New experimental schemes have also been developed by the research community, adopting a data-driven methodology to study social dynamics and human activity, and making most of the collected data freely available to the scientific community. Specially noteworthy in this context is the data on face-to-face interactions recorded by the SocioPatterns interdisciplinary research collaboration [173], which collected longitudinal data on the physical proximity and face-to-face contacts of individuals in numerous real-world environments, such as schools, museums and hospitals. New fundamental questions regarding the properties of network dynamics arise from the newly gathered empirical data. In order to address these challenges, new theoretical models have been designed, aimed at explaining both the temporal patterns observed and their influence on the corresponding integrated networks [82, 155, 158, 183].

Empirical data analyses have revealed rich and complex patterns of dynamic evolution [10, 34, 70, 71, 76, 85, 112, 128, 165, 172], calling for renewed modeling efforts [164, 183]. Besides, researchers have tried to understand how dynamical processes such as epidemic spreading [78, 92, 146, 165], random walks [14, 109], percolation [10, 130] and social consensus [3, 5, 31] are affected by the temporal evolution of the underlying network substrate. Indeed, the irregularity of the links, and their rate of appearance, can impact critically a dynamical process developing on a temporal network [68, 138, 159, 175]. This intense investigation into the properties of social relationships led in particular to the discovery of a cornerstone of human social dynamics, namely the "bursty" nature of human interactions, characterised by intervals of rapidly occurring events separated by long periods of inactivity [34, 71, 76, 127, 128, 172]. This observation dramatically questions the traditional frameworks positing Poisson distributed processes. Several mechanisms, such as the circadian cycle and weekly patterns [81], reinforcement dynamics [183], and decision-based queuing process [11] have been proposed as explanations for the observed bursty nature of human social behaviour. Nevertheless, burstiness turned out to be ubiquitous in nature, appearing in a wide range of systems in nature, ranging from earthquakes [39]

to neuronal activity [91] and sunspots [182]. The universality of this bursty behaviour reveals a corresponding omnipresence of memory effects [87]. The burstiness of social interactions and its consequences on the dynamical phenomena possibly considered in social gatherings point out the necessity of designing new models taking into account the temporal dimension of social networks. In this chapter we introduce the basics of the time-varying networks formalism.

1.1. Basic concepts and formalism of static networks

Network theory [124] applies to any system that admits an abstract mathematical representation in terms of a graph, whose nodes (vertices) identify the elements acting in the system and in which the set of connecting links (edges) represent the presence of a pairwise interaction among those elements. A graph is formally defined as a pair of sets $\mathcal{G} = (\mathcal{V}, \mathcal{E})$, where $\mathcal{V} = \{i, j, k, ...\}$ is a set of vertices and $\mathcal{E} = \{(i, j), (j, k), ...\}$ is a set of edges connecting the nodes pairwise. The number of nodes is usually denoted by N and the number of edges by E. A graph can be directed if the edges are defined as ordered pairs of nodes, i.e. distinguishing the links (i, j) and (j, i), or undirected if the links are defined as unordered pairs of nodes. In a graphical representation, for undirected graphs the presence of an edge between vertices i and j connects the vertices in both directions, whereas the presence of an edge from i to j in a directed graph does not necessarily imply the presence of the reverse edge from j to i. Additional information may be considered in the network representation, encoded through the definition of a weight w_{ij} assigned to each edge (i, j) [17].

1.1.1. Adjacency matrix

From a mathematical point of view, it is convenient to define a graph by means of the adjacency matrix $X = (x_{ij})$. It is a $N \times N$ matrix defined such that

$$x_{ij} = \begin{cases} 1 & \text{if } (i, j) \in \mathcal{E} \\ 0 & \text{if } (i, j) \notin \mathcal{E} \end{cases} . \tag{1.1}$$

For undirected graphs, the adjacency matrix is symmetric, $x_{ij} = x_{ji}$ and thus contains redundant information.

1.1.2. Paths and connected components

A central concept in the inquiry of graph structure is the reachability of vertices, i.e. the possibility of going from one vertex to another following the connections given by the edges in the network. A network is said to be connected if every

vertex is reachable from any other vertex, i.e. if a virtual walker travelling on a graphical representation of the graph can reach any vertex following the (possibly oriented) arrows representing the edges of the graph. A path from a node i_1 to another node i_n is formally defined as an ordered list of vertices $\mathcal{P} = \{i_1, ..., i_n\}$ containing at least two nodes, such that all the (possibly oriented) edges connecting two successive nodes of the list exist, $(i_k, i_{k+1}) \in \mathcal{E}$, $\forall 1 \leqslant k \leqslant n-1$. A connected component of the graph is then simply defined as a subset of nodes, such that every pair of elements in the subset is connected by at least one path. The knowledge of the distribution of connected components of the graph represents a valuable information, and in particular the possible existence of a giant connected component, defined as a subset of nodes whose size scales with the number of vertices of the graph. The presence of a giant connected subgraph implies that a macroscopic fraction of the graph is connected, and therefore its size diverges in the limit $N \to \infty$. Besides, this giant connected component is a pivotal notion for the analysis of the percolation phenomenon, as we will see in chapter 3.

1.1.3. Statistical characterization of networks

The concept of adjacency matrix is very useful in analytical approaches to dynamical processes that explicitly take into account the actual connectivity of the network [32, 178]. However, in large systems, asymptotic regularities are not easily detected by looking at the local connectivity of the network, and one has to shift the attention to statistical measures that take into account the global behaviour of the system. As in the rest of the manuscript we will consider undirected graphs only, all the concepts defined hereafter implicitly suppose that the graph is undirected, but most of them may be extended to directed graphs.

1.1.3.1. Degree distribution

The key concept of degree, defined as the number of adjacent edges to a given vertex, concretely the number of neighbours of a node, allows to define the degree distribution $P(k)$, equal to the probability that any randomly chosen vertex has degree k. It is obtained by constructing the normalized histogram of the degree of the nodes in a network. Alternatively, the dispersion of the degree in the network may be described in terms of the moments of order n of the distribution

$$\langle k^n \rangle = \sum_k k^n P(k). \tag{1.2}$$

To completely define the network, we need to specify also how the different degree classes are connected. To this end, one defines the conditional probabilities $P(k', k'', ..., k'^{(n)}|k)$ that a vertex of degree k is simultaneously connected to a number n of other vertices with corresponding degrees $k', k'', ..., k'^{(n)}$. These

quantities are the simplest theoretical tools that encode the degree correlations in the network.

1.1.3.2. Two nodes degree correlations

The first case usually considered is the two-point conditional probability $P(k'|k)$ that any edge emitted by a vertex with degree k is connected to a vertex with degree k'. In general, two nodes degree correlations can be represented as the three-dimensional histograms of $P(k'|k)$. However, this quantity is highly affected by statistical fluctuations and, thus, the study of the network structure is completed by the definition of the average degree of the nearest neighbours of a vertex of degree k. Both quantities are related by the expression

$$\overline{k}^{nn}(k) = \sum_{k'} k' P(k'|k). \tag{1.3}$$

In the presence of correlations, the behaviour of $\overline{k}^{nn}(k)$ discriminates two general classes of networks. If it is an increasing function of k, vertices with high degree have a larger probability of being connected with large degree vertices. This corresponds to an assortative mixing [123]. On the contrary, a decreasing behaviour of $\overline{k}^{nn}(k)$ defines a disassortative mixing, in the sense that high degree vertices have a majority of neighbours with low degree, while the opposite holds for low degree vertices [123].

1.1.3.3. Three nodes degree correlations

Triadic correlations can be measured by means of the probability $P(k', k''|k)$ that a vertex of degree k is simultaneously connected to two vertices with degrees k' and k''. A fortiori in this case, these probabilities are difficult to estimate directly from real data because of finite size statistical fluctuations, so that the concept of clustering coefficient has been proposed to help elucidate the connectivity structure of networks. This quantity refers to the tendency to form triangles or triadic closures in the network, and may be defined as the uniparametric probability that a vertex of degree k is connected to vertices of degree k' and k'' and that those two vertices are, on their turn, joined by an edge, averaged over all the possible values of the degrees of the neighbours. Therefore, one writes

$$\bar{c}(k) = \sum_{k',k''} P(k', k''|k)\Pi(k', k''), \tag{1.4}$$

where the function $\Pi(k', k'')$ is the probability that the vertices k' and k'' are connected, and depends on the particular network considered and can also be a function of the degree k of the common vertex.

All these quantities can of course be obtained directly from the adjacency matrix X, but most importantly the statistical description allows to develop powerful network models and mean-field approaches to dynamical processes on complex systems.

1.2. Time-varying graphs

The network formalism can be easily extended to include time dependent graphs, also known as temporal or time-varying networks [70]. In temporal networks, the nodes are defined by a static set of elements, and the edges represent pairwise interactions, which now appear and disappear over time. This temporal evolution is thus embodied in the time dependency of the adjacency matrix X_t, whose elements are now discontinuous functions of time, switching alternatively between the values 0 and 1:

$$x_{ij}(t) = \begin{cases} 1 & \text{if } (i,j) \text{ is active at time } t \\ 0 & \text{otherwise} \end{cases} . \tag{1.5}$$

This formulation implicitly assumes that the links have a finite duration, and in order to include links with infinitely small duration, we write

$$x_{ij}(t) = \sum_{k \geqslant 1} \Theta(t - T^{(ij)}_{k,start}) - \Theta(t - T^{(ij)}_{k,end}) + \delta(t - T^{(ij)}_{k,0}) \tag{1.6}$$

where $\Theta(x)$ is the Heaviside step function such that $\Theta(x) = 1$ if $x > 0$ and $\Theta(x) = 0$ if $x \leqslant 0$, and $\delta(x)$ is the Dirac delta function. In this manner, $x_{ij}(t)$ is equal to one in the intervals $[T^{(ij)}_{k,start}, T^{(ij)}_{k,end}]$ where the link is active, is infinite at the epochs $T^{(ij)}_{k,0}$ standing for punctual activations of the link, and is equal to zero otherwise. Depending on the system under scrutiny, characteristic timescales may be at play, emerging from natural or technical constraints. For example, in scientific collaboration networks [122] the interval of time between consecutive editions of the journal considered imposes a periodic evolution, while in physical proximity networks [34], the internal clock of the experimental setup imposes a time step to the network evolution. Moreover, discrete-time approaches to investigate dynamical processes on networks naturally posit a fundamental time interval subsequently imposed to the network dynamics. In any case, while an exact representation of the temporal network is given by the temporal adjacency matrix, in practice one has access to a coarse-grained information about the dynamical interactions in the network. This translates into a time-aggregation procedure of the instantaneous network over successive time windows of length Δt. Formally, a static projection is created from the links dynamics observed during the interval $[(\ell - 1)\Delta t\,,\, \ell\Delta t]$, and the elements of the adjacency matrix

$A_\ell^{(\Delta t)}$ hereby defined are expressed as

$$a_{ij,\ell}^{(\Delta t)} = \Theta\left(\int_{(\ell-1)\Delta t}^{\ell\Delta t} x_{ij}(t)\, dt\right) \tag{1.7}$$

In this sense, the detailed activation pattern of a link inside the interval Δt is encapsulated into a binary bit of information. The resulting graph defined by $A_\ell^{(\Delta t)}$ is a snapshot of the temporal network under study, which can be completed by assigning a weight $w_{ij,\ell}^{(\Delta t)}$ to the edge (i, j)

$$w_{ij,\ell}^{(\Delta t)} = \int_{(\ell-1)\Delta t}^{\ell\Delta t} x_{ij}(t)\, dt \tag{1.8}$$

Repeating this procedure over L successive time steps Δt, one obtains a sequence $\{\mathcal{G}_\ell^{(\Delta t)}, \ell = 1, ..., L\}$ of instantaneous snapshot graphs, representing a discrete version of the corresponding continuous time-varying network in the time window $[0, L\Delta t]$. The choice of the aggregation window Δt is a crucial issue as it may severely impact the structure of the resulting discrete time-varying networks [96] and have non-trivial effects in the analysis of dynamical processes taking place on top of them [143]. However, this operation is standard in the investigation of temporal networks, and represents a fruitful and satisfying approximation as long as the aggregation window Δt is not too large compared to the characteristic timescales of the dynamics [143].

The discrete-time sequence representing the temporal network may in its turn be projected onto an aggregated static network $\mathcal{G}^{agg}$, whose graph is formed by the union of the snapshot graphs, i.e., calling $\mathcal{E}^{agg}$ the set of edges of $\mathcal{G}^{agg}$ and $\mathcal{E}_\ell^{(\Delta t)}$ the set of edges of $\mathcal{G}_\ell^{(\Delta t)}$ (the set of vertices being the same for all graphs), $(i, j) \in \mathcal{G}^{agg} \Leftrightarrow [\exists\ 1 \leqslant \ell_0 \leqslant L,\ (i, j) \in \mathcal{G}_{\ell_0}^{(\Delta t)}]$. While this graph informs about the total number of neighbours of a node, the total time (counted as the number of time steps Δt) spent in contact by a pair of nodes is encoded in the weights $w_{ij}^{agg} = \sum_\ell a_{ij,\ell}^{(\Delta t)}$ associated to each link of the graph [70, 78, 128]. The alternative definition $w_{ij}^{agg} = \sum_\ell w_{ij,\ell}^{(\Delta t)}$, measuring the real time spent in interaction, also ensures the equivalence between the aggregated weighted graph $\mathcal{G}^{agg}$ and the single snapshot graph $\mathcal{G}_1^{(L\Delta t)}$ obtained through the coarse-graining procedure with a time step $L\Delta t$. We also conveniently define the strength of node i, $s_i^{agg} = \sum_j w_{ij}^{agg}$, gauging the total time spent in contact by the node. The aggregated representation facilitates the identification of interesting properties of the system. More in general, the tools presented in this chapter help to unravel the topological properties of social networks, and most importantly they give a novel insight into the dynamics of a wide range of phenomena emerging from collective human behaviours, such as the formation of communities and the spreading of information and social influence or rumours [66, 128].

1.3. Empirical contact networks

The recent accumulation of large volumes of data has contributed to the quantitative understanding of various phenomena that had previously been examined only from a qualitative perspective [12, 79]. Examples range from the analysis of political trends [2, 29, 98] and human behaviour as economic agents [140, 141], to human mobility patterns [22]. Various technological innovations have also enabled this data avalanche, such as mobile phones and GPS devices [49, 113, 171], or radio-frequency wearable sensors [34]. Moreover, the ascent of widespread online social networks has provided an optimal research field for the social scientists [8, 36, 75, 97].

The so-called face-to-face contact networks represent a crucial substrate for the creation of social bonds [168], the transmission of ideas, and the spreading of infectious diseases [102, 148], and thus occupy a pivotal position in the collection of human social networks. The singularity of these networks stems from the fact that the richest information flow is generally obtained from face-to-face communication [42]. This fundamental form of interaction is necessary to workplace efficiency or sustaining social relationships, among others, and so far outperforms in this respect other modes of communication [1]. Face-to-face interaction networks, for these reasons, have long drawn an important attention [6, 19, 80], but the scarcity of high resolution time-resolved data represented a serious impediment to the quantitative analysis of the dynamics of human contacts.

Recently, new experimental methods using electronic devices were developed to monitor physical proximity interactions, allowing to reconstruct with relatively good spatial and temporal resolutions face-to-face contact networks [173]. Mobile phone traces permit to scan social relationships among large populations [49, 63], but do not allow to track face-to-face contacts, unless a specific software is provided [41]. WiFi and Bluetooth devices can be used to evaluate spatial proximity, but are limited by a spatial resolution of a few meters and are generally not a good proxy for physical proximity interactions. Finally, the MIT Reality Mining project gathered profitable data on face-to-face interactions, by means of specifically conceived “sociometric badges" [50, 99]. Here we focus on the SocioPatterns collaboration [173], which designed an experimental procedure associating resolution and scalability, by operating economical and non-intrusive radio frequency identification devices (RFID). This original setup can be deployed at social gatherings involving up to several hundreds of individuals, and probes interactions at different scales, from co-presence in a given area, to face-to-face proximity of individuals, thanks to an adjustable spatio-temporal resolution. The deployment of the SocioPatterns experimental scheme requires each volunteer to wear on their chest a badge equipped with an active RFID device. These instruments are designed to emit and receive very low power radio waves within a

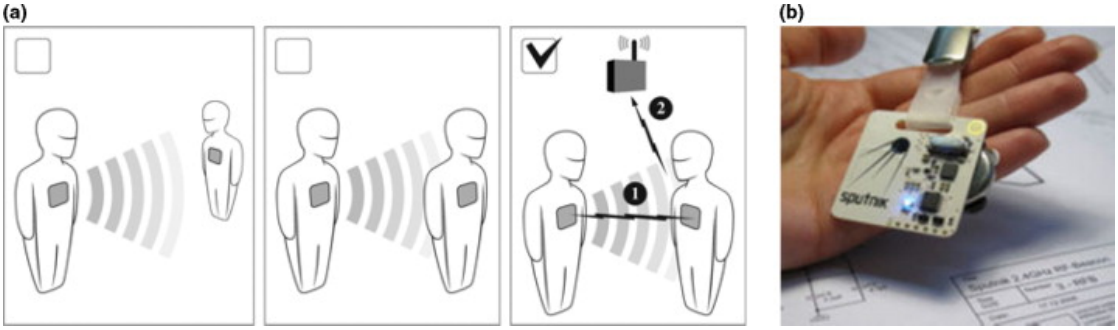

Figure 1.2.: (a): Schematic illustration of the RFID sensor system. RFID tags, shown in panel (b), are worn as badges by the individuals participating to the experiments. A face-to-face contact is detected when two persons are close and facing each other. The interaction signal is then sent to the antenna. Figure courtesy of SocioPatterns.

spatial cone roughly coinciding with the field of view of the carrier, and relay the data about the proximity of other devices to RFID readers installed in the scenery beforehand. The infrastructure is tuned so that interactions are recorded within a proximity of one to two meters and with a time-resolution of 20 seconds. The resulting data is coarse-grained, in the sense that two individuals are considered to be “in contact" during an interval of 20 seconds as soon as their RFID devices have exchanged at least one packet during that interval. A schematic illustration of the monitoring mechanism is shown in Fig. 1.2 The empirical datasets collected by the SocioPatterns collaboration are naturally described in terms of time-varying networks [70, 118], whose nodes represent the individuals wearing the sensors, and whose links stand for pairwise interactions appearing and disappearing over time. The properties of the electronic equipments and the experimental protocol imply an implicit coarse-graining of the real temporal contact network, as described in section 1.2. The elementary time step considered here is $\Delta t = 20$ seconds. In the following we briefly present datasets gathered in two different social contexts. The first one is a recording of the contacts between students of five classes of a high school (Lycée Thiers, Marseille, France), collected during seven days in November 2012 (“Thiers” dataset) [54, 153]. The second dataset consists in the temporal network of contacts between the participants of a conference (2009 Annual French Conference on Nosocomial Infections, Nice, France) during two days (“SFHH” dataset) [166]. The SFHH (Société Française d’Hygiène Hospitalière) data correspond to a rather homogeneous contact network, while the Thiers (high school) population is structured in classes of similar sizes and presents contact patterns that are constrained by strict and repetitive school schedules. In Table 1.1 we provide a brief summary of the main properties of these two datasets. In particular, we focus on

- N: number of individuals engaged in interactions.

Dataset	N	T	$\overline{p}$	$\langle \Delta t_c \rangle$	$\langle k \rangle$	$\langle s \rangle$
Thiers	180	14026	5.67	2.28	24.66	500.5
SFHH	403	3801	26.14	2.69	47.47	348.7

Table 1.1.: Some properties of the SocioPatterns datasets under consideration.

- T: total duration of the contact sequence, in units of the elementary time interval $\Delta t = 20$ seconds.
- $\overline{p} = \sum_t p(t)/T$: average number of individuals $p(t)$ interacting at each time step.
- $\langle \Delta t_c \rangle$: average duration of a contact.
- $\langle k \rangle$: average degree of the nodes in the projected binary network, aggregated over the whole time sequence.
- $\langle s \rangle$: average strength of the nodes in the projected weighted network, defined as the mean number of interactions per agent.

Furthermore, those networks exhibit non-trivial dynamical features, such as a bursty behaviour, indicated by broad-tailed distributions of the gaps separating successive social events. On Fig. 1.3 we plot the distributions of the waiting time between two consecutive interactions, for a single individual and for the whole network. More detailed analysis of these datasets can be found in Refs. [23, 78, 129, 167]. Such behaviour can impact dramatically the development of spreading phenomena on the network. Besides, the fact that these dynamical properties are shared across very different social contexts [23, 78, 129, 167] hints at a universality of these behaviours. These analysis thus ask for a twofold effort: On the one hand, a modeling endeavour, aimed at capturing the probabilistic regularities exhibited by empirical networks, and on the other hand, an investigation into dynamical processes running on top of temporal networks confronting the models and the empirical data. These two axes will both be explored in the next chapters.

1.4. Temporal network models

Network modeling is fundamental in order to identify the basic mechanisms underpinning the structural and dynamical regularities observed in many complex systems. Its development is rooted in the powerful graph theory [51, 117], and some of the models designed, such as the class of growing network models based on preferential attachment [13, 47], reach successes in different fields [46]. Recently, the temporal dimension of networks has drawn an increasing attention,

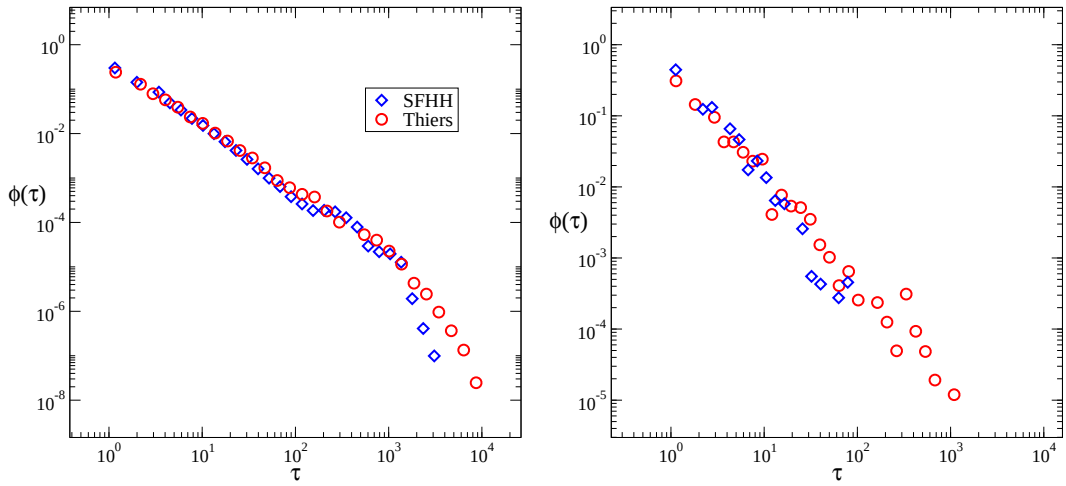

Figure 1.3.: (Left): Probability distribution $\psi(\tau)$ of the gap times τ between consecutive interactions for all nodes. (Right): Probability distribution $\psi(\tau)$ of the gap times τ between consecutive interactions of the most active node in the network. On both panels we have $\psi(\tau) \sim \tau^{-1-\alpha}$ with $\alpha \simeq 0.5$.

especially through the presence of complex and universal temporal patterns revealed by the analysis of empirical data concerning various types of social interactions such as mobile phone communications and face-to-face interactions [70, 71, 76, 165, 172] as discussed earlier. These achievements point out the need to surpass the traditional network modeling paradigm, deploying static graphs and thus unable to apprehend the crucial dynamical characteristics of human social behaviour. Efforts in this direction unfold over different fields of investigation ranging from social mobility [149] to air transportation [58], and call on original concepts such as dynamic centrality [67], memory [88] or reinforcement dynamics [183]. The Activity Driven network model, recently introduced by Perra et al. [136] deserves a special attention for its convenient tractability and its success in bridging the gap between the structural properties of real social networks and the microscopic mechanisms yielding the observed topology. The cornerstone in the definition of this model lies in the observation that the onset of social interactions is driven by an intrinsic *activity* of individuals, urging them to interact with their peers, along with the empirical evidence that individuals exhibit very heterogeneous levels of social activity. The dynamics of this agent based model is described at the individual level, and the activation pattern of a particular node obeys a stochastic discrete-time sequence of Bernoulli trials whose probability of success is proportional to the *activity potential* of the individual, defined as the probability per unit time that he/she engages in a social interaction. The outcome of this process is thus given by a sequence of static graphs, updated at each elementary time step Δt of the model, and depending on the distribution $F(a)$ of

the activity potential. Among the temporal network models that have flourished in the last years, the activity driven model has the peculiarity of allowing for analytic treatment. Its basic ingredients, indeed, suggest an analogy with a class of hidden variables models [20, 25, 154], and through a convenient mapping of the activity driven network to this model, it is possible to compute analytic expressions for the topological properties of the time-integrated network, as a function of the time span of observation T and the activity potential functional form $F(a)$ [160]. Moreover, the time-integrated activity driven network may be regarded as a growing network, which subsequently raise the question of the onset of a giant connected component, in other words the temporal percolation of the network [162]. Last but not least, the framework proposed allows to apprehend the dynamics of some processes of interest running on the top of the activity driven networks [103, 109, 136].

1.4.1. Activity Driven Network Model

The activity driven network model is defined in terms of N individuals or agents, endowed with an intrinsic activity potential, defined as the probability that she/he solicits a social connection/act with other agents per unit time. The activity or firing rate of the agents is a (quenched) random variable, extracted from the activity distribution $F(a)$ taken as a parameter of the model, and which can take a priori any form. The model proceeds by creating a succession of instantaneous graphs $\mathcal{G}_t$, updated at each time step Δt, and assuming a simple generative process obeying the following rules:

- At each discrete time step t the network $\mathcal{G}_t$ starts with N disconnected vertices.
- Each node i becomes active with probability $a_i \Delta t$ and generates a link that is connected to another individual selected uniformly at random.
- Time is updated $t \to t + \Delta t$, and all the edges in the network $\mathcal{G}_t$ are deleted. From this definition it follows that all the interactions have a constant duration equal to Δt.

We notice that $a_i \Delta t$ is a probability, which implies that the activity parameter is restricted to values such that $a_i \leqslant 1/\Delta t$. The model hereby described is Markovian in the sense that agents do not have memory of the previous time steps. The full dynamics of the network and its ensuing structure is thus completely determined by the activity potential distribution $F(a)$. In particular, the degree distribution of the aggregated network integrated over a time window T, is functionally related to the activity distribution $P_T(k) \sim T^{-1} F(kT^{-1} - \langle a \rangle)$. This interesting property is corroborated by empirical evidence [136] and constitutes a key result of this model. The AD model has proved to be very flexible and analytically suitable to study dynamical processes on time-varying networks [136,

138, 139]. However, it is easy to see that in the continuous time limit, i.e. for a vanishing Δt, the discrete-time sequence of activations of a node with activity a described above is equivalent to a Poisson process of rate a. In this interpretation, the activations of the nodes are punctual events stochastically distributed in time, with an inter-event time between two activations distributed according to $\psi(\tau) = a \exp(-a\tau)$. Described in these terms, it is clear that the activity driven network model fails to reproduce the bursty nature of social interactions [7], revealed by the observation of waiting times between two consecutive interactions of the same individual following heavy tailed distributions that can be approximated as power laws of the form $\psi(\tau) \sim \tau^{-(1+\alpha)}$, with $0 < \alpha < 2$ in general. Meeting this challenge, we aim at designing a natural generalization of the Activity Driven network model, where the distribution $\psi(\tau)$ of holding times between consecutive activations of the agents is taken as an entry of the model and can take a priori any form.

1.4.2. Generalized Activity Driven networks

Previous modeling efforts have shown that the concept of memory can induce non-Poissonian interevent time distributions in temporal networks [38, 69, 105, 158, 177]. Here we propose a model extending the activity driven framework and compatible with the empirically observed bursty nature of social interactions, which allows for a simple mathematical treatment. Our model is defined as follows: Each agent i in the network is endowed with a generalized activity parameter c_i extracted from an arbitrary distribution $\eta(c)$ taken as an entry of the model. The activation pattern of agent i then follows a renewal process [40], i.e. a series of punctual events separated by independently and equally distributed random times, with a waiting time distribution between two activations given by $\psi_{c_i}(\tau)$. The functional form of the holding times distribution is thus common to all the agents, and the possible heterogeneity among the individuals is encompassed in the parameter c playing the role of a generalized firing rate (i.e. inversely proportional to the average waiting time when it exists). When an agent activates, a peer is selected at random, and a link is drawn connecting both nodes, and lasting an infinitesimally small time. For reasons that will be detailed in chapter 5, the time origin of a renewal process, i.e. the epoch of the 0-th counted event, must be specified. In particular in our model, we suppose that all the individual renewal processes start and are synchronized at time $t = 0$. The model dynamics, observed throughout a time window $[0, t]$, is then generated as follows:

- We start with a set of N disconnected and synchronized nodes at time $t = 0$.
- Each one of them is assigned an activity parameter c, extracted from a given distribution $\eta(c)$.

- For each agent i, we repeatedly extract waiting times τ_k from the same probability distribution $\psi_{c_i}(\tau)$, until the last activation time $T_\ell^{(i)} = \sum_{k=1}^{\ell} \tau_k$ is such that $T_\ell^{(i)} > t$ and $T_{\ell-1}^{(i)} < t$ (by convention $T_0^{(i)} = 0$). In this way, the total number of times r_i that an individual i has activated in the time interval $[0, t]$ is equal to the total number of successive inter-event times τ generated minus one ($r_i = \ell - 1$).

- Each time an agent i is active, an individual $j \neq i$ is chosen uniformly at random and an edge is created between i and j. We do not consider time extensions of links i.e. they are instantaneously removed.

In terms of the adjacency matrix, the temporal network hereby defined is undirected and

$$x_{ij}(\tau) = \sum_{k=1}^{r_i(t)} \delta(\tau - T_k^{(i)}) \delta_{(i)_k, j} + \sum_{k=1}^{r_j(t)} \delta(\tau - T_k^{(j)}) \delta_{(j)_k, i} \tag{1.9}$$

where $\delta(\cdot)$ is the Dirac delta function, $\delta_{\cdot,\cdot}$ is the Kronecker symbol, and $(i)_k$ is the peer chosen by agent i at his/her k-th activation.

The Generalized Activity Driven framework hereby presented will be extensively studied throughout this Thesis, and many topological and dynamical properties of these networks will be elucidated in the next chapters. As we pointed out earlier, the original Activity Driven network constitutes a particular case of our model with an exponential waiting time distribution $\psi_{c_i}(\tau) = c_i \exp(-c_i \tau)$. However the discrete-time description is not convenient (although formally possible) to study a Non-Poissonian network in the general case, which can represent a disadvantage in the investigation of some dynamical processes running on top of the network as we shall see in chapter 6 and chapter 7. For this reason, although the exponential holding time distribution assumed in the Activity Driven network model is clearly at odds with empirical evidence, we will extensively use it in the manuscript, when the assumption of a Non-Poissonian network substrate does not allow for a mathematical tractability of the particular process under scrutiny.

The models under consideration exhibit numerous limitations that we will discuss at the end of chapter 2. In particular, the fact that the peers solicited for social interaction by activated agents throughout the dynamics are selected uniformly at random is obviously not realistic. We release this strong assumption by considering two more sophisticated pairing mechanisms that will be used in the rest of the manuscript, and for which analytic treatment will be developed as far as possible.

1.4.3. Reinforcement law

There is empirical evidence [86] that the establishment of connections is correlated in time. Part of the explanation lies in the fact that the social sphere of a person is divided into different classes of ordered intimacy, leading to the establishment of strong ties repeatedly activated and weak ties sporadically activated. A local reinforcement mechanism proposed in [89] was able to mimic characteristic aspects of social networks, among which the emergence of such strong and weak ties. This mechanism is based on a distinction made by an individual between the persons he/she has interacted with in the past and the rest of the population. In the event of the activation of agent i, he/she will decide to interact with one of his $q_i(t)$ known relatives with probability $p_i(t)$ and with a new individual with probability $1 - p_i(t)$. Both new individuals and known relatives are chosen uniformly at random among their respective subgroups. Defining

$$p_i(t) = \frac{q_i(t)}{1 + q_i(t)} \tag{1.10}$$

and starting with an empty network at time $t = 0$ the model reproduces both a growth of the social circle and a reinforcement of the contacts with its members. However it is worth noticing that this mechanism does not lead to a community structure, as the social circles of the relatives of a given individual do not necessarily coincide because new members are selected uniformly at random.

1.4.4. Attractiveness

In certain circumstances local mechanisms alone cannot explain the creation of social ties. In social contexts that imply the interaction with unknown people, the rules driving the establishment of social interactions are most likely different from those driving the emergence of close social ties. For example on the online social platform Twitter, one may start taking an interest in someone based on the knowledge of some consensually established popularity. The same mechanism may be put forward to explain how unfamiliar people relate when attending to a congress [158]. Although in general the popularity is a complex emergent property of a social network and may be evaluated differently by two distinct individuals, a modelling of such quantity ignoring a possible time dependency and local preferences is a good start for the sake of simplicity as previously mentioned. Thus we will use a model in which people are assigned a quenched popularity index or attractiveness b and apply a linear preferential attachment rule [13], i.e. when an agent i activates, s/he will connect to another agent j with probability $p_j = \frac{b_j}{N\langle b\rangle}$.

Those pairing mechanisms may straightforwardly be added to the Generalized

	homogeneous PM	reinforcement PM	attractiveness PM
arbitrary WTD $\psi(t)$	GAD0	GADM	GADA
exponential WTD	expAD0	expADM	expADA
PL WTD $\psi(t) \sim t^{-1-\alpha}$	PLAD0	PLADM	PLADA

Table 1.2.: Nomenclature of the models used in the thesis. PM stands for pairing mechanism, WTD for waiting time distribution, and PL for power law.

Activity Driven model as they do not affect the activation dynamics. In the rest of the manuscript, we will refer to the model defined with the random pairing rule as GAD0, to the model with individual memory kernels as GADM, and to the model with attractiveness as GADA. Besides, the original Activity Driven model will be denoted expAD(0-M-A), as it is a particular case of our extension with exponential waiting time distribution, and the model with power-law distributed holding times will be referred to as PLAD(0-M-A). This nomenclature is summarized in Table 1.2. In the next chapter, we present a mathematical treatment of the GADA model, which is further developed in the case of a homogeneous attractiveness (i.e. the GAD0 model).

2. Generalized Activity Driven Network

2.1. Introduction

In the study of complex systems, one of the main assets of statistical physics consists in the postulation of simple models capable to reproduce one given relevant property of the system under consideration. This approach allows to simplify the study, by focusing on the property under scrutiny, independently of other complicating factors. In the case of static complex networks, the configuration model fulfills this role with respect to the degree distribution, by considering networks characterized exclusively by this degree distribution, and completely random regarding all other properties. In the field of temporal networks, the generalized activity driven (GAD) model fills this niche, providing a simple model characterized by an arbitrary inter-event time distribution, that assumes any form, in particular that dictated by empirical evidence.

In this chapter we present a detailed mathematical analysis of the GADA model defined in subsection 1.4.2, focusing in the properties of the static networks that can be constructed integrating the contacts in the temporal dynamics. Indeed, within the mathematical framework of temporal networks, a static representation can be recovered by integrating a time-varying graph in a time interval $[0, t]$. The study of this integrated network is relevant, since traditional static social networks [79] are constructed in this way, and it is important to know how the features of the temporal dynamics affects the topological properties of its integrated counterpart. The inclusion of non-Poissonian dynamics in the process of links addition, given by the waiting time $\psi(t)$ with a non-exponential form, has a deep impact on the topology of the resulting time-aggregated network. By performing a mapping of our model to the class of networks with hidden variables [20], we readily derive analytical expressions for different topological observables of the integrated network. For the particular case of a GAD0 network, i.e. when the attractiveness of the agents is homogeneous in the network, and for a power-law waiting time distribution between successive activations of the agents, we prove that the degree distribution of the aggregated network is also broad-tailed, and we check our analytical result with numerical simulations of the model.

2.2. Mapping to the hidden variable formalism

We are interested in the integrated network $\mathcal{G}_1^{(t)}$ obtained by applying the coarse-graining procedure of section 1.2 to the temporal graph characterized by the instantaneous adjacency matrix of (1.9). This network is undirected, has no multiple edges, and even though a weight increment may be considered for the links (i, j) that have been generated several times by the GADA dynamics throughout the time window $[0, t]$, we do not study this feature in the rest of the manuscript. The topological properties of the integrated networks generated by the GADA model can be worked out by applying a mapping to the class of network models with hidden variables, proposed in Ref. [20] (see also [25, 154]). Hidden variables network models are defined as follows: starting from a set of N initially disconnected nodes, each node i is assigned a (possibly multidimensional) variable h_i, drawn at random from a probability distribution $\rho(h)$. Each pair of nodes i and j, with hidden variables h_i and h_j, are connected with an undirected edge with probability $\Pi(h_i, h_j)$ (the connection probability). The model is fully defined by the functions $\rho(h)$ and $\Pi(h, h')$, and all the topological properties of the resulting network can be derived through the propagator $g(k|h)$ [20], defined as the conditional probability that a vertex with hidden variable h ends up connected to exactly k other vertices (has degree k). From this propagator, expressions for the topological properties of the model can be readily obtained [20]:

- Degree distribution:
$$P(k) = \sum_h g(k|h)\rho(h). \tag{2.1}$$

- Probability to arrive at a node of degree k', following an edge emanating from a vertex with degree k:
$$P(k'|k) = \frac{1}{P(k)} \sum_{h,h'} g(k'-1|h')p(h'|h)\rho(h)g(k|h) \tag{2.2}$$
where we defined
$$p(h'|h) = \frac{N\rho(h')\Pi(h, h')}{\overline{k}(h)}. \tag{2.3}$$

- Degree correlations, as measured by the average degree of the neighbours of the vertices of degree k, $\overline{k}^{nn}(k)$ [132]:
$$\overline{k}^{nn}(k) = 1 + \frac{1}{P(k)} \sum_h \rho(h)g(k|h)\overline{k}^{nn}(h), \tag{2.4}$$

where we have defined

$$\overline{k}^{nn}(h) = \frac{N}{\overline{k}(h)} \sum_{h'} \rho(h')\overline{k}(h')\Pi(h,h'), \tag{2.5}$$

and

$$\overline{k}(h) = \sum_{k} kg(k|h) \tag{2.6}$$

which is the average degree of the vertices with hidden variable h.

- Average clustering coefficient $\langle c \rangle$, defined as the probability that two vertices are connected, provided that they share a common neighbour [180]

$$\langle c \rangle = \sum_{h} \rho(h)\bar{c}(h), \tag{2.7}$$

where we have defined

$$\bar{c}(h) = \sum_{h',h''} p(h'|h)\Pi(h',h'')p(h''|h), \tag{2.8}$$

Additionally, one can define the clustering spectrum, as measured by the average clustering coefficient of the vertices of degree k, $\bar{c}(k)$ [132, 142]

$$\bar{c}(k) = \frac{1}{P(k)} \sum_{h} \rho(h)g(k|h)\bar{c}(h), \tag{2.9}$$

We can apply the hidden variables formalism to the integrated GADA network model by identifying the mapping to the corresponding hidden variables and connection probability. From the definition of the model, the parameter that determines the connectivity of a node i is the number of times r_i that it has become active in the considered time window (its activation number). This number depends on its turn of the parameter c_i characterizing the waiting time distribution of node i. Moreover, a node receives a number a connections from other nodes that depends on its own attractiveness b. Therefore, we choose as hidden variables

$$h \to (r, c, b). \tag{2.10}$$

It is worth noticing that these quantities are not independent, and it is convenient to describe the variable r with its conditional distribution $\chi_t(r|c,b)$. This quantity corresponds to the probability that the number of activations counted between 0 and t for a node with activity c and attractiveness b is equal to r. By definition of the model, it does not depend on b. Besides it can be computed in terms of $\psi_c(\tau)$ [93]. The hidden variable probability distribution thus reads

$$\rho(h) \to \rho_t(r,c,b) \equiv \eta(c,b)\chi_t(r|c). \tag{2.11}$$

Finally, it is easy to see that the connection probability does not explicitly depend on the activity parameter c,

$$\Pi(h, h') \to \Pi(r, r', b, b') \tag{2.12}$$

As the connection attempts are independent, it is straightforward to derive the connection probability Π from the complementary probability that each one of the $r + r'$ attempts between two nodes to reach one another has failed:

$$\Pi(r, r', b, b') = 1 - \left(1 - \frac{b}{N\langle b\rangle}\right)^{r'} \left(1 - \frac{b'}{N\langle b\rangle}\right)^{r} \tag{2.13}$$

Thus, in the limit $N \gg rb'/\langle b\rangle$ and $N \gg r'b/\langle b\rangle$, we have

$$\Pi(r, r', b, b') \simeq \frac{r\,b' + r'\,b}{N\langle b\rangle} \quad [1] \tag{2.14}$$

Given the form of the connection probability, the corresponding propagator will be independent of c, $g(k|r, b)$. To find its functional form, one notices that a node with activation number r will have a degree k equal to the sum of an in-degree and out-degree, $k = k_{\text{out}} + k_{\text{in}}$, which accounts for the edges created by the activation of the node, and by the activation of all other nodes, respectively. In the case of a constant attractiveness $b = 1$, the probability that r activations lead to outgoing links targeting r different people is equal to

$$g_{\text{out}}(k = r) = \frac{N!}{(N - r)!N^r} \tag{2.15}$$

In the limit $N \gg r$, at first order we have $g_{\text{out}}(k = r) \simeq 1 - \dfrac{r(r-1)}{2N}$, which is very close to one. In other terms, the propagator of the out-degree is in a good approximation given by a delta function centered at r, $g_{\text{out}}(k|r) = \delta(k - r)$. This approximation still holds if we assume a regular distribution of the attractiveness b (in the sense that there are no mega-attractors concentrating all the popularity). In the rest of the chapter we suppose that this hypothesis is fulfilled. For the in-degree we can write $k_{\text{in}} = \sum_{r'} k_{\text{in}}(r')$, where $k_{\text{in}}(r')$ is the number of connections received from other nodes with hidden variable r'. Following [20] we obtain that the generating function of the in-degree propagator, $\hat{g}_{\text{in}}(z|b) = \sum_k g_{\text{in}}(k|b)z^k$, fulfils the equation

$$\ln \hat{g}_{\text{in}}(z|b) = N \sum_{r',c',b'} \rho_t(r', c', b') \ln\left[1 - (1 - z)\pi(r', b)\right] \tag{2.16}$$

[1] The symbol $\simeq$ means, in all the manuscript, equal to at dominant order: $[f(x) \underset{x\to a}{\simeq} g(x)] \Leftrightarrow [f(x) \underset{x\to a}{=} g(x) + o(g(x))]$

where $\pi(r', b) = 1 - [1 - \frac{b}{N\langle b\rangle}]^{r'}$ is the probability that a node with attractiveness b is reached at least once by a node with activation number r'. Therefore, for a sparse network (in the limit $\langle r\rangle/N \ll 1$), the in-degree propagator reads [20]

$$g_{\text{in}}(k|b) = \exp\left(-\frac{\langle r\rangle b}{\langle b\rangle}\right) \frac{[\langle r\rangle \frac{b}{\langle b\rangle}]^k}{k!}. \tag{2.17}$$

Finally, we obtain the total propagator as the convolution of the in-degree and the out-degree propagators, having the form

$$g(k|r, b) = \begin{cases} \exp\left(-\frac{\langle r\rangle b}{\langle b\rangle}\right) \frac{[\langle r\rangle \frac{b}{\langle b\rangle}]^{k-r}}{(k-r)!} & \text{for } k \geq r \\ 0 & \text{otherwise} \end{cases}. \tag{2.18}$$

In the limit $\langle r\rangle \gg 1$, the previous exact expression can be approximated by the simple shifted Poissonian form

$$g(k|r, b) = e^{-(r+\langle r\rangle \frac{b}{\langle b\rangle})} \frac{(r + \langle r\rangle \frac{b}{\langle b\rangle})^k}{k!}, \tag{2.19}$$

which we will use in the rest of the chapter to allow for mathematical tractability. Note that this approximation corresponds to the general result derived in [20] for sparse networks, i.e.

$$g(k|h) = e^{-\overline{k}(h)} \frac{\overline{k}(h)^k}{k!} \tag{2.20}$$

where in our case $\overline{k}(h) = r + \langle r\rangle \frac{b}{\langle b\rangle}$.

2.3. Topological observables

2.3.1. Degree distribution

2.3.1.1. General case

The most relevant topological property of any static network is its degree distribution $P(k)$, defined as the probability that a randomly chosen node has degree k [125]. The degree distribution generated by the GADA model in an integration window $[0, t]$ can be expressed in terms of the propagator $g(k|r, b)$ as [20]

$$P_t(k) = \sum_{r,c,b} \rho_t(r, c) g(k|r, b). \tag{2.21}$$

The general asymptotic form of the degree distribution can be obtained by performing a steepest descent approximation. For $\langle r\rangle \gg 1$, using the Poissonian propagator Eq. (2.19), and considering r as a continuous variable, we can write

Eq. (2.21) as

$$P_t(k) \simeq \sum_{c,b} \eta(c,b) \int dr\, e^{\phi(r)} \chi_t(r|c) \tag{2.22}$$

where

$$\phi(r) = -\langle r \rangle \frac{b}{\langle b \rangle} - r + k \ln\left(r + \langle r \rangle \frac{b}{\langle b \rangle}\right) - \ln(k!). \tag{2.23}$$

This function has a maximum at $r_m = k - \langle r \rangle \frac{b}{\langle b \rangle}$ and its second derivative at this point is $\phi''(r_m) = -\frac{1}{k}$. By expanding ϕ up to second order, one can obtain

$$e^{\phi(r)} \simeq \frac{e^{-(r-r_m)^2/2k}}{\sqrt{2\pi k}} \simeq \delta(r - r_m), \tag{2.24}$$

where we have used Stirling's approximation, and replaced the ensuing Gaussian function by a Dirac delta function. Therefore, the degree distribution reads

$$P_t(k) \simeq \sum_{c,b} \eta(c,b)\, \chi_t\left(k - \langle r \rangle \frac{b}{\langle b \rangle} |\, c\right) \tag{2.25}$$

2.3.1.2. Exponential waiting time

If we consider the simple case of a Poissonian inter-event time distribution, $\psi_c(\tau) = ce^{-c\tau}$, as in the original AD model, the activation number distribution is simply given by the Poisson distribution [40],

$$\chi_t(r|c) = e^{-ct} \frac{(ct)^r}{r!}, \tag{2.26}$$

with an average activation number $\langle r \rangle = \langle c \rangle t$. In a continuous c approximation, defining $\chi_t(r_m|c) = e^{\varphi(c)}$ with

$$\varphi(c) = -ct + r_m \ln(ct) - \ln(r_m!) \tag{2.27}$$

and applying once again a steepest descent approximation around the maximum at $c_m = \frac{r_m}{t}$, with the condition $|\varphi''(c_m)| = \frac{t^2}{r_m} \gg 1$, one finally obtains

$$P_t(k) \simeq \sum_{c,b} \eta(c,b)\, \delta\left(k - \left[ct + \langle c \rangle t \frac{b}{\langle b \rangle}\right]\right) \tag{2.28}$$

In particular, when $b = 1$ is constant, we recover the asymptotic form of the integrated degree distribution obtained in [160], $P_t(k) \simeq t^{-1}\eta(k/t - \langle c \rangle)$, the limits of its validity being $\langle c \rangle t \gg 1$, and $t^2 \gg (k - \langle c \rangle t) \gg 1$.

2.3.2. Moments of the degree distribution

The moments of the degree distribution read

$$\langle k^n \rangle = \sum_h \rho(h) \overline{k^n}(h) \tag{2.29}$$

where we define the moments $\overline{k^n}(h)$ averaging over all the nodes with hidden variable h

$$\overline{k^n}(h) = \sum_k k^n g(k|h) \tag{2.30}$$

The form of the degree propagator Eq. (2.18) indicates that at fixed values of r the variable $k-r$ is distributed according to a Poisson distribution, for which the moments can be expressed as polynomials expressions of the rate $\langle r \rangle \frac{b}{\langle b \rangle}$. Thus we write [144]

$$\overline{(k-r)^n}(h) = T_n\left(\langle r \rangle \frac{b}{\langle b \rangle}\right) \tag{2.31}$$

where

$$T_n(x) = \sum_{i=0}^{n} \left\{ {n \atop i} \right\} x^i \tag{2.32}$$

and $\left\{ {n \atop i} \right\}$ is the Stirling number of the second kind

$$\left\{ {n \atop i} \right\} = \frac{1}{i!} \sum_{j=0}^{i} (-1)^{i-j} \binom{i}{j} j^n \tag{2.33}$$

This expressions indicates that the moments $\langle k^n \rangle$ cannot be computed directly but are obtained by induction. As an example we give the expressions for the first two moments:

$$\langle k \rangle = \langle r \rangle + \sum_h \rho(h) \overline{(k-r)}(h) = 2\langle r \rangle \tag{2.34}$$

and the second moment is deduced from the first one as follows:

$$\overline{(k-r)^2}(h) = \overline{k^2} - 2r\,\overline{k}(h) + r^2 = \langle r \rangle \frac{b}{\langle b \rangle} + \langle r \rangle^2 \frac{b^2}{\langle b \rangle^2} \tag{2.35}$$

which leads to

$$\langle k^2 \rangle = \langle r^2 \rangle + 2\langle r \rangle \frac{\langle rb \rangle}{\langle b \rangle} + \langle r \rangle + \langle r \rangle^2 \frac{\langle b^2 \rangle}{\langle b \rangle^2} \tag{2.36}$$

We see that for a network with homogeneous attractiveness, the first and second moment of the degree distribution are functions of the moments of the activation number distribution $\langle r \rangle$ and $\langle r^2 \rangle$. In the appendix section B we develop a method providing the Taylor series expansions of these two quantities for an ar-

bitrary inter-event time distribution $\psi_c(t)$.

Until now we have presented a description of the GADA model, unfortunately the pairing process rule based on attractiveness does not allow for further mathematical tractability, in particular no simple expressions can be obtained for the average degree of the neighbours of the vertices of degree k, $\overline{k}^{nn}(k)$, nor for the average clustering coefficient $\langle c \rangle$. We will therefore focus on the generalized activity driven network model with a random pairing rule GAD0 in the rest of the chapter.

2.3.3. Degree correlations of a GAD0 network

The average degree of the vertices with hidden variable h reads

$$\begin{aligned} \overline{k}(h) &= \sum_k k\, g(k|r) \\ &= r + \langle r \rangle \end{aligned} \tag{2.37}$$

then using Eq.(2.5) we deduce

$$\begin{aligned} \overline{k}^{nn}(h) &= \frac{N}{r + \langle r \rangle} \sum_{r',c'} \eta(c')\chi_t(r'|c')(r' + \langle r \rangle) \left[\frac{r + r'}{N} \right] \\ &= 2\langle r \rangle + \frac{\langle r^2 \rangle - \langle r \rangle^2}{r + \langle r \rangle} \end{aligned} \tag{2.38}$$

Inserting this expression into Eq.(2.6) and using the Poissonian approximation of the propagator Eq. (2.19), we obtain

$$\overline{k}^{nn}(k) = 1 + 2\langle r \rangle + \frac{P(k-1)}{k\, P(k)} (\langle r^2 \rangle - \langle r \rangle^2) \tag{2.39}$$

In the limit of large k, one generally has $\frac{P(k-1)}{P(k)} \sim 1$ (it is not true for Erdős–Rényi networks for example but in practice the distribution of the activity $\eta(c)$ is chosen such that the resulting network exhibits fat-tail degree distribution) and we can write

$$\overline{k}^{nn}(k) \simeq 1 + 2\langle r \rangle + \frac{\sigma_r^2}{k} \tag{2.40}$$

From this expression we conclude that, in general, the integrated networks resulting from the GAD0 model shows disassortative mixing by degree. This behaviour is at odds with the assortative form observed for degree correlations in real social networks [125]. However it is not surprising since the neighbours are chosen uniformly at random during the network expansion.

2.3.4. Clustering coefficient of a GAD0 network

Combining Eqs.(2.3) and (2.8) we find

$$\bar{c}(h) = \frac{2}{N}\left(\langle r\rangle + \frac{\langle r^2\rangle - \langle r\rangle^2}{r + \langle r\rangle}\right) \tag{2.41}$$

Inserting this expression into Eq.(2.9) and using the poissonian approximation of the propagator Eq. (2.19), we obtain

$$\bar{c}(k) = \frac{2\langle r\rangle}{N} + \frac{2\,P(k-1)\sigma_r^2}{k\,P(k)N} \tag{2.42}$$

The first term of this equation corresponds to the average clustering coefficient of a Erdős–Rényi network (i.e. where all possible links are drawn independently with a fixed probability p) with the same density $2\langle r\rangle/N$.

2.4. GAD0 network with power-law waiting time distribution

2.4.1. Degree distribution

Here we focus on the particular case of power-law waiting time distributions, of the form $\psi_c(t) \sim t^{-1-\alpha}$, with $0 < \alpha < 1$, empirically observed. In the case of heavy tailed waiting time distributions, we expect to observe strong departures from the simple result in Eq. (2.28). Let us focus in particular on the simple power law form

$$\psi_c(t) = \alpha\, A_c\,(A_c\, t + 1)^{-(\alpha+1)}\,, \tag{2.43}$$

where $A_c = c\,(\Gamma_{1-\alpha})^{\frac{1}{\alpha}}$, c being the parameter quantifying the (possible) heterogeneity of waiting times in the population, and where we have defined $\Gamma_z \equiv \Gamma(z)$, the gamma function. For $\alpha > 1$ the parameter c is inversely proportional to the average waiting time and thus represents an activation rate. We will explore in particular the case $0 < \alpha < 1$, for which the first moment of the waiting time distribution diverges. We can still consider in this case the fractional moment $\langle \tau^{\alpha/2}\rangle^{2/\alpha}$, which is proportional to $1/c$, thus defining a generalized firing rate.

As we can see from Eq. (2.25), the degree distribution $P_t(k)$ depends mainly on the activation time distribution $\chi_t(r|c)$. This probability may be expressed as

$$\chi_t(r|c) = \int_0^t \Psi_r(u|c)\tilde{\psi}_c(t-u)\,du \tag{2.44}$$

where $\Psi_n(t|c)$ is the probability that the r-th activation of a node with activity c occurs at time t and $\tilde{\psi}_c(t) = \int_t^\infty \psi_c(u)du$ is the survival probability, i.e. the proba-

bility that a node having activated at $t = 0$ waits for a time longer than t before activating again. This equation translates the fact that $\chi_t(r|c)$ is equal to the sum of the probabilities that the r-th occurs at some time $0 < u < t$, and that the node waits at rest for the remainder of the time, $t - u$. The time T_r of occurrence of the r-th activation is the sum of the successive inter-event times, which are identically and independently distributed, so that the distribution $\Psi_r(t|c)$ is the convolution of $\psi_c(t)$ with itself repeated r times. Therefore, in the Laplace space we write $\Psi_r(s|c) = \psi_c(s)^r$, where the Laplace transform is defined as

$$f(s) = \int_0^\infty d\tau \; f(\tau) e^{-\tau s}. \tag{2.45}$$

Besides, we straightforwardly prove that $\tilde{\psi}_c(s) = (1 - \psi_c(s))/s$. Finally, Eq. (2.44) takes the form

$$\chi_s(r|c) = \psi_c(s)^r \frac{1 - \psi_c(s)}{s} \tag{2.46}$$

From this equation, we also derive (see details in section B) the average and average square number of activations:

$$\overline{r}_c(s) = \sum_r r \, \chi_s(r|c) = \frac{\psi_c(s)}{s(1 - \psi_c(s))} \tag{2.47}$$

$$\overline{r^2}_c(s) = \sum_r r^2 \, \chi_s(r|c) = \overline{r}(s) + \frac{2 \, \psi_c^2}{s(1 - \psi_c(s))^2} \tag{2.48}$$

By virtue of the Tauberian theorem n°1, for $\frac{s}{c} \ll 1$ we can expand the Laplace transform of the waiting time distribution

$$\psi_c(s) \simeq 1 - \left(\frac{s}{c}\right)^\alpha, \tag{2.49}$$

and inserting into the previous equations, we obtain

$$\chi_s(r|c) \simeq -\frac{1}{\alpha \, r} \frac{\partial}{\partial s} e^{-r(s/c)^\alpha} \tag{2.50}$$

$$\overline{r}_c(s) \simeq c^\alpha s^{-1-\alpha} \tag{2.51}$$

$$\overline{r^2}_c(s) \simeq 2 \, c^{2\alpha} s^{-1-2\alpha} \tag{2.52}$$

Then, using the Tauberian theorem n°2 we deduce

$$\chi_t(r|c) \simeq \frac{1}{\alpha\, r}\, \frac{c\, t}{r^{1/\alpha}}\, \mathfrak{L}\left(\frac{c\, t}{r^{1/\alpha}}\right) \tag{2.53}$$

$$\overline{r}_c(s) \simeq \Gamma^{-1}_{1+\alpha}(ct)^{\alpha} \tag{2.54}$$

$$\overline{r^2}_c(s) \simeq 2\,\Gamma^{-1}_{2\alpha+1}(ct)^{2\alpha} \tag{2.55}$$

valid for $ct \gg 1$, and where $\mathfrak{L}(z)$ is a one-sided Lévy distribution with Laplace transform $\mathfrak{L}(s) = e^{-s^{\alpha}}$ [93, 151]. Using the expansion at large r [61]

$$\chi_t(r|c) \simeq \frac{(c\,t)^{-\alpha}}{\Gamma_{1-\alpha}} \exp\left(-(1-\alpha)\left[\left(\frac{\alpha}{ct}\right)^{\alpha} r\right]^{\frac{1}{1-\alpha}}\right),$$

and inserting it into Eq. (2.25), we arrive at

$$P_t(k) \simeq \frac{(k-\langle r\rangle)^{\frac{1}{\alpha}-1}}{\Gamma_{1-\alpha} t} \int \eta\left(\frac{u}{t}\,(k-\langle r\rangle)^{\frac{1}{\alpha}}\right) \frac{e^{\xi(\alpha,u)}}{u^{\alpha}}\, du, \tag{2.56}$$

where we have considered c continuous, and defined $\xi(\alpha,u) = -(1-\alpha)\,(\alpha/u)^{\frac{\alpha}{1-\alpha}}$.

Expression Eq. (2.56) depends now only on the waiting time heterogeneity distribution $\eta(c)$. While the parameter c of an agent is not directly accessible from empirical data, it can be argued that it is directly related to the average activity potential a of a node [136], defined as the rate of activation averaged over a time window of given length T. Indeed, for a single renewal process parametrized by $\psi_c(t)$, we identify this rate to

$$a = \frac{\overline{r}_c}{T} \tag{2.57}$$

which is the average number of activation per unit time. Besides, using the expression (2.54), we deduce that the activity potential and the generalized activity parameter are related by $a \sim c^{\alpha}$. Given the power law distribution of the activity potential measured in real temporal networks [137], we deduce that the parameter c is also distributed with a power law. Thus we posit

$$\eta(c) = \frac{\beta}{c_0}\left(\frac{c}{c_0}\right)^{-(\beta+1)}, \quad \beta > 0, \quad c > c_0. \tag{2.58}$$

With this form of $\eta(c)$, the average activation number takes the form, for large t,

$$\langle r\rangle = \int \overline{r}_c(t)\,\eta(c)\,dc \simeq \frac{\beta\,\Gamma^{-1}_{1+\alpha}}{(\beta-\alpha)}\,(c_0 t)^{\alpha}, \tag{2.59}$$

and the integral in Eq. (2.56) has a lower bound at $u_0 = c_0\, t\, (k - \langle r \rangle)^{-\frac{1}{\alpha}}$. Taking the limit $k - \langle r \rangle \gg (c_0 t)^\alpha$, u_0 vanishes, and we finally obtain the asymptotic result

$$P_t(k) \sim (c_0 t)^\beta (k - \langle r \rangle)^{-\gamma} \quad [2] \tag{2.60}$$

with $\gamma = 1 + \frac{\beta}{\alpha}$. Now, keeping the notation $F(a)$ for the activity distribution defined in Ref. [136], and recalling that we defined $a \sim c^\alpha$, a simple transformation between probability distribution allows to write $\eta(c) \sim F[a(c)]\frac{da}{dc}(c)$. Besides, the activity potential was reported to be power-law distributed with an exponent δ, $F(a) \sim a^{-\delta}$, thus we obtain for the generalized activity parameter $\eta(c) \sim c^{-1-\alpha(\delta-1)}$. From here, we recover the postulated heterogeneity distribution of c, Eq. (2.58), with an exponent $\beta = \alpha(\delta - 1)$. Most remarkably, for this value of β , the integrated network exhibits a degree distribution decaying with an exponent $\gamma = 1 + \beta/\alpha = \delta$, i.e. we recover the main result of the activity driven model, stating the equivalence between degree and activity potential distributions. In order to check our analytic predictions, we have performed numerical simulations of the PLAD0 model with the waiting time and heterogeneity distributions Eqs. (2.43) and (2.58), respectively. In Fig. 2.1 we show the degree distribution $P_t(k)$ for different values of the exponents α and β of the waiting time and heterogeneity distributions. As one can see, the scaling relation of Eq. (2.60) is fulfilled remarkably well. In the same Figure we validate the scaling of the degree distribution with the integration time t, showing the collapse of the degree distribution for different t. The result Eq. (2.60) is noteworthy in two respects. Firstly, it relates two fundamental features found in real social networks, a broad tailed inter-event time distribution, as represented by the waiting time distribution $\psi(\tau)$, and a scale free degree distribution $P_t(k)$, whose exponent γ is simply related to the parameters α, controlling $\psi(\tau)$, and β, related to the heterogeneity of the individuals' social activity. Secondly, it shows transparently that non-Markovian effects are related to an exponent $\alpha < 1$, associated with a diverging first moment of the waiting time distribution. Indeed, in the limit $\alpha \to 1$, Eq. (2.60) recovers the Poissonian results Eq. (2.28), which means that even if the second moment of the waiting time distribution is infinite ($1 < \alpha < 2$), the structure of the integrated network will not be significantly different (at dominant order in t) to that of a Poissonian AD network.

2.4.2. Degree correlations

In this section we test the validity of the expression of the average degree $\overline{k}^{nn}(k)$ of the neighbours of a node with degree k given by Eq. (2.40). We perform numerical simulations of the PLAD0 network, for an activity distribution $\eta(c) \sim c^{-1-\beta}$ with $c \in [c_0, c_{max}]$. We set a cut-off c_{max} to avoid unnecessary numerical

[2] The symbol $\sim$ means, in all the manuscript, proportional to at dominant order: $[f(x) \underset{x\to a}{\sim} g(x)] \Leftrightarrow [\exists A \neq 0, f(x) \underset{x\to a}{=} A\, g(x) + o(g(x))]$

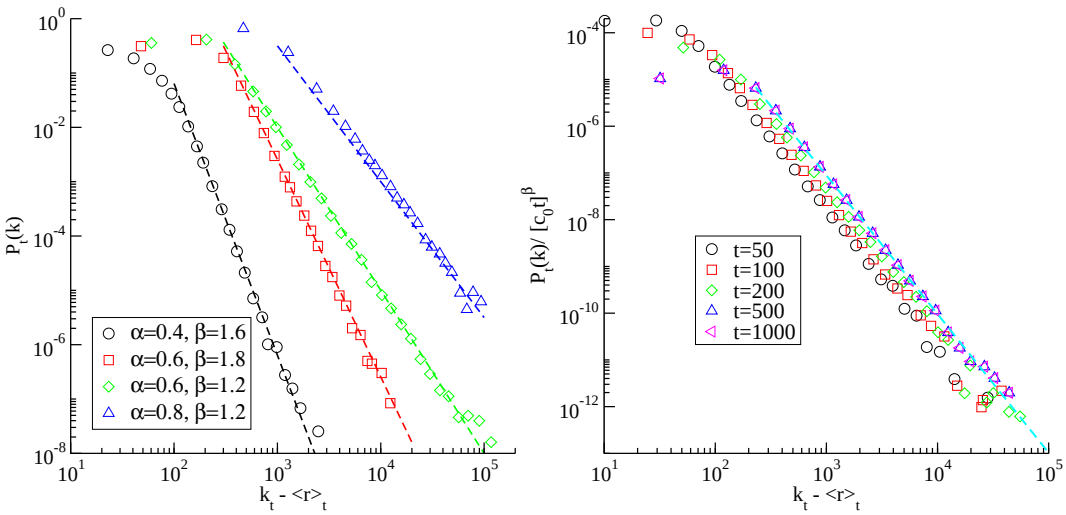

Figure 2.1.: (Left): Degree distribution $P_t(k)$ at time $t = 10^4$ as a function of the rescaled degree $k - \langle r \rangle_t$ from numerical simulation of the PLAD0 model with a network of size $N = 10^6$, $c_0 = 1$, and different values of α and β. The exponent $\gamma = 1 + \beta/\alpha$ is plotted in dashed line. (Right): Rescaled degree distribution $P_t(k)/(c_0 t)^\beta$ for different times t, in networks size $N = 10^6$, $c_0 = 1$, $\alpha = 0.6$, and $\beta = 1.2$. The theoretical decay exponent $\gamma = 3$ is plotted as dashed line.

costs. On Fig. 2.2 we plot the rescaled average degree of the neighbours $(\overline{k}^{nn}(k) - 1 - 2\langle r \rangle)/\sigma_r^2$ as a function of k for different values of α and β and observe that at large k the behaviour predicted by Eq. (2.40) perfectly fits the simulations. Moreover, in order to assess the intensity of the disassortativity of the network, we report the ratio

$$\kappa = \frac{\overline{k}^{nn}(1) - \overline{k}^{nn}(\infty)}{\overline{k}^{nn}(\infty)} = \frac{\sigma_r^2}{1 + 2\langle r \rangle} \tag{2.61}$$

evaluated with the simulations. For $(\alpha, \beta) = (0.7, 1.5)$, $\kappa \simeq 250$. For $(\alpha, \beta) = (0.5, 1.5)$, $\kappa \simeq 30$ and for $(\alpha, \beta) = (0.3, 0.8)$, $\kappa \simeq 8$. Those values indicate a quite strong decrease of $\overline{k}^{nn}$ as a function of k, at odds with what is observed in real social networks. Moreover, this implies that the generating functions framework [117] traditionally used to study the percolation of static uncorrelated graphs is not suitable for the case of an aggregated PLAD0 network as we shall see in chapter 3.

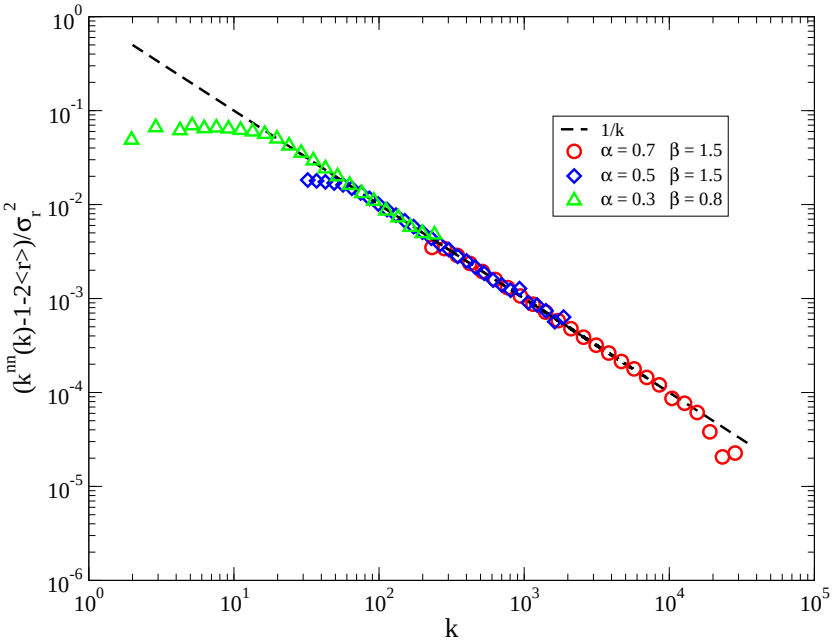

Figure 2.2.: Degree correlations of the PLAD0 network for different values of α and β. We plot the rescaled average degree of the neighbours as a function of k, $(\overline{k}^{nn}(k) - 1 - 2\langle r\rangle)/\sigma_r^2$. $c_0 = 1$, $c_{max} = 10^3$, $t = 10^3$ and network size $N = 10^6$.

2.5. Discussion and perspectives

In this chapter we have presented a detailed mathematical study of the properties of the time-integrated networks emerging from the dynamics of the GAD model. We have focused on the topological properties of the integrated networks. These properties are determined as a function of the model's parameters, namely the exponent α of the waiting time distribution $\psi_c(t)$, and the exponent β of the agents' heterogeneity distribution $\eta(c)$, by applying a mapping of the network's construction algorithm to the hidden variables class of models. For the case of the degree distribution $P(k)$, we recover the intimate connection between the scale-free nature of static social networks, $P(k) \sim k^{-\gamma}$, and two main characteristics of social temporal networks, namely a power-law distributed waiting time, $\psi_c(t) \sim (ct)^{-1-\alpha}$, and a power-law form of the heterogeneity distribution, $\eta(c) \sim c^{-1-\beta}$, as deduced from the distribution of average activity [115, 137]. This relation is quantified in the identity $\gamma = 1 + \beta/\alpha$.

In our model, the individual social behaviours are defined in terms of renewal processes counting the outgoing links of the agents. In real social networks on the other hand, it is usually not possible to determine who actually initiated an interaction, and social bonds are thus considered to be symmetrical. As we jus-

tify the power-law form of the waiting time distribution of the GAD model with the empirical evidence that social interactions are usually separated by broad-tailed distributed random times, we ought to explicit the relation between both processes. Indeed, in our model, the process counting all the interactions of an agent i is the superposition of the activation process of i, and the $N-1$ processes counting the activations of all the other agents with a subsequent link targeting i. Although the inter-event time distribution corresponding to this process cannot be derived explicitly, we may argue that this process counts on average $\overline{r}_{c_i} + \langle r \rangle$ events, which is equal to the integrated degree $\overline{k}(r) = r + \langle r \rangle$ of a node with activation number r, averaged over all possible values of r. Besides, assuming a power-law form $\psi_c(t) \sim (ct)^{-1-\alpha}$, this quantity is proportional to $((c_i + \langle c \rangle)t)^{\alpha}$ in the large time limit, i.e. it is equal to the average number of events counted for a renewal process with a waiting time distribution $\phi_i(t) \sim ((c_i + \langle c \rangle)t)^{-1-\alpha}$. Thus, the process counting the interactions of agent i with activity c_i, regardless of who initiated the social act, is similar to a renewal process with the same inter-event distribution, but with activity $c + \langle c \rangle$. The equivalence between both formulations cannot be confirmed because the superposition of several renewal processes is not in general a renewal process [40], however it is a strong argument supporting the relevance of the GAD model.

The framework presented in this chapter constitutes a minimal model of temporal networks with long tailed inter-event time distribution. As such, it has a wide potential to serve as a synthetic controlled environment to check both numerically and analytically several properties of these networks, and in particular their effect on dynamical processes, in much the same way as the configuration model has played this role for static networks. Moreover, due to its simple definition, it can be easily modified to make it more realistic. We envision as the more interesting of those improvements the introduction of temporal correlations in the activation patterns of the nodes. Indeed, in the mapping to hidden variables networks, no particular assumption are made concerning the activation number distribution $\chi_t(r|c)$, and this quantity may be taken as the fundamental parameter characterizing the counting process of the agents, thus allowing for temporal correlations. The nodes are then directly assigned a distribution $\chi_i(r,t)$, replacing the parameter c_i, in such a way that the mapping performed in section 2.2 remains valid, and in particular the propagator in Eq. (2.19). We also contemplate the introduction of a finite duration for the social contacts between nodes. Last but not least, the GAD0 integrated networks exhibit disassortative degree correlations, at odds with empirical observations in real static social networks. Correcting this effect emerges also as an important future objective.

3. Percolation

3.1. Short overview of percolation theory

A crucial topic in the field of network science is the question of the existence of a giant connected component also called giant cluster [26, 124]. This connected set of nodes plays a predominant role in the investigation of all dynamical processes that may unfold on the network. For instance in spreading processes, whether such a connected subgraph, whose size is proportional to the size N of the system, is present or not, will determine if the diffusing quantity under consideration may possibly pervade a sizeable fraction of the network [121]. On the other hand, the resilience of networked systems, defined as their ability to remain functional when they are subject to physical damage translating into links or nodes removal, is deeply related to the conditions of existence of a giant connected cluster [163]. More generally, the fact that a macroscopic fraction of the network is connected is a necessary condition to an efficient navigability in the system.

Percolation theory provides the natural theoretical framework to determine the conditions of existence of such a giant connected cluster. In the context of static Erdős–Rényi graphs, the percolation problem considers a random graph of size N in which each of the $N(N-1)/2$ edges is present with a probability $0 < p < 1$. The bond percolation problem hereby defined focuses on the properties of the clusters, and in particular their sizes, as a function of the occupation probability p. It is clear that if p is close to 0, the network is sparse and only small and independent clusters can be formed, while at large p the network is densely connected and is complete (i.e. fully connected $E = N(N-1)/2$) for $p = 1$. As the size of the network goes to infinity, the switch from sparsity to completeness defines a phase transition at a critical value p_c. For $p < p_c$, the network is fragmented into a myriad of small subgraphs, while for $p > p_c$, a giant connected component containing a finite fraction of the total number of vertices appears, and thus becomes of infinite size in the thermodynamic limit corresponding to $N \to \infty$. This bond percolation problem may be extended to arbitrary degree distributions [26, 124]. In this context, the existence of a giant connected component translates into conditions on the connectivity properties of the network.

Furthermore, it is clear that all network models implying the growth of the

graph, in the sense that more and more edges are drawn between a fixed number of vertices, will at some point meet the conditions of existence of a giant cluster, thus defining a temporal percolation process. In particular, the time-integrated network obtained through the GAD dynamics and thoroughly studied in chapter 2 is potentially the theater of the birth of a giant connected component. Indeed, as time passes, more connections will be established in the integrated network, forming a growing connected component until at some time T_p this component will percolate, i.e. it will have a size proportional to the network size N. The percolation threshold T_p is particularly relevant for the evolution of dynamical processes running on top of the underlying network [17], since any process with a characteristic lifetime $\tau < T_p$ will be unable to explore a sizeable fraction of the network. In this chapter we derive a self-consistent equation which establishes a very general criterion implicitly defining the percolation time T_p of a GAD0 time-integrated network. We check our result with numerical simulations.

3.2. Percolation dynamics

The investigation of the percolation transition as a function of the connectivity properties of uncorrelated random graphs finds a convenient formulation within the generating functions framework [26, 124]. This technique allows for the derivation of a necessary and sufficient condition for the existence of a giant connected component, depending on the first and second moment of the degree distribution

$$\frac{\langle k^2 \rangle}{\langle k \rangle} > 2 \tag{3.1}$$

This inequality, known as the Molloy-Reed (MR) [117] criterion, is exact if cycles are statistically irrelevant in the network, which is the case for random uncorrelated graphs in the thermodynamic limit close to the transition. In the context of time-aggregated GAD0 networks, $\langle k \rangle_t$ and $\langle k^2 \rangle_t$ are functions of the integration time t, so that the criterion implicitly defines the transition time T_p^0 of the temporal percolation process. Using the expressions Eqs. (2.34) and (2.36) for the first and second moment of the degree distribution, T_p^0 is given by the solution of the equation

$$3\langle r \rangle^2_{T_p^0} + \langle r^2 \rangle_{T_p^0} - 3\langle r \rangle_{T_p^0} = 0 \tag{3.2}$$

As we saw in chapter 2 however, the activity driven networks are in general not rigorously uncorrelated, and the MR criterion can lead to a substantial inaccuracy in the evaluation of the percolation threshold, depending on the particular activity distribution considered [162]. We thus resort to a more powerful framework, adequate for the study of the percolation of correlated random networks. The use of this formalism will be further justified in the next sections.

3.2.1. General case

In order to find an expression for the percolation threshold, we will follow the general formalism valid for correlated random networks, where the effect of degree correlations are accounted for by the branching matrix [62, 162]

$$B_{kk'}(t) = (k'-1)P_t(k'|k), \tag{3.3}$$

which implicitly depends on time through the conditional probability $P_t(k'|k)$ that a node with degree k is connected to a node with degree k', in the time window $[0,t]$ [132]. The percolation threshold is determined by the largest eigenvalue $\Lambda(t)$ of the branching matrix $B_{kk'}(t)$. Simplification of this matrix may be worked out, using the hidden variable formalism presented in section 2.2. We use the Poissonian form of the propagator derived in the previous chapter

$$g(k|h) = e^{-\overline{k}(h)}\frac{\overline{k}(h)^k}{k!} \tag{3.4}$$

where $\overline{k}(h) = r + \langle r\rangle$. Moreover, we proved that the probability $\Pi(h,h')$ that two nodes with hidden variables h and h' end up connected in the aggregated network at time t is equal to

$$\Pi_t(h,h') = \frac{r+r'}{N} = \frac{\overline{k}(h)+\overline{k}(h')-\langle k\rangle}{N} \tag{3.5}$$

This allows us to simplify the conditional probability

$$\begin{aligned} P(k'|k) &= \frac{1}{P(k)}\sum_{h,h'} g(k'-1|h')p(h'|h)\rho(h)g(k|h) \\ &= \frac{1}{P(k)}\sum_{h,h'} g(k'-1|h')\rho(h')\frac{(\overline{k}(h)+\overline{k}(h')-\langle k\rangle)}{\overline{k}(h)}\rho(h)g(k|h) \\ &= \frac{1}{p_k}\left(p_{k'-1}p_k + \frac{k'}{k}p_{k'}p_{k-1} - \frac{\langle k\rangle}{k}p_{k'-1}p_{k-1}\right) \end{aligned} \tag{3.6}$$

where we have written $P(k) = p_k$ for brevity. The largest eigenvalue of the matrix $B_{kk'}$ is then derived by means of the Perron-Frobenius theorem [56]. Following the last few steps of Ref. [162], we look for an eigenvector with positive components. Positing $\nu_k = 1 + \omega p_{k-1}/(kp_k)$, we derive two necessary conditions for ν_k to be an eigenvector with eigenvalue Λ:

$$\begin{aligned} \Lambda &= \langle k\rangle + \omega\sum_k \frac{(k-1)p_{k-1}^2}{kp_k} \\ \Lambda\omega &= \langle k^2\rangle - \langle k\rangle - \langle k\rangle^2 + \omega\langle k\rangle\left(1 - \sum_k \frac{(k-1)p_{k-1}^2}{kp_k}\right) \end{aligned} \tag{3.7}$$

In the limit of large N, we use the approximation $\sum_k \frac{(k-1)p_{k-1}^2}{kp_k} \simeq 1$, so that we obtain a single equation for Λ:

$$\Lambda^2 - \langle k \rangle \Lambda - \langle k^2 \rangle + \langle k \rangle^2 + \langle k \rangle = 0 \tag{3.8}$$

whose non-negative solution reads

$$\Lambda(t) = \frac{\langle k \rangle}{2} + \frac{1}{2}\sqrt{4\langle k^2 \rangle - 4\langle k \rangle - 3\langle k \rangle^2}, \tag{3.9}$$

where the first and second moment of the degree distribution are computed on the network integrated in the time window $[0, t]$. One can express Λ as a function of $\langle r \rangle$ and $\langle r^2 \rangle$ using Eqs. (2.34) and (2.36), as

$$\Lambda(t) = \langle r \rangle_t + \sqrt{\langle r^2 \rangle_t - \langle r \rangle_t}. \tag{3.10}$$

The percolation time T_p determined by imposing the condition $\Lambda(T_p) = 1$ [162], is thus given by the solution T_p of the implicit equation

$$\langle r^2 \rangle_{T_p} - \langle r \rangle_{T_p}^2 = 1 - \langle r \rangle_{T_p}. \tag{3.11}$$

No explicit expressions exist for $\langle r \rangle_t$ and $\langle r^2 \rangle_t$, except for an exponential waiting time distribution (Poisson process) $\psi_c(t) = c\, e^{-ct}$, in which case we recover the result derived in [162]

$$\left.\begin{array}{rcl} \langle r \rangle_{T_p} & = & \langle c \rangle T_p \\ \langle r^2 \rangle_{T_p} & = & \langle c \rangle T_p + \langle c^2 \rangle T_p^2 \end{array}\right\} \Rightarrow \quad T_p^{AD} = \frac{1}{\langle c \rangle + \sqrt{\langle c^2 \rangle}} \tag{3.12}$$

Since the network percolation occurs at relatively short times (such that $\langle r \rangle < 1$), the approximations for χ_t at large times performed in the previous chapter cannot be applied, and one must resort in principle to numerical simulations to estimate T_p.

In the following, we will study the percolation time T_p for a PLAD0 network with an inter-event time distribution of the form $\psi_c(t) = \alpha c(ct+1)^{-1-\alpha}$ with $0 < \alpha < 1$ and a parameter c distributed according to $\eta(c) = (c/c_0)^{-\beta-1}$. The temporal threshold is evaluated as the peak of the clusters' susceptibility $\xi(t)$ [162, 163]. This quantity is defined as $\xi(t) = \sum_s s^2\, n_s$, where n_s is the number of clusters of size s per node and the sum is restricted to all clusters, except the largest one. On Fig. 3.1 we plot the size of the largest connected component S_{GCC}, divided by the total size N of the network, as a function of time, as well as the susceptibility $\xi(t)$. We observe that the peak of $\xi(t)$ corresponds to the birth of a giant connected component spanning a finite fraction of the total size N.

On the other hand, in order to check the validity of our general criterion, we solve numerically Eq. (3.11), by means of a dichotomic search, with $\langle r^2 \rangle_{T_p}$

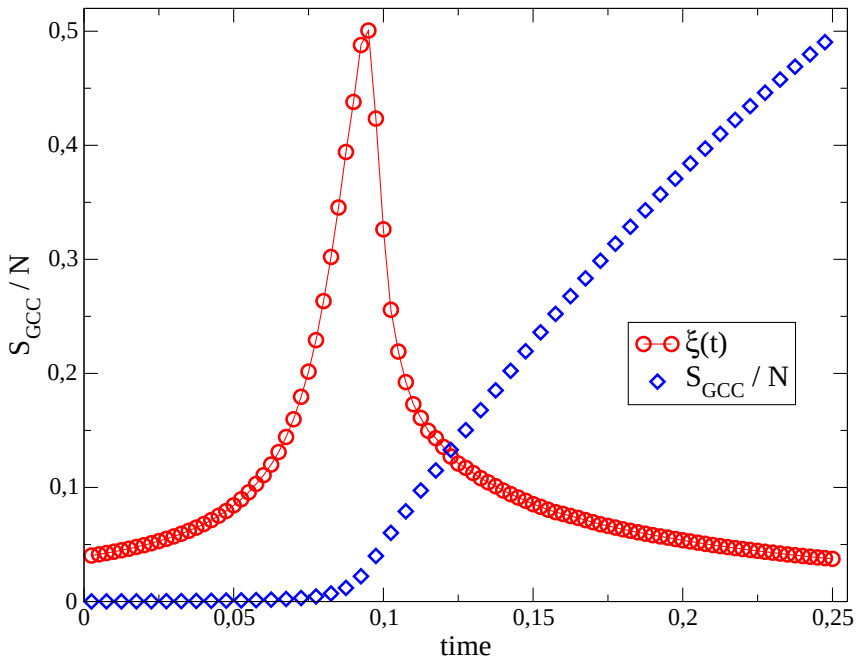

Figure 3.1.: Temporal percolation of a PLAD0 network. We plot the reduced susceptibility $\frac{\xi(t)}{2\xi_{max}}$ and the size of the largest connected component S_{GCC}/N as functions of time. $\alpha = 0.9$, $\beta = 1.1$, $c_0 = 1$, $c_{max} = 10^3$ and network size $N = 10^5$. Results are averaged over 100 iterations.

and $\langle r \rangle_{T_p}$ evaluated from numerical simulations of the corresponding renewal processes. We proceed as follows:

1. Evaluate $\theta_0 = 1 - \langle r \rangle_{t_0} - \langle r^2 \rangle_{t_0} + \langle r \rangle_{t_0}^2$ at some small starting time t_0 such that $\theta_0 > 0$ (this is always possible because $\theta(t = 0) = 1$)

2. Set $a = 0$ (see next step)

3.
   - Evaluate recursively θ_1, θ_2, ..., θ_k, at times $t_i = (1 + 1/10^a) \times t_{i-1}$
   - Stop when $\theta_k < 0$ ($\theta_{k-1} > 0$). As $\theta(t)$ is a monotonically decreasing function of t one has $t_k > T_p > t_{k-1}$
   - Set $t_0 = t_{k-1}$ and repeat step 3. with $a = a + 1$

The process stops and return t_{k-1} when a predefined precision (corresponding to a given value of a) is reached (for $a = 4$, $0.9999\, T_p < t_{k-1} < T_p$). Fig. 3.2 contrasts the result of this numerical evaluation of Eq. (3.11) with estimations of the threshold T_p from numerical simulations of the PLAD0 model, by means of the peak of the susceptibility. We observe on the figure a very good agreement between both methods for all values of α and β, although the threshold obtained

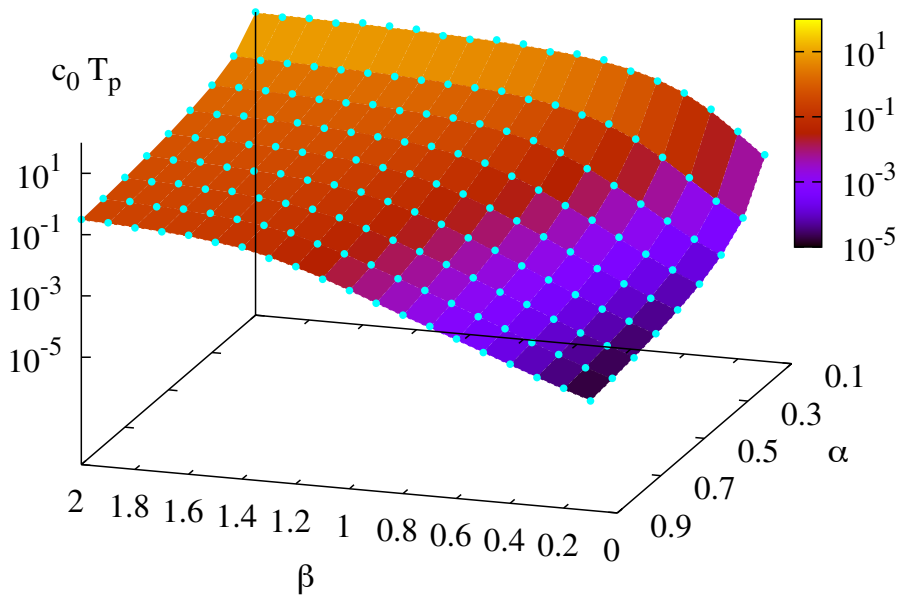

Figure 3.2.: Percolation threshold T_p as a function of α and β. Blue dots correspond to estimations of T_p as given by the peak of the clusters' susceptibility; the surface is obtained by a numerical solution of Eq.(3.11). Network size is $N = 10^8$, $c_0 = 1$ and $c_{max} = 10^6$ (see main text).

by means of $\xi(t)$ tends to be slightly superior to that predicted by Eq. (3.11), with an average error of 6%.

One can see that the percolation time T_p rapidly decreases toward zero in a region of the (β, α) space. This is due to the fact that, as Eq. (3.11) shows, if the second moment $\langle r^2 \rangle_t$ diverges, then T_p tends to zero in the thermodynamic limit, $N \gg 1$. According to (2.55), one has, for $ct \gg 1$

$$\overline{r^2}_c(t) \sim (ct)^{2\alpha}. \tag{3.13}$$

Thus for $\beta < 2\alpha$, $\langle r^2 \rangle_t = \int dc\, \eta(c) \overline{r^2}_c(t)$ is infinite at large times. This implies that $\langle r^2 \rangle$ is infinite $\forall t > 0$, since otherwise there would be a discontinuity at some arbitrary time $t > 0$, which is absurd. Therefore, the percolation time is zero in the thermodynamic limit for $\beta < 2\alpha$, while it is finite otherwise. To avoid these finite size effects, one needs to set a cutoff c_{max} for the parameter c (in Fig. 3.2 this cutoff is set to $c_{max} = 10^6$). We explore the impact of the cutoff in Fig. 3.3, which shows the percolation time T_p in the (β, α) space for different values of c_{max}. We choose a network size N such that $N \geq 100\, c_{max}$ in order to hinder sampling errors on the values of c. As expected, we observe a strong decay of T_p towards zero in the region $\beta < 2\alpha$, as c_{max} grows.

We also compare the percolation threshold obtained within the correlated networks formalism, T_p, with the prediction valid for uncorrelated networks T_p^0, as given by the Molloy-Reed criterion of Eq. (3.2). This equation can be solved

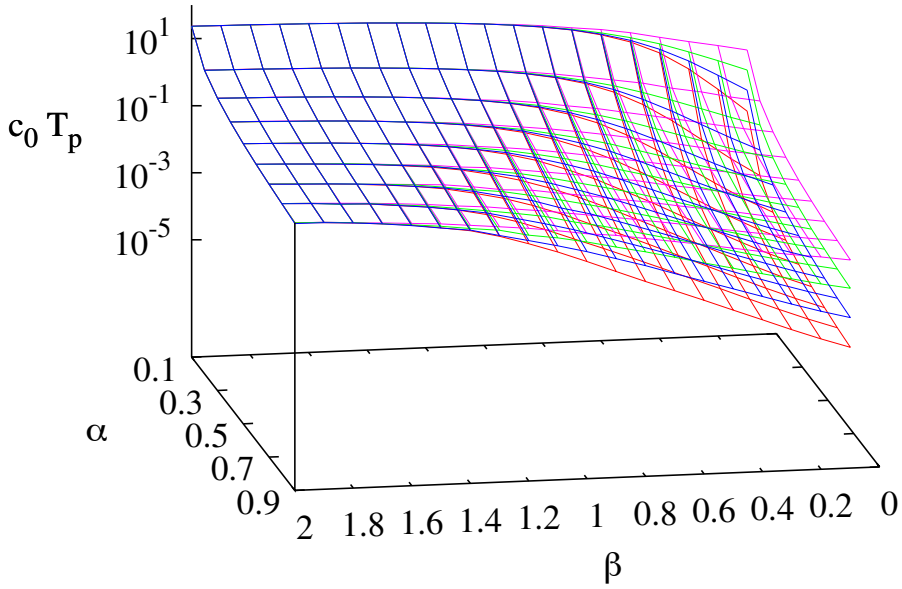

Figure 3.3.: Percolation threshold T_p as a function of α and β for different values of c_{max}. T_p is calculated numerically from Eq. (3.11), with $c_0 = 1$. From top surface to bottom one, values of $c_{max} = 10^3, 10^4, 10^5, 10^6$. Network size is $N = 10^8$.

numerically applying the dichotomic search method described above. Fig. 3.4 shows the relative error between T_p and T_p^0, in the (β, α) space. One can see that only for large values of β the MR criterion is close to the real percolation threshold, justifying the necessity of using the correlated networks formalism.

Another interesting observation comes from relating the behavior of the percolation time T_p as a function of α and β, shown in Fig. 3.2, with the average number of activation events counted in the time window $[0, T_p]$, $\langle r \rangle_{T_p}$, which is a measure of the density (average degree) of the integrated network. On the one hand, increasing β while keeping constant α decreases $\langle r \rangle_{T_p}$, and so it increases the percolation threshold T_p. On the other hand, increasing α while keeping β constant accelerates the growth of the integrated network, so $\langle r \rangle_{T_p}$ increases and T_p is smaller. The average number of activations $\langle r \rangle_{T_p}$, thus, as a measure of the density of the network at time $t = T_p$, provides useful additional information on the characteristics of the percolation process. Fig. 3.5 displays $\langle r \rangle_{T_p}$ as a function of α and β, showing that this density has a minimum value which appears to be close to the region $\alpha = \beta$. In this region, agents form a giant component even though they hardly have interacted, indicating that the link emission pattern is more efficient for this particular set of parameters. A partial explanation of this feature can be derived from an evaluation of Eq. (3.11) in the large time limit, even though the network percolates at times where asymptotic expansions of $\langle r \rangle_t$ and $\langle r^2 \rangle_t$ are not relevant. In this limit we write $\langle r^n \rangle \simeq \frac{\Gamma_{n+1}}{\Gamma_{\alpha n+1}\Gamma^n_{1-\alpha}} \langle c^{\alpha n} \rangle t^{\alpha n}$

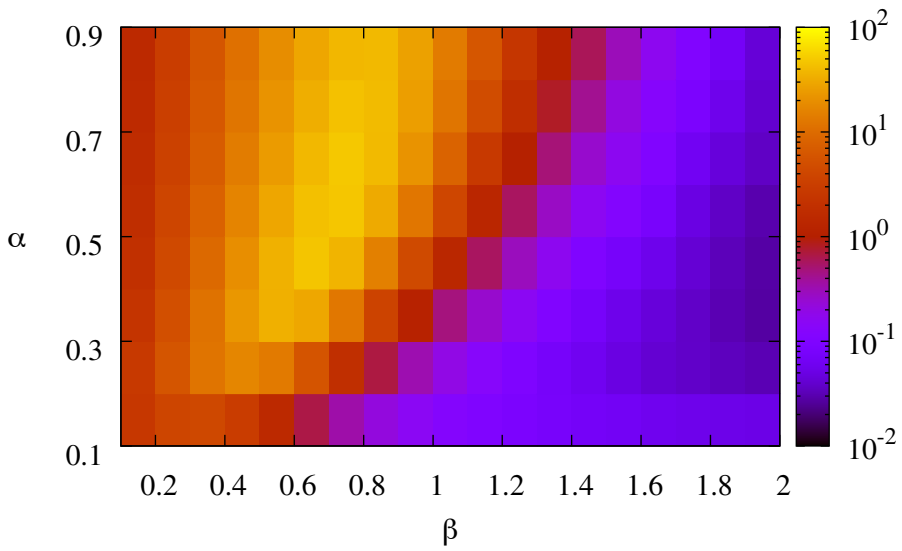

Figure 3.4.: Relative error $(T_p - T_p^0)/T_p^0$ as a function of α and β. T_p^0 is obtained by numerically solving the implicit equation ensuing from the Molloy-Reed criterion, T_p is given by the numerical solution of Eq. (3.11). Network size is $N = 10^8$, $c_0 = 1$ and $c_{max} = 10^6$.

[151], which gives an average activation number at the threshold T_p

$$\langle r \rangle_{T_p} \simeq \frac{\sqrt{1 + 4R(\alpha, \beta)} - 1}{2R(\alpha, \beta)}, \tag{3.14}$$

where $R(\alpha, \beta) = 2\,\Gamma^2_{\alpha+1}\langle c^{2\alpha}\rangle / \Gamma_{2\alpha+1}\langle c^{\alpha}\rangle^2 - 1$. We look for possible extremes in Eq. (3.14), for a given value of α, and with a maximum $c_{\max}$ to avoid divergences.

$$\begin{aligned} & \frac{\partial \langle r \rangle_{T_p}}{\partial \beta} = 0 \\ \Leftrightarrow \quad & \frac{\partial_\beta R}{2R^2\sqrt{1+4R}}(-1 - 2R + \sqrt{1+4R}) = 0 \end{aligned} \tag{3.15}$$

The term between parenthesis is equal to zero if and only if $R = 0$, however $R > 1$ for $0 < \alpha < 1$, so that we deduce

$$\begin{aligned} & \frac{\partial \langle r \rangle_{T_p}}{\partial \beta} = 0 \\ \Leftrightarrow \quad & \frac{\partial R}{\partial \beta}(\alpha, \beta) = 0 \\ \Leftrightarrow \quad & \frac{\partial}{\partial \beta} \frac{\langle c^{2\alpha} \rangle}{\langle c^{\alpha} \rangle^2} = 0 \end{aligned} \tag{3.16}$$

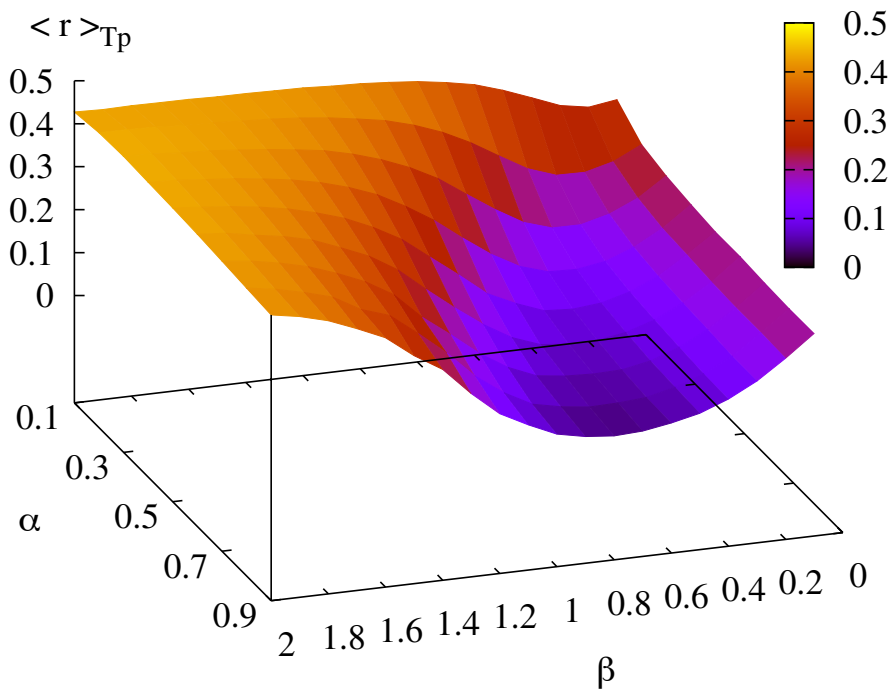

Figure 3.5.: Average activation number at the threshold, $\langle r \rangle_{T_p}$, as a function of α and β. Network size $N = 10^7$, $c_0 = 1$ and $c_{max} = 10^6$.

Moreover, we write

$$\frac{\langle c^{2\alpha} \rangle}{\langle c^{\alpha} \rangle^2} = \frac{(\beta - \alpha)^2 (1 - c_1^{-\beta})(1 - c_1^{2\alpha - \beta})}{\beta(\beta - 2\alpha)(1 - c_1^{\alpha - \beta})^2} \tag{3.17}$$

where $c_1 = c_{\max}/c_0$. The factor $(\beta - \alpha)^2$ in the numerator implies that the derivative with respect to β is equal to zero at $\beta = \alpha$. We thus observe a minimum in $\langle r \rangle_{T_p}$ located precisely at $\beta = \alpha$, in qualitative agreement with Fig. 3.5.

As stated above, for the general form of the waiting time distribution given by Eq. (2.43), neither explicit expressions are available for $\langle r \rangle_{T_p}$ and $\langle r^2 \rangle_{T_p}$, nor are approximations valid close to the percolation time T_p, so that one must resort to numerical simulations to estimate T_p. An exception is the case of a power law waiting time distribution with exponent $\alpha = 1/2$, which corresponds to the one-sided Lévy distribution [93]

$$\psi_c(t) = \frac{e^{-1/(ct)}}{\sqrt{\pi c}\, t^{3/2}}. \tag{3.18}$$

In this case, the distribution of activation numbers at time t reduces to

$$\chi_t(r|c) = \operatorname{erf}\left(\frac{r+1}{\sqrt{ct}}\right) - \operatorname{erf}\left(\frac{r}{\sqrt{ct}}\right), \tag{3.19}$$

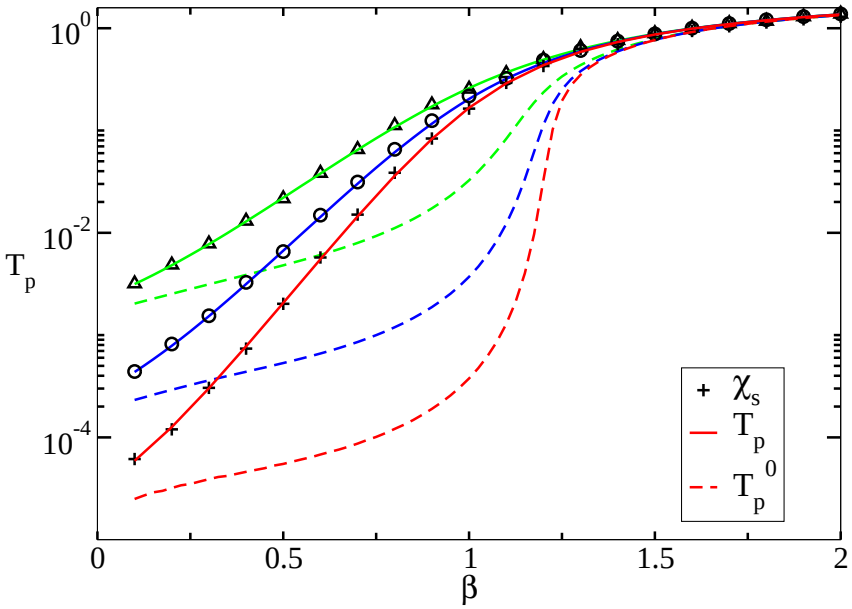

Figure 3.6.: Percolation threshold T_p on a Lévy NoPAD network as a function of β. Three different values of the parameter c_{max} are shown. Symbols represent T_p evaluated by means of the peak of the susceptibility $\chi(s)$. Continuous lines represent T_p evaluated numerically from Eq. (3.20) and Eq. (3.11). Dashed lines represent the threshold T_p^0 given by the Molloy-Reed criterion. Triangles correspond to $c_{max} = 10^4$, circles to $c_{max} = 10^5$ and crosses to $c_{max} = 10^6$. The corresponding dashed lines follow the same downward progression. Lower bound activity $c_0 = 1$. Network size $N = 10^8$.

where $\mathrm{erf}(z)$ is the error function. The moments of the activation distribution can be analytically expressed as

$$\langle r^n \rangle_t = \int dc\, \eta(c) \sum_{r=0}^{\infty} r^n \left(\mathrm{erf}\left(\frac{r+1}{\sqrt{ct}} \right) - \mathrm{erf}\left(\frac{r}{\sqrt{ct}} \right) \right), \tag{3.20}$$

and the percolation time T_p can be computed by introducing Eq. (3.20) into the general criterion Eq. (3.11), and solving numerically the ensuing self-consistent equation.

Fig. 3.6 shows the percolation time T_p on a Lévy NoPAD network as a function of the activity distribution exponent β. One can see that the theoretical prediction fits very well the numerical estimation of T_p given by the peak of the cluster susceptibility $\xi(t)$. In the same Fig. 3.6, we also plot the percolation threshold T_p^0 as predicted by the MR criterion, showing that this is a good approximation

only if β is close to 2, in accordance with what is observed in Fig. 3.4, for an inter-event time distribution with a general form given by Eq. (2.43).

3.3. Summary

In this chapter we have presented a detailed mathematical study of the connectivity properties of the time-integrated networks emerging from the dynamics of the GAD0 model introduced in chapter 1. The systematic recording of the instantaneous contacts prescribed by the dynamics of this model allows to define the temporal percolation of the ensuing aggregated network, as determined by the time T_p at which a giant connected component, spanning a finite fraction of total number of nodes in the network, first emerges. Applying the branching matrix formalism [62, 162], appropriate to elucidate the percolation of correlated random static graphs, we derive a general criterion defining implicitly the percolation time and featuring the first and second moments of the activation number distribution $\langle r \rangle_{T_p}$ and $\langle r^2 \rangle_{T_p}$. Unfortunately the equation is not directly solvable for an arbitrary waiting time distribution $\psi_c(t)$ and a distribution $\eta(c)$ quantifying the heterogeneity of the activity parameter c. However the criterion successfully describes a phenomenon depending intrinsically on the connectivity properties of the network in terms of quantities related to the local activation dynamics of the agents only, regardless of who is connected to whom. We test the validity of this criterion for a PLAD0 network, described in section 2.4, and characterized by the exponent α of the waiting time distribution and the exponent β of the distribution $\eta(c)$ of the activity parameter. We compare, as a function of α and β, the percolation time evaluated by a numerical resolution of the general criterion and the real threshold evaluated as the peak of the clusters' susceptibility [162, 163]. A very good agreement is found between the real percolation threshold and that provided by the criterion. Besides, a relevant result revealed by our analysis is that the percolation time vanishes in the thermodynamic limit in the region $\beta < 2\alpha$, where the fast aggregation of connections leads to a giant component in a very short interval of time. The investigation of the percolation process of integrated temporal networks opens new interesting tracks for future research, related in particular to the properties of dynamical processes running on top of them. Indeed, in the context of epidemic spreading, the SIR model (see chapter 6) on expAD0 networks was shown to be conveniently mappable a temporal percolation problem. Although such an equivalence is not guaranteed on generalized activity driven networks, we hope that our work will motivate further research in this direction, and bring fruitful insights to the study of dynamical processes on non-Markovian temporal networks.

4. Temporal network poissonization and consequences on the percolation

4.1. Introduction

While the structural properties of the static representation of a networked system play a crucial role in its description, the temporal nature of the elements of the network itself implies new dynamical phenomena that do not have a counterpart in the corresponding time-aggregated graph [34, 59, 73, 88, 104, 112].

Moreover, we have now empirical evidence that Poisson processes, characterized by inter-event times between consecutive interactions that are exponentially distributed, do not faithfully describe real interaction patterns in a variety of physical and social systems. The times between successive contacts are better described by heavy-tailed distributions, reflecting the so-called bursty behaviour of the links dynamics. The recent discovery of this non-trivial feature has incited renewed efforts aimed at unravelling the interplay between a variety of dynamical processes and the temporal and structural properties of the underlying networks. In general, it has been reported that the broad-tailed inter-contact time distributions found in empirical datasets contribute to slow down the dynamics of stochastic processes on networks, compared with what happens when randomization procedures are applied to the network substrate [77, 86, 88, 128, 175]. However, other studies reveal the existence of regimes exhibiting an acceleration of the dynamical processes with respect to these null models [147, 150]. In this chapter, we quantify the error made in the evaluation of the temporal percolation threshold when an arbitrary annealed static graph, resulting from the time-aggregation of a given temporal contact sequence, is supposed to be generated by Poissonian activation processes of the agents, i.e. when the network is mapped onto an activity driven network topology. This simple analysis allows us to call attention to the crucial influence of not only the tail, but also the early behaviour of the inter-event time distribution on the birth of a giant connected component in the corresponding time-aggregated network.

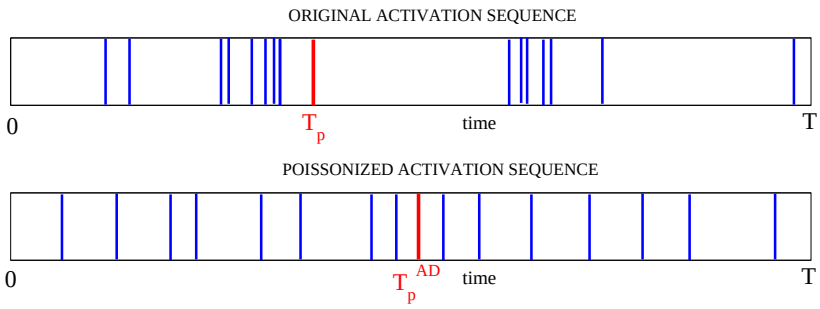

Figure 4.1.: Schematic illustration of a poissonization process. (top): arbitrary sequence of activations in a time window $[0, T]$. (bottom): possible outcome of the randomization procedure. We display the percolation time of the growing network corresponding to the time-aggregation of the overall contacts sequence, and the percolation time of the activity driven network obtained through the poissonization. Note that the activation sequences do not correspond to any actual simulation or empirical data, nor do the times T_p and T_p^{AD}, but rather constitute an illustration of the general principle of the method.

Let us consider a set of N nodes, each activating according to a counting process, i.e. a succession of punctual events occurring stochastically in time. We suppose that subsequently to an activation, a node connects to a peer chosen uniformly at random, defining a general temporal network dynamics. Besides, suppose an external observer arriving at time T, and having only access to the total number of activations counted in the interval $[0, T]$ for each node, $\{r_i\,,\ i \in [1, N]\}$, and ignoring the epochs of occurrence of these activations. Having no prior information about the dynamics of the network, this observer might want, in a first approximation, to map the individual activation processes onto Poissonian processes. In the following, we define three such *poissonization* methods, and derive for each of them the percolation threshold T_p^{AD} of the activity driven network obtained through the randomization process. On Fig. 4.1 we sketch an arbitrary sequence of activations for a single node in the interval $[0, T]$, and a possible sequence obtained by a poissonization procedure. The estimated threshold T_p^{AD} does not in general coincide with the threshold T_p of the original network. The methodology developed here is aimed at describing a real world situation in which an observer has access to a static graph, usually rather dense and thus having percolated, and is willing to infer a possible underlying temporal network dynamics. For this reason in the rest of the chapter we assume that the observation time T is larger than the percolation time T_p of the network under scrutiny.

4.2. Definition of the procedures

4.2.1. Direct poissonization

The intuitive direct poissonization consists in defining for agent i its activity rate as

$$a_i = \frac{r_i}{T} \tag{4.1}$$

The average temporal percolation threshold of an activity driven network is given by (3.12)

$$T_p^{AD} = \frac{1}{\langle a \rangle + \sqrt{\langle a^2 \rangle}} \tag{4.2}$$

where the brackets $\langle \cdot \rangle = \frac{1}{N} \sum_i (\cdot)_i$ mean averaging over all the agents. From equation (4.1) we have

$$\langle a \rangle = \frac{\langle r \rangle_T}{T} \tag{4.3}$$

$$\langle a^2 \rangle = \frac{\langle r^2 \rangle_T}{T^2} \tag{4.4}$$

From which we write

$$T_p^{AD} = \frac{T}{\langle r \rangle_T + \sqrt{\langle r^2 \rangle_T}} \tag{4.5}$$

At time T the average number of activations of the poissonized network matches that of the original network, i.e. $\langle r \rangle_T^{AD} = \langle r \rangle_T$, but the average square number of activations is overestimated because $\langle r^2 \rangle_T^{AD} = \langle r \rangle_T + \langle r^2 \rangle_T$. In particular, if we suppose that the original network has Poissonian dynamics, this direct poissonization procedure fails to recover the actual activity distribution, and subsequently leads to a systematic error in the evaluation of the percolation time, which is not satisfying. On Fig. 4.2, panel (c), we compare the percolation threshold T_p of an expAD0 network to the threshold obtained with a direct poissonization at $T = 10T_p$. We plot the fraction of nodes belonging to the largest connected component of the original network as a function of time (black circles), along with the function $\theta(t) = -1 + \langle r \rangle_t + \langle r^2 \rangle_t - \langle r \rangle_t^2$ (red circles) which intersects the zero horizontal axis at $t = T_p$ as we saw in chapter 3. Meanwhile, a list $\{r_i\}$ is generated through a single realization of the network's dynamics during a time $T = 10T_p$ ($T_p = 2.93$) and the corresponding list of activities defining the poissonized network is evaluated as $\{a_i = r_i/T\}$. The poissonized threshold is subsequently evaluated as the intersection between the zero horizontal axis and the curve $\theta^{AD}(t) = -1 + 2\langle a \rangle t + \langle a^2 \rangle t^2 - \langle a \rangle^2 t^2$ (green circles). We clearly see that the threshold of the poissonized network is not equal to that of the expAD0 network, $T_p^{AD} \neq T_p$. The weakness of this method stems from the fact that we try to determine the supposed underlying activity distribution based on the knowledge

of a single realization of a stochastic process, which induces an inevitable statistical error. To overcome this difficulty, we now assume a stronger prior knowledge about the initial process.

4.2.2. Averaged direct poissonization

We now suppose that each agent i activates according to a renewal process starting at $t = 0$, with inter-event time distribution $\psi_i(t)$, and that instead of a single realization of these processes, we have access to an ensemble average for each node:

$$\overline{r}_i = \sum_r r\, \chi_T(r|\psi_i) \tag{4.6}$$

where $\chi_T(r|\psi_i)$ is the probability that agent i activates r times in the time interval $[0, T]$. Thus we define

$$a_i = \frac{\overline{r}_i}{T} \tag{4.7}$$

The moments of the poissonized network are then given by

$$\langle a \rangle = \frac{\langle r \rangle_T}{T} \tag{4.8}$$

$$\langle a^2 \rangle = \frac{\langle \overline{r}^2 \rangle_T}{T^2} \tag{4.9}$$

Then

$$T_p^{AD} = \frac{T}{\langle r \rangle_T + \sqrt{\langle \overline{r}^2 \rangle_T}} \tag{4.10}$$

This procedure, by definition, allows to recover the exact activity distribution when the original network has a Poissonian dynamics because in this case the average number of activation $\overline{r}_i$ of the node i is equal to the original activity of the node times the observational time T. However, if the poissonization is applied to a network with an arbitrary inter-event time distribution $\psi_i(t)$ at its threshold, i.e. for $T = T_p$, we have in general $\langle r^2 \rangle_{T_p} \neq \langle r^2 \rangle_{T_p}^{AD}$. Combined with the fact that $\langle r \rangle_{T_p} = \langle r \rangle_{T_p}^{AD}$, and that $\theta(T_p) = 0$ by virtue of the general percolation criterion, we deduce $\theta^{AD}(T_p) \neq 0$. In other words, for $T = T_p$, the poissonized percolation time is not equal to the original threshold T_p. On Fig. 4.2(c), we first check that the curve $\theta^{AD}(t)$ (brown circles) evaluated via this second poissonization procedure is equal to the curve $\theta(t)$ of the original expAD0 network. On panel (b), we plot the relative size of the largest connected component of a PLAD0 network as a function of time, the corresponding function $\theta(t)$, and the functions $\theta^{AD}(t)$ resulting from the poissonization procedures applied to the PLAD0 network at $T = T_p$ ($T_p = 0.084$). We see that both methods fail to recover the correct percolation threshold. We consider that the threshold should be conserved under the

application of a satisfying poissonization procedure applied at $T = T_p$, and we thus define a third method to overpass this flaw.

4.2.3. Reshuffling of the activation times

The two methods presented before constitute attempts to define explicitly the activity of a node i, a_i based on the knowledge of r_i. Here we apply a more practical randomization procedure, assigning to each activation a random time of occurrence, uniformly at random, in the interval $[0, T]$, so that the list $\{r_i, i \in [1, N]\}$ stays unchanged. Through this method, the actual activity distribution of the poissonized network is not explicitly defined any more, but the first and second moment are implicitly obtained with

$$\begin{aligned} \langle r \rangle_T &= \langle r \rangle_T^{AD} = \langle a \rangle T \\ \langle r^2 \rangle_T &= \langle r^2 \rangle_T^{AD} = \langle a^2 \rangle T^2 + \langle a \rangle T \end{aligned} \tag{4.11}$$

which is equivalent to

$$\begin{aligned} \langle a \rangle &= \frac{\langle r \rangle_T}{T} \\ \langle a^2 \rangle &= \frac{\langle r^2 \rangle_T - \langle r \rangle_T}{T^2} \end{aligned} \tag{4.12}$$

From $\langle a \rangle$ and $\langle a^2 \rangle$ we then deduce the percolation threshold of the poissonized network

$$T_p^{AD} = \frac{T}{\langle r \rangle_T + \sqrt{\langle r^2 \rangle_T - \langle r \rangle_T}} \tag{4.13}$$

This method ensures that when poissonizing a network at the percolation threshold, i.e. at $T = T_p$, one recovers $T_p^{AD} = T_p$, which is not true with the first two procedures. On Fig. 4.2(c) we check that this method, applied to an expAD0 network, leads to $\theta^{AD}(t) = \theta(t)$ and subsequently T_p^{AD}. On panel (b), we check that the percolation time is left unchanged by the reshuffling method applied at $T = T_p$, as indicated by the fact that $\theta^{AD}(T_p) = \theta(T_p) = 0$. On panel (a), we plot the curves $\theta^{AD}(t)$ corresponding to the application of the three procedures defined in this section to the same PLAD0 network at $T = 10T_p$. As expected, we observe that the corresponding poissonized percolation time are erroneous. In the following we will see that depending on the existence of a finite average waiting time between consecutive interactions of the agents in the network, the methods described above may lead to dramatically incorrect evaluations of the threshold.

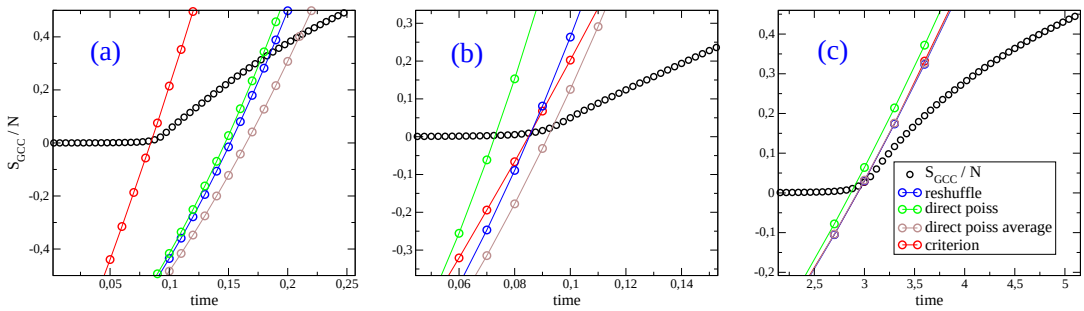

Figure 4.2.: (a) Poissonization of a PLAD0 network at $T = 10T_p$ ($T_p = 0.084$) with $\alpha = 0.9$, $\eta(c) \sim c^{-2.1}$ and $c \in [1, 10^3]$. (b): Poissonization of the same PLAD0 network at $T = T_p$. (c): Poissonization of an expAD0 network at $T = 10T_p$ ($T_p = 2.93$) with $\eta(c) \sim c^{-1.1}$ and $c \in [10^{-3}, 1]$. In each case we plot the relative size of the largest connected component S_{GCC}/N as a function of time (black circles), the function $\theta(t)$ of the original network (red circles) and the functions $\theta^{AD}(t)$ corresponding to the direct poissonization (green circles), the averaged direct poissonization (brown circles) and the reshuffling poissonization (blue circles).

4.3. Poissonization of a network far from the threshold

In this section we focus on the poissonization procedures applied to a network at a time T much larger than the percolation threshold of the original network, i.e. for $T \gg T_p$. We distinguish two cases: networks with finite average waiting times and networks with infinite average waiting times.

4.3.1. Network with finite average waiting time

For a general waiting time distribution with finite first moment τ, the first and the second moments of the distribution of the number of activations read, at large time t [61]

$$\begin{aligned} \overline{r_i} &\simeq \frac{t}{\tau_i} \\ \overline{r_i^2} &\simeq \frac{t^2}{\tau_i^2} \end{aligned} \tag{4.14}$$

Then when poissonizing a network having a threshold T_p at large $T \gg T_p$, and for which an agent i has a finite average waiting time τ_i, the ensuing percolation

time reads

$$T_p^{AD} \simeq \frac{1}{\langle 1/\tau \rangle + \sqrt{\langle 1/\tau^2 \rangle}} \tag{4.15}$$

We notice that this threshold, obtained in the large time limit, is the same for the three procedures defined above, and does not depend on the observation window T. Indeed, when the average waiting time is finite, the relative fluctuations of the number of renewals around its average value vanish at large times, so that the three poissonization procedures defined above are practically equivalent for $T \gg \langle \tau \rangle$.

4.3.2. Waiting time distribution lacking a first moment

In this section we evaluate the percolation time obtained through the application of the reshuffling method applied to a temporal network whose agents activate according to a renewal process with a waiting time distribution lacking a first moment, more precisely for $\psi(t) \underset{\infty}{\sim} t^{-1-\alpha}$ with $\alpha < 1$. According to Eqs. (2.54) and (2.55), the first and the second moments of the distribution of the number of activations read, at large time t,

$$\begin{aligned} \overline{r} &\underset{\infty}{\sim} t^{\alpha} \\ \overline{r^2} &\underset{\infty}{\sim} t^{2\alpha} \end{aligned} \tag{4.16}$$

so that the poissonized percolation time, obtained from Eq.(4.13), diverges with T

$$T_p^{AD} \underset{\infty}{\sim} T^{1-\alpha} \tag{4.17}$$

This result of course holds for the three procedures presented above, nevertheless it can be further analysed in the light of the mapping performed in the second method. Indeed, in this procedure we impose that for each node, the average number of interactions counted in the interval $[0, T]$ must be the same in both representations of the network (Poissonian and non-Poissonian), i.e. $a_i = \overline{r}_i/T$. As the growth of $\overline{r}_i$ is sublinear at large times, the resulting activity, averaged over the time window $[0, T]$, vanishes, $a_i \sim T^{\alpha-1}$. For all agents in the poissonized network, the activity thus trivially tends to zero, and the corresponding percolation time inexorably tends to infinity.

4.4. Numerical analysis

We want to use the reshuffling method on two different temporal networks characterized by the following fat-tailed inter-event time distributions:

$$\psi_1(t) = \alpha c_1 \, (c_1 t)^{-\alpha-1} \, e^{-(c_1 t)^{-\alpha}} \tag{4.18}$$

$$\psi_2(t) = \alpha c_2 \, (c_2 t + 1)^{-\alpha-1} \tag{4.19}$$

where $\alpha > 1$, i.e. with finite average waiting time. Note that ψ_1 is a Weibull distribution with a negative shape parameter $-\alpha$. We want to compare the percolation time of the temporal PLAD0 networks hereby defined and their poissonized versions. For the sake of simplicity, we choose to consider homogeneous networks, and we impose $c_1 = \Gamma(1 - 1/\alpha)/2$ and $c_2 = 0.5/(\alpha - 1)$ so that the average times between two activations are $\tau_1 = \tau_2 = 2$. On Fig. 4.3 we plot the ratio T_p/T_p^{AD} as a function of α for different values of the observational time T. The percolation times of the original networks are evaluated with prior numerical resolution of the general criterion established in chapter 3, while the poissonized thresholds are computed with Eq. (4.13) (in which $\langle r \rangle_T$ and $\langle r^2 \rangle_T$ are calculated with numerical simulations). In particular for $T = \infty$ the poissonized percolation time in Eq. (4.15) is equal to 1, so that $T_p/T_p^{AD}(T = \infty) = T_p$. We see that the network parametrized by ψ_2 always percolates before its poissonized version and that at fixed values of α the poissonized percolation time grows with T. This phenomenology can be given some insight when looking at the behaviour of $\langle r \rangle_t$ at small times. Indeed, poissonizing at T consists in creating a poissonian AD network whose average number of activations coincides with that of the original network at time T. Determining which network percolates first is equivalent to determine if the original network grows faster or slower at short times than the poissonized version, which can be determined graphically comparing $\langle r \rangle_t$ and the straight line joining the origin and the point $(T, \langle r \rangle_T)$.

In the Laplace domain, we recall that (see Eq. (2.54))

$$\langle r \rangle_s = \frac{\psi(s)}{s(1 - \psi(s))} \tag{4.20}$$

the behaviour of $\langle r \rangle_t$ at short times is determined by the behaviour of $\langle r \rangle_s$ at large s, i.e.

$$\langle r \rangle_t \underset{0}{\simeq} \mathcal{L}^{-1}\left[\frac{\psi(s)}{s}\right] = \int_0^t \psi(t')dt' \tag{4.21}$$

where $\mathcal{L}^{-1}$ is the inverse Laplace transform. If $\psi(0) > 0$ this simplifies into $\langle r \rangle_t \simeq \psi(0)t$, otherwise the integral must be computed. For the network with ψ_2, we simply have

$$\langle r \rangle_t \underset{0}{\simeq} \alpha c_2 t \tag{4.22}$$

and we also know that at large times

$$\langle r \rangle_t \underset{\infty}{\simeq} (\alpha - 1) c_2 t \tag{4.23}$$

We extrapolate that at all times the curve $\langle r \rangle_t$ is always above its asymptote $(\alpha - 1)c_2 t$, and subsequently that $\forall T$ and $\forall t < T$, $\langle r \rangle_t > \langle r \rangle_t^{AD}$. Thus it is not surprising to observe in Fig. 4.3 that the original network percolates faster than its poissonized version. However, this naive picture of the percolation process is not exact. Indeed the threshold depends also on the second moment $\langle r^2 \rangle$, and is implicitly determined by the condition $1 - \langle r \rangle_{T_p} = \langle r^2 \rangle_{T_p} - \langle r \rangle_{T_p}^2$, so that the poissonized network may percolate later than its original version even though its density grows faster at small times. For the network parametrized by ψ_1, indeed, the phenomenology observed in Fig. 4.3 is much richer than for ψ_2 and is clearly in contradiction with the qualitative reasoning performed earlier. For small values of α and large values of T, the poissonized network percolates after the original network even though the initial growth of the network's density is sublinear $\langle r \rangle_t \underset{0}{\simeq} e^{-(c_1 t)^{-\alpha}}$, i.e. slower than for the poissonized network. Furthermore, depending on the value of α, T_p^{AD} may either be an increasing (for $\alpha \lesssim 1.25$) or decreasing (for $\alpha \gtrsim 2.5$) function of T, or even exhibit a minimum at some finite value of T (for $\alpha \simeq 1.75$). As a conclusion, it seems that there is no systematic way to determine if the poissonized network percolates before or after the original network, without computing T_p and T_p^{AD}. In particular the probability density functions ψ_1 and ψ_2 are both fat-tailed with the same power-law decay but they lead to totally different results when comparing T_p and T_p^{AD}.

4.5. Conclusion

In this chapter, we analysed the implications of the poissonization procedure, which lies at the core of the analysis of empirical temporal networks. Indeed, for technical reasons, in a variety of situations an observer has only access to an aggregated static version of a network. Then in order to infer the actual contacts sequence that originated the network, or at least a faithful probabilistic representation of it, the simplest assumption he can make, which has been extensively used in the literature, is that of a contact pattern following a Poissonian process, and more specifically an agent based description in terms of activity driven temporal networks [136]. Here the situation is slightly different, as we assume that the dynamics of the network is that of the synthetic PLAD0 network defined in Introduction. This approach allows us to perform a quantitative analysis of the consequences of the application of such a method in the estimation of the temporal percolation threshold of the network. We give an expression of the estimated percolation time, i.e. the percolation time of the inferred activity driven network,

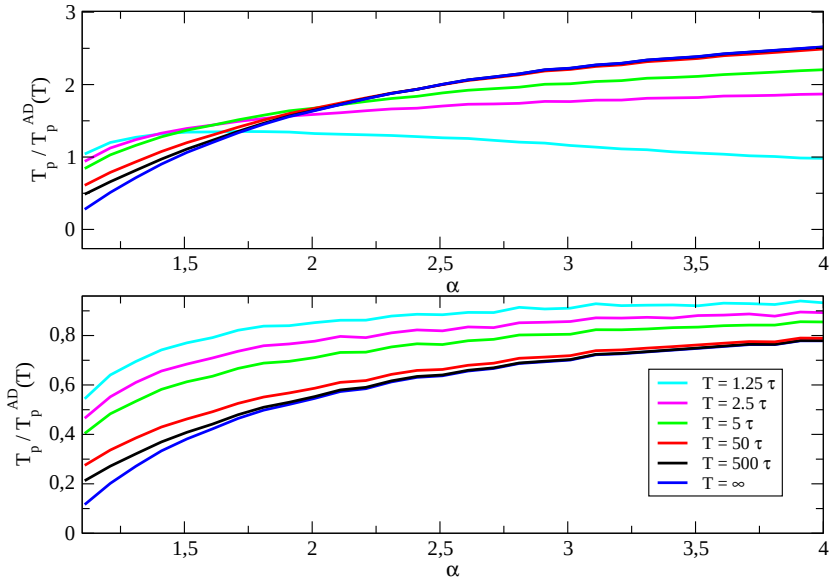

Figure 4.3.: (top): poissonization of a Weibull network (WTD ψ_1). (bottom): poissonization of a PLAD0 network (WTD ψ_2) as a function of α, for different values of T.

as a function of the average number and average square number of activations in the network counted in the interval $[0, T]$ (or equivalently as a function of the average degree and average square degree of the aggregated PLAD0 network as explained in subsection 2.3.2). In the case of a power-law inter-event distribution with finite first moment, this threshold can either be larger or smaller than the real threshold, depending on the value of the exponent α considered, and the observation window T. In particular, we exhibit two different inter-event distributions sharing a common power-law decay behaviour at large times with the same exponent, but leading to an opposite result when comparing T_p and T_p^{AD}. We deduce that the traditional classification opposing bursty and Poissonian-like behaviour is not entirely relevant, and we point out the necessity to take into account the early behaviour of the inter-event time distribution in the dynamical analysis of the network. Moreover, our investigation reveals that mapping a bursty network with infinite average waiting time onto an activity driven network leads to a dramatic error in the evaluation of the time of birth of a giant connected component in the network. Indeed, in this case the threshold trivially tends to infinity when the observational time T tends to infinity because the activity of the agents of the poissonized network vanishes as T grows. In this sense, this analysis goes along the same lines as what is found in the literature, indi-

cating that the Poissonian model fails to capture the essential ingredients of the network's dynamics, and leads to a misleading picture of the unfolding of dynamical processes running on top of it. However, two major criticisms can be made of the investigation presented in this chapter. First, further effort should be devoted to proving that the PLAD0 model succeeds in capturing the major traits of real empirical networks, and more specifically the percolation threshold. Indeed, if this model was to be proven irrelevant, then our work would simply amount to a proof of the incompatibility between two unrealistic models, regarding the percolation of the networks, and thus would have no practical consequences as far as empirical networks are concerned. Secondly, while it was proven with qualitative arguments that the temporal percolation of an activity driven network is equivalent to an SIR spreading process [162], such a mapping still needs to be confirmed in the case of a GAD network. This means that, although it seems reasonable to anticipate that the inaccuracy of the evaluated percolation threshold of a PLAD0 network obtained through a poissonization procedure will have a similar repercussion on the evaluation of the epidemic threshold of a spreading process, the present work does not constitute a rigorous proof of this statement.

5. Aging Effects

5.1. Aging of a renewal process

The analysis of the GAD model presented in this Thesis is rooted in the previously mentioned renewal theory. In very general terms, any stochastic process $r(t)$ counting the number of a certain type of instantaneous events occurring during a time interval $[0, t]$, with identically and independently distributed time spans between consecutive events, may be called a renewal process, or renewal counting process. Renewal theory does not specify the exact meaning or effect of a single event, and is for this reason found at the core of many stochastic problems throughout many different fields of science. In fact, the renewal formalism generalizes a Poisson process, defined as a series of events occurring with exponentially distributed waiting times, to arbitrary distributions $\psi(t)$ of the holding times. For a Poisson process, $\psi(t) = \tau^{-1} \exp(-t/\tau)$ so that the events are observed at a constant rate τ^{-1} and thus define a memoryless process. For arbitrary holding times on the other hand, the counting process is in general non-Markovian, but any memory of the past is erased with the occurrence of an event.

The form of the inter-event time distribution $\psi(t)$ can impact heavily the statistics of the overall counting process. In particular, when this distribution is power-law tailed, i.e. $\psi(t) \underset{\infty}{\sim} t^{-1-\alpha}$, the average holding time $\langle t \rangle = \int_0^\infty t\psi(t)dt$ is infinite for $0 < \alpha < 1$. Such a distribution is said to be scale free because the largest waiting time generated during a single realization of the renewal process is statistically of the order of the observation duration. On the contrary, for distributions possessing a finite average holding time τ, the corresponding renewal process behaves quasi deterministically on large time scales, i.e. $r(t) \simeq t/\tau$ when $t \gg \tau$.

Figure 5.1 shows the realizations of a deterministic renewal with $\psi(t) = \delta(t - 1)$, of a Poissonian renewal, $\psi(t) = e^{-t}$, and of a heavy-tailed distribution of the form $\psi(t) = 4.5 \times (5t + 1)^{-1.9}$. While the regularity of the deterministic process is distinct, we observe that the two random processes cannot be clearly identified by the observation of their initial evolution at short time scales. On the other hand, the realizations of the deterministic and Poissonian renewal processes look almost identical at larger time scales, $r(t) \simeq t$ for $t \gg 1$. On the contrary, for the power-law tailed renewal process, large holding times persist and are statistically relevant on arbitrarily long time scales. The counting process remains non trivial,

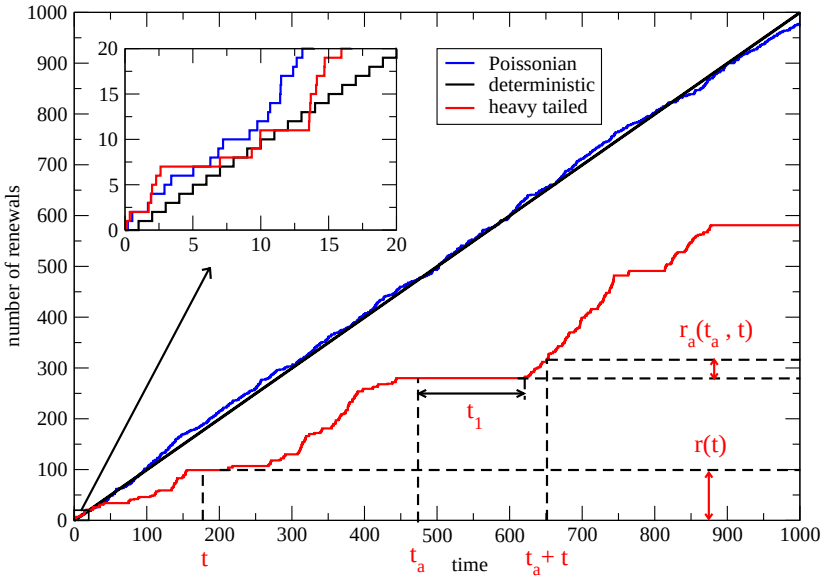

Figure 5.1.: Sample realizations for three different types of renewal processes. Events are separated by waiting times, which are independently and identically distributed according to a probability density function $\psi(t)$. In black, we plot the deterministic process counting one event at each unit time step: $\psi(t) = \delta(t-1)$. In blue, we plot a realization of a Poissonian renewal with rate 1: $\psi(t) = e^{-t}$. In red, we plot the realization of a scale free process, $\psi(t) = 4.5 \times (5t+1)^{-1.9}$, the average inter-event time is infinite in this case.

even when $t \gg 1$.

That being said, we put forward at this point the notion of aged measurements: considering a renewal process starting at time $t = 0$, an observer might only be able or willing to count events starting from a later epoch $t_a > 0$. Instead of the total number of renewals $r(t)$, s/he then witnesses the counted fraction $r_a(t_a, t) = r(t_a + t) - r(t_a)$. As the inter-event times are independently and equally distributed, the fundamental statistical difference between the renewal processes r and r_a is completely encompassed in the statistics of the time t_1 elapsed between the start of the measurement at t_a and the first observation of an event. This interval is called the forward recurrence time [151] and its probability distribution is denoted $h(t_a, t_1)$. If the observer counts the events from the beginning of the process, $t_a = 0$ the forward recurrence time is of course simply distributed like any other waiting time, $h(t_a = 0, t_1) = \psi(t_1)$. But for deferred, aged measurements, $t_a > 0$, the distribution is distinct, as indi-

cated in Fig. 5.1. The dependence of the statistical properties of the counted renewals r_a on the starting time of the observation t_a is called an aging effect. Its intensity critically depends on the specific waiting time distribution under consideration. For instance, a Poissonian renewal process is Markovian, which means that events occur at a constant rate at all times, so that $h(t_a, t_1) = \psi(t_1)$, $\forall t_a$. In other words, a Poissonian renewal process does not age. For any other distribution, $h(t_a, t) \neq \psi(t)$ and aging is at play. However, the fact that a renewal behaves quasi deterministically at large times when the average waiting time is finite clearly means that the aging effects fade at such time scales. Contrariwise, infinite average waiting times imply non trivial behaviour of the corresponding counting processes at all time scales, and aging effects should be taken into careful consideration in this case.

The investigation of a general aged renewal process finds a convenient formulation in the Laplace domain. Keeping the notations of chapter 2, we give an expression for the distribution $\chi_{t_a,t}(r|c)$ of the number of events counted in the interval $[t_a, t_a + t]$, for a renewal process with waiting time distribution $\psi_c(t)$, c being an arbitrary parameter having the dimension of a firing rate. Defining the double Laplace transform

$$\chi_{u,s}(r|c) = \int_0^\infty dt_a \int_0^\infty dt\ \chi_{t_a,t}(r|c) e^{-ut_a} e^{-st} \tag{5.1}$$

we have [14, 61, 151]

$$\chi_{u,s}(r|c) = \begin{cases} (us)^{-1} - h_c(u,s)s^{-1} & r = 0 \\ h_c(u,s)\psi_c(s)^{r-1}[1-\psi_c(s)]s^{-1} & r \geqslant 1 \end{cases}, \tag{5.2}$$

where

$$h_c(u,s) = \frac{\psi_c(u) - \psi_c(s)}{s-u} \frac{1}{1-\psi_c(u)} \tag{5.3}$$

is the double Laplace transform of the forward waiting time distribution $h_c(t_a, t)$. This expression is derived in the same manner as for the non-aged case (2.46), except that here the time T_r of occurrence of the r-th renewal, for $r \geqslant 1$, is the sum of r independent variables, the first one distributed with $h_c(t_a, t)$ and the other ones with $\psi_c(t)$. Besides, the probability to count zero events is equal to the survival probability $\tilde{h}_c(t_a, t)$ associated to the forward waiting time distribution: $\chi_{t_a,t}(r = 0|c) = \int_t^\infty h_c(t_a, u)du$. In the following, we will study the aging of a renewal process with a power-law waiting time distribution, and we assume a distribution of the form (2.43). In the case $t_a > 0$, and working in the large time limit $ct \gg 1$ and $ct_a \gg 1$, the expression of the forward waiting time in Laplace space, Eq. (5.3), takes, using Eq. (2.49), the form

$$h_c(u,s) = \frac{s^\alpha - u^\alpha}{u^\alpha(s-u)}, \tag{5.4}$$

while Eq. (5.2) becomes [151]

$$\chi_{t_a,t}(r|c) = \delta(r)[1 - m_c(t_a,t)] + h_c(t_a,t) *_t \chi_t(r|c) \tag{5.5}$$

where $m_c(t_a,t) = \int_0^t h_c(t_a,t')dt'$, the symbol $*_t$ means convolution with respect to the variable t, and $\chi_t(r|c) = \chi_{t_a=0,t}(r|c)$. For $t_a > 0$, we observe an increasing probability of counting exactly $r = 0$ events during the time interval $[t_a, t_a + t]$, with a relative weight given by $1 - m_c$, which will have an important impact in the shape of the degree distribution of the temporal network models considered.

In chapter 2, we investigated the properties of the GAD network, in which the activations of a node i obeys a renewal process parametrized by $\psi_{c_i}(t)$. In all the developments, we implicitly considered that the epoch of the beginning of the observation coincided with the onset of the renewal processes, additionally assumed to be all synchronized at $t = 0$. In this chapter, we still make the hypothesis, that the renewal processes start at the same time $t = 0$ for all nodes, but we now investigate the properties of the aggregated network, based on the observation of the link dynamics throughout the interval $[t_a, t_a + t]$. We obviously expect repercussions of the statistical aging effects at the individual level on the overall properties of the network.

5.2. Degree distribution of an aged PLAD0 network

5.2.1. Degree distribution of slightly aged networks

We expect different aging effects according to the relative importance of the aging time t_a and the observation time window t. For slightly aged networks, in which $1 \ll t_a \ll t$ ($1 \gg u \gg s$), Eq. (5.4) reduces to

$$h_c(u,s) \simeq \frac{1}{u} - \frac{s^\alpha}{u^{\alpha+1}}, \tag{5.6}$$

and Eq. (5.5) is expressed as [151]

$$\begin{aligned}
\chi_{u,s}(r|c) &\simeq \delta(r)\left(\frac{1}{us} - \frac{h_c(u,s)}{s}\right) + h_c(u,s)\chi_s(r|c) \\
&\simeq \delta(r)\frac{s^{\alpha-1}}{u^{\alpha+1}} + \frac{\chi_s(r|c)}{u} - c^\alpha \frac{(s/c)^\alpha \chi_s(r|c)}{u^{\alpha+1}} \\
&\simeq \delta(r)\frac{s^{\alpha-1}}{u^{\alpha+1}} + \frac{\chi_s(r|c)}{u} + \frac{c^\alpha}{u^{\alpha+1}}\frac{\partial \chi_s}{\partial r}
\end{aligned} \tag{5.7}$$

Then, by means of the Tauberian theorem n°2 we deduce

$$\chi_{t_a,t}(r|c) \simeq \frac{\delta(r)(t_a/t)^\alpha}{\Gamma_{1+\alpha}\Gamma_{1-\alpha}} + \chi_t + \frac{(c\,t_a)^\alpha}{\Gamma_{1+\alpha}}\frac{\partial \chi_t}{\partial r}, \tag{5.8}$$

where we write $\chi_t \equiv \chi_t(r|c)$ for brevity. Inserting this expression into Eq. (2.21) we obtain

$$\begin{aligned} P_{t_a,t}(k) &= \sum_c \eta(c) \int_0^\infty \left(\frac{(c\,t_a)^\alpha}{\Gamma_{1+\alpha}} \frac{\partial \chi_t}{\partial r} + \chi_t \right) g(k|r) dr \\ &+ \mathcal{P}(k, \langle r \rangle) \frac{(t_a/t)^\alpha}{\Gamma_{1+\alpha}\Gamma_{1-\alpha}} \end{aligned} \tag{5.9}$$

where $\mathcal{P}(k, \langle r \rangle)$ is a Poisson distribution centered at $\langle r \rangle$. Noticing that for $\langle r \rangle \gg 1$, the Poissonian propagator in Eq. (2.19) tends to a Gaussian distribution and is as such a quasi-symmetric function with respect to the axis $k = r + \langle r \rangle$, we write $g(k|r) \simeq g(k - r - \langle r \rangle)$. Moreover, the dependence of g on the aging time is fully included in the average number of activation $\langle r \rangle \equiv \langle r \rangle_{t_a,t}$, thus we can use the following relation between $g_0 = g_{0,t}$ and $g = g_{t_a,t}$:

$$g(k|r) \simeq g(k_a - r - \langle r \rangle_{0,t}) \simeq g_0(k_a|r), \tag{5.10}$$

where $k_a = k + \langle r \rangle_{0,t} - \langle r \rangle_{t_a,t}$. Moreover, the derivative of $g_0(k_a|r)$ with respect to r reads

$$\begin{aligned} \frac{\partial g_0}{\partial r}(k_a|r) &\simeq \frac{\partial}{\partial r}\left[e^{-r-\langle r \rangle} \frac{(r + \langle r \rangle)^k}{k!} \right] \\ &\simeq g_0(k_a - 1|r) - g_0(k_a|r) \end{aligned} \tag{5.11}$$

Inserting this result in Eq. (5.9), and integrating by parts, we obtain

$$\begin{aligned} P(k) &\simeq \frac{(ct_a)^\alpha}{\Gamma_{1+\alpha}} \Big[\chi_t(r|c) g_0(k_a|r) \Big]_0^\infty + P_0(k_a) + \frac{t_a^\alpha}{\Gamma_{1+\alpha}} \sum_c \eta(c) c^\alpha [P_0(k_a|c) - P_0(k_a - 1|c)] \\ &+ \mathcal{P}(k, \langle r \rangle) \frac{(t_a/t)^\alpha}{\Gamma_{1+\alpha}\Gamma_{1-\alpha}} \end{aligned} \tag{5.12}$$

where $P_0(k|c) = \sum_r \chi_t(r|c) g_0(k|r)$ is the non-aged degree distribution for a constant activity c. In this equation the bracket term $[\,\cdot\,]_0^\infty$ vanishes for $r = \infty$ and cancels out the poissonian term $\mathcal{P}(k, \langle r \rangle)$ for $r = 0$. Indeed, $g_0(k_a|0) = \mathcal{P}(k, \langle r \rangle)$ and $\chi_t(0|c) = \tilde{\psi}_c(t) \simeq \Gamma_{1-\alpha}^{-1}(ct)^{-\alpha}$. This gives, for a distribution $\eta(c)$ with a power-law form given by Eq. (2.58),

$$P(k) \simeq P_0(k_a) + \frac{\beta\,(c_0 t_a)^\alpha}{(\beta - \alpha)\Gamma_{1+\alpha}} [\widetilde{P}_0(\tilde{k}_a) - \widetilde{P}_0(\tilde{k}_a - 1)], \tag{5.13}$$

where we have defined $\widetilde{P}_0(k) = \sum_c \tilde{\eta}(c) \sum_r \chi_t(r|c)\tilde{g}_0(k|r)$ as the non-aged degree distribution with a modified activity distribution $\tilde{\eta}$ of parameter $\tilde{\beta} = \beta - \alpha$, and used the approximation $g(k|r) \simeq g_0(k_a|r) \simeq \tilde{g}_0(\tilde{k}_a|r)$ with $\tilde{k}_a = k + \langle r\rangle_{0,t}^{(\tilde{\eta})} - \langle r\rangle_{t_a,t}$, and $\langle r\rangle_{0,t}^{(\tilde{\eta})} = \sum_c \tilde{\eta}(c) \sum_r \chi_t(r|c)$. Thus, at large degree and leading order in t_a/t, the second term of the equation is negligible and the aged degree distribution is simply equal to the non-aged distribution P_0 evaluated at $k = k_a$

$$P_{t_a,t}(k) \sim (c_0 t)^{\beta}(k - \langle r\rangle_{t_a,t})^{-\gamma}. \tag{5.14}$$

Unsurprisingly, the degree distribution $P(k)$ of the slightly aged network exhibits the same scaling behavior as that of the non-aged one at large k, and we recover the expected expression for a vanishing t_a. Interestingly, in Eq.(5.13) the aged degree distribution is expressed with two non-aged distributions P_0 and $\widetilde{P}_0$, and the dependence on the aging time t_a is entirely embedded in the degree k_a and a scaling factor t_a^{α}. This allows for a direct evaluation of the aged distribution, whatever t_a, with the prior knowledge of P_0 and $\widetilde{P}_0$ only. In practice however, those two functions are evaluated via numerical simulations.

Fig. 5.2 checks the previous results by means of numerical simulations of the GAD model in the slightly aged regime. We numerically estimate the distributions P_0, $\widetilde{P}_0$ and P for a network of size $N = 10^7$, with three different sets of parameters (α, β, t_a, t). For each case we compare the aged degree distribution, the non-aged degree distribution and the degree distribution given by Eq. (5.13). One can see that Eq. (5.13) nicely predicts the aged degree distribution. Moreover, we observe a bump in the aged degree distribution for small degree values with respect to the non-aged distribution, more or less visible depending on the aging time t_a. The fact that more individuals have a smaller degree in the aged networks means that the dynamics in this case is slowed down with respect to the non-aged case. Panel (d) of Fig. 5.2 confirms that the exponent of the power law decay, $\gamma = 1 + \beta/\alpha$, predicted by Eq. (5.14), is correct.

5.2.2. Degree distribution of strongly aged networks

The strongly aged network regime emerges for $1 \ll t \ll t_a$ $(1 \gg s \gg u)$. In this limit, the forward waiting time distribution in the Laplace space can be approximated as

$$h_c(u, s) \simeq \frac{s^{\alpha-1}}{u^{\alpha}}, \tag{5.15}$$

and the aged activation distribution is given by

$$\begin{aligned} \chi_{u,s}(r|c) &\simeq \delta(r)\left(\frac{1}{us} - \frac{s^{\alpha-2}}{u^{\alpha}}\right) + c^{\alpha}\frac{(s/c)^{\alpha}\chi_s(r|c)}{s\,u^{\alpha}} \\ &\simeq \delta(r)\left(\frac{1}{us} - \frac{s^{\alpha-2}}{u^{\alpha}}\right) - \frac{c^{\alpha}}{u^{\alpha}\,s}\frac{\partial\chi_s}{\partial r} \end{aligned} \tag{5.16}$$

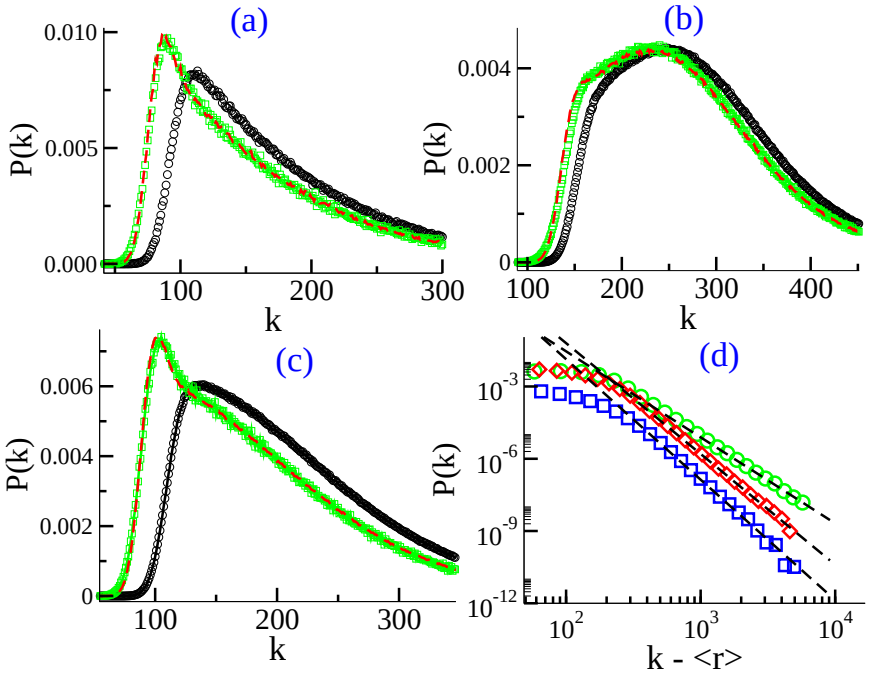

Figure 5.2.: Slightly aged degree distribution $P(k)$ for different values of α, β t_a and t. Plots (a), (b) and (c) show the non-aged distribution in black circles and the aged distribution in green squares. The behavior predicted by Eq. (5.13) (with P_0 and $\widetilde{P}_0$ previously calculated numerically) is plotted in red dashed line. Plot (d) shows the power law behavior at large k for the three aged distributions shown in the other plots: (a) squares, (b) circles, and (c) diamonds. Eq. (5.14) is plotted as a dashed line. Network size $N = 10^7$, results are averaged over 50 runs. The values of the parameters are the following. (a): $(\alpha, \beta) = (0.3, 1.2)$, $t = 10^6$ and $t_a = 10^3$. (b): $(\alpha, \beta) = (0.7, 1.8)$, $t = 500$ and $t_a = 10$. (c): $(\alpha, \beta) = (0.5, 1.8)$, $t = 5.10^3$ and $t_a = 100$.

Then, by means of the Tauberian theorem n°2, we obtain

$$\chi_{t_a,t}(r|c) \simeq \left(1 - \frac{(t/t_a)^{1-\alpha}}{\Gamma_\alpha \Gamma_{2-\alpha}}\right)\delta(r) - \frac{c^\alpha t_a^{\alpha-1}}{\Gamma_\alpha}\int_0^t \frac{\partial \chi_{t'}}{\partial r} dt'.$$

Using the same approximations as in the slightly aged case, we find, for $\eta(c)$ given by Eq. (2.58),

$$P(k) \simeq \mathcal{P}(k, \langle r \rangle) - \frac{\beta c_0^\alpha}{\tilde{\beta}\,\Gamma_\alpha t_a^{1-\alpha}} \int_0^t dt' [\widetilde{P}_{0,t'}(\tilde{k'}_a) - \widetilde{P}_{0,t'}(\tilde{k'}_a - 1)], \tag{5.17}$$

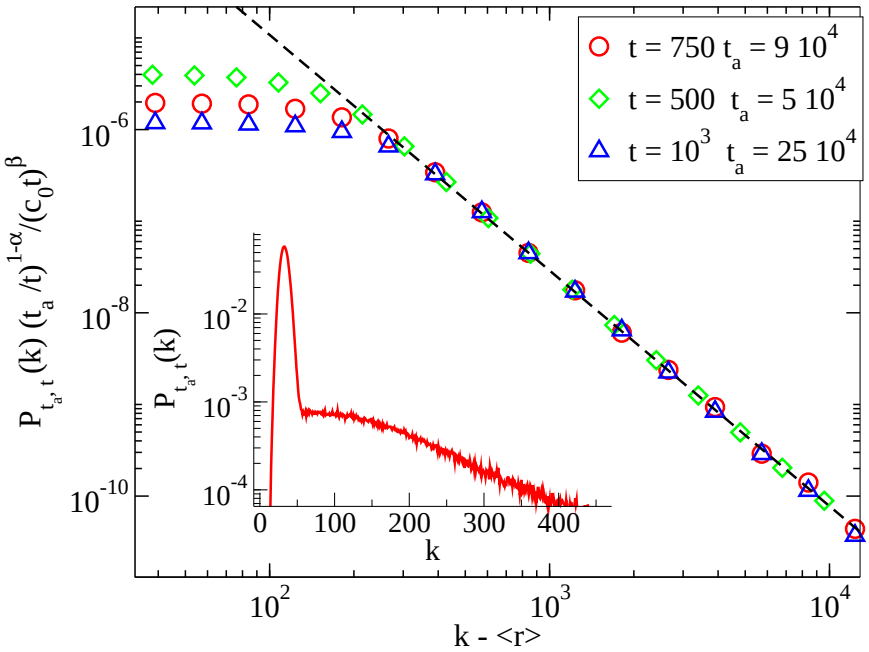

Figure 5.3.: Rescaled degree distribution $P_{t_a,t}(k)$ in case of strong aging. Different values of the time window t and the aging time t_a are shown. Inset: Poissonian behavior of the degree distribution $P(k)$ for small k with $t_a = 10^5$, $t = 500$. Network size $N = 10^7$. Parameters are set at $\alpha = 0.7$ and $\beta = 1.1$.

where $\tilde{k'}_a = k + \langle r \rangle_{0,t'}^{(\tilde{\eta})} - \langle r \rangle_{t_a,t}$. This expression shows the presence of a population splitting: A majority of individuals remain inactive over the whole observation time window t, while they still receive connections from the active part of the population. This leads to a dominant Poisson term in the degree distribution. Again, we find a power law behavior at large k, using the approximation $\widetilde{P}_{0,t'}(\tilde{k'}_a) - \widetilde{P}_{0,t'}(\tilde{k'}_a - 1) \sim (c_0 t')^{\tilde{\beta}}(k - \langle r \rangle)^{-\tilde{\gamma}-1}$

$$P_{t_a,t}(k) \sim (c_0 t)^{\beta}(t/t_a)^{1-\alpha}(k - \langle r \rangle)^{-\gamma} \tag{5.18}$$

but this time the tail of the distribution vanishes when t_a tends to infinity. Fig. 5.3 shows the validity of the scaling with the aging time t_a predicted by Eq. (5.18) and the Poissonian term highlighted in Eq. (5.17).

5.3. Temporal percolation of aged networks

Here we consider the effects of aging on the percolation threshold. We can prove that the criterion Eq. (3.11) is valid also in presence of aging. Indeed, no particular hypothesis on the distribution of the activation number $\chi(r|c)$ is

required to derive the topological properties of the integrated-network, and in particular the addition of a dependency on the aging time t_a does not affect the reasoning made in section 2.2 to perform a mapping of the model to a hidden variable network. In the slightly aged regime, no expansions may be used for the first and second moment of the activation number distribution. The threshold is thus evaluated by a numerical resolution of the criterion just as for the non-aged case, and we do not present it here. Most interestingly however, one can determine the asymptotic behaviour of the percolation threshold T_p as a function of the aging time t_a, in the limit of strong aging, as follows. Since the main effect of aging is to delay the growth of the integrated network, we expect the same consequences for the birth of the giant component. Therefore, T_p must be an increasing function of t_a. Three different asymptotic behaviours are to be considered when t_a tends to infinity: T_p/t_a either tends to 0, to a positive constant, or it diverges. It is straightforward to discard the latter, since in this case one would have $\langle r\rangle_{t_a,T_p} \simeq \langle r\rangle_{0,T_p} \gg 1$, which is contradictory with the condition $\langle r\rangle_{T_p} < 1$. Thus, one can look for a solution satisfying $T_p/t_a \to 0$ for $t_a \to \infty$, and if a solution is found, then it is the correct one, since it is a lower bound for any other. Using the expansions for the strong aging regime proposed in [151], for $t_a \gg T_p \gg 1$ one has

$$\langle r^n\rangle_{t_a,T_p} \simeq \frac{\Gamma_{n+1}}{\Gamma_\alpha \Gamma_{\alpha n+2-\alpha}} \langle c^{\alpha n}\rangle \, t_a^{\alpha-1} \, T_p^{1-\alpha+\alpha n}. \tag{5.19}$$

By inserting the moments of r in Eq. (3.11), one finds

$$T_p \simeq A(\alpha,\beta) \; t_a^{\frac{1-\alpha}{1+\alpha}}, \tag{5.20}$$

where $A(\alpha,\beta) = [\Gamma_\alpha \Gamma_{2+\alpha}/2\langle c^{2\alpha}\rangle]^{\frac{1}{1+\alpha}}$.

Fig. 5.4 shows the percolation time T_p evaluated from Eq. (3.11), using a dichotomic search strategy, as a function of the aging time t_a, and computed from direct numerical simulations using the susceptibility peak, for a GAD network with $\beta = 1.5$ and different values of α. One can observe that aging has practically no effect on the percolation time T_p for t_a smaller than the percolation threshold with no aging. On the contrary, for $t_a \gg T_p \gg 1$, the asymptotic behavior of T_p as a function of t_a is very well predicted by Eq. (5.20).

5.4. Poissonization of an aged network

5.4.1. Finite average waiting time

As discussed in section 5.1, a renewal process with finite average waiting time τ behaves quasi deterministically at large times, i.e. $\overline{r}(t) \simeq t/\tau$ for $t \gg \tau$. This straightforwardly implies that on average, the number of renewals $r_a(t_a,t)$

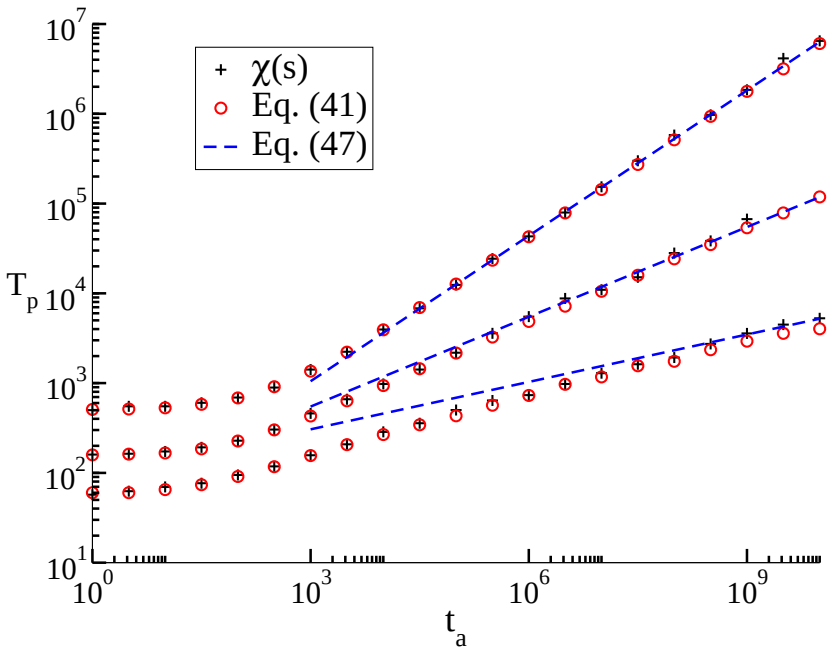

Figure 5.4.: Percolation threshold T_p as a function of the aging time t_a. Parameters are set to $\beta = 1.5$, $c_0 = 0.001$, $c_{max} = 1$ and $\alpha = 0.3, 0.5, 0.7$ from top to bottom. Circles represent T_p evaluated numerically from (3.11). Crosses are an estimation of T_p as given by the peak of the susceptibility. The asymptotic behavior predicted by (5.20) is plotted in dashed line. Network size $N = 10^6$.

counted between t_a and $t_a + t$ for a process starting at $t = 0$ is independent of t_a for $t_a \gg \tau$ and is equal to $r_a(t_a, t) = r(t_a + t) - r(t_a) \simeq t/\tau$. In other words, there are no aging effects at large times, because the dynamics becomes stationary. This allows to define the so-called equilibrium process, which simply corresponds to a renewal process having started infinitely far in the past. In particular, the forward recurrence time no longer depends on the aging time t_a, and one has [108]

$$h(t_a = \infty, t) = h(t) = \frac{1}{\tau} \int_t^{+\infty} \psi(u) du \tag{5.21}$$

However, while the average number of counted events of such an equilibrium process grows linearly with the time of observation, the second moment $\overline{r^2}(t)$ of the distribution of renewals is still non-trivial at short times for a general process ψ, i.e. it is neither deterministic nor Poissonian. Thus if we simultaneously observe a non-aged network between 0 and T and the corresponding equilibrium network over a time window of length T (independently of the starting point because the dynamics is stationary), the dynamics at small times are different, but at large times $\overline{r^n}_{eq}(t) \simeq \overline{r^n}(t) \simeq (t/\tau)^n$. In particular, their percolation

thresholds are distinct, as well as the thresholds estimated via the reshuffling poissonization method presented in chapter 4. However in the large T limit the poissonized thresholds coincide: $(T_p^{eq})^{AD} = T_p^{AD} \simeq 1/(\langle 1/\tau \rangle + \langle 1/\tau^2 \rangle)$.

5.4.2. Infinite average waiting time

When the waiting time distribution lacks a first moment, we saw that strong aging effects are at play. We consider here the poissonization of a strongly aged network with a power-law waiting time distribution of the form $\psi(t) \sim t^{-1-\alpha}$ with $0 < \alpha < 1$, the possible heterogeneity of the agents having no relevant impact on what follows. The observation is made throughout a time window $[t_a, t_a + T]$, so that we have to distinguish between two cases, i.e. $1 \ll T \ll t_a$ and $1 \ll t_a \ll T$. In the limit $T \gg t_a$, the aging effects are not relevant any more, and the poissonized percolation threshold is the same as that obtained for the non-aged network $T_p^{AD} \sim T^{1-\alpha}$. For $1 \ll T \ll t_a$ on the other hand, we may use the approximation of Eq. (5.19), which combined with Eq. (4.13) gives, at dominant order in t_a/T

$$T_p^{AD} \simeq \frac{T}{\langle r^2 \rangle^{\frac{1}{2}}} \sim (T\, t_a)^{\frac{1-\alpha}{2}} \tag{5.22}$$

From which we deduce, with Eq. (5.20)

$$\frac{T_p^{AD}}{T_p} \sim t_a^{\frac{-(1-\alpha)^2}{2(1+\alpha)}}\, T^{\frac{1-\alpha}{2}} \tag{5.23}$$

This ratio is thus a growing function of T, but more insight is given if we fix a relation $T(t_a)$ and analyse the behaviour of the ratio as a function of t_a. For T proportional to the real threshold T_p given by Eq. (5.20) we obtain that $T_p^{AD} \sim T_p$, the error is in this case independent of t_a. If we alternatively impose an observation time T proportional to t_a, we have

$$T_p^{AD} \sim t_a^{\frac{\alpha(1-\alpha)}{1+\alpha}} \tag{5.24}$$

which means that the poissonized threshold highly overestimates the real threshold in this case. We conclude that for a network with infinite average waiting times, the estimation of the percolation threshold using a poissonization procedure is dramatically erroneous, whether the network is aged or not.

5.5. Conclusion

In this chapter, we analysed a renewal process for which the average holding time between consecutive events is infinite. Such a process is subject to a non-trivial phenomenon called aging: the statistics of the number of events counted within a finite time window strongly depends on the specific instant at which the observation starts. The most striking aging effect is an increasing probability to count zero event during the observation. Simultaneously, the distribution of the non-zero number of renewals is also modified. Being structured upon parallel renewal processes of the agents, the generalized activity driven model developed in this thesis is obviously subject to aging effects. Distinguishing between the strongly aged and the slightly aged regime, we provide effective expressions of the degree distribution of the time-integrated aged PLAD0 network, as a function of the corresponding non-aged degree distribution, i.e. integrated throughout a time window of same length t. In the slightly aged regime, the aging implies the birth of a small bump on the distribution at small degrees, and only brings higher order corrections in t_a/t to the tail of the distribution. In the strongly aged case however, the distribution is essentially Poissonian due to a majority of agents staying inactive throughout the time interval of observation, and still exhibit a vanishing power-law tail. Our expressions are successfully confronted to numerical analysis in both cases. Furthermore, we investigated the percolation of an aged time-integrated GAD0 network. The general criterion derived in chapter 3 giving implicitly the threshold T_p is still valid for aged networks. Because the aging essentially acts as a slowdown of the dynamics, the percolation threshold is an increasing function of the aging time t_a. This allows us to derive analytical expressions of the threshold in the strongly aged regime, using accurate approximations of the first and second moment of the distribution of the activation number $\langle r \rangle$ and $\langle r^2 \rangle$. The resulting expression is confirmed by numerical analysis on Fig. 5.4. Finally, we discuss the poissonization procedure presented in the previous chapter in the presence of aging. In the strongly aged regime, the poissonization of a PLAD0 network with finite average waiting times leads to an incorrect, although finite, error in the evaluation of the real percolation time. For a PLAD0 network with infinite average waiting times on the other hand, the poissonization leads to a diverging estimation of the threshold when the procedure is applied at very large T. The main picture of the poissonization method thus remains the same as in the non-aged case, and assuming a Poissonian dynamics to explain a given time-integrated network structure may lead to a dramatic error in the evaluation of the real percolation threshold of the network. To sum up, aging effects are inherent to the generalized activity driven model we developed, and affect in particular the structural and connectivity properties of the corresponding time-aggregated network.

The aging phenomenon points out the crucial importance of the starting time of a renewal process. This naturally leads to question the strong assumption

we made about the synchronization of all the individual renewal processes in the network. Indeed, a more realistic hypothesis would be to define a different aging time for all agents, describing more faithfully the real-life scenario in which new people regularly enter the network. However such an assumption renders the model dramatically more complex, and does not allow for mathematical tractability. Nevertheless, we may argue that a desynchronized network, i.e. with heterogeneous aging times, is equivalent in the strongly aged regime to our synchronized GAD model. Indeed, if we suppose that the individual process of agent i starts at $t_{0,i}$ and that the observation of the dynamics starts at a time T_a much larger than the largest starting time $t_{0,max}$ among the agents, then for each agent the time elapsed since the beginning of the process is $t_{a,i} = T_a - t_{0,i}$ which is equal in a first approximation to T_a. In conclusion, one of the main assets of the GAD model is that it allows to transparently observe the aging effects introduced by arbitrary waiting time distributions, and is thus a suitable null model for the detection of statistical aging effects, as opposed to a possible physical aging effects of the agents [111, 184].

6. Epidemic spreading with risk perception

6.1. Introduction

The propagation patterns of an infectious disease depend on many factors, including the number and properties of the different stages of the disease, the transmission and recovery mechanisms and rates, and the hosts' behavior (e.g., their contacts and mobility) [4, 90]. Given the inherent complexity of a microscopic description taking into account all details, simple models are typically used as basic mathematical frameworks aiming at capturing the main characteristics of the epidemic spreading process and in particular at understanding if and how strategies such as quarantine or immunization can help contain it. Such models have been developed with increasing levels of sophistication and detail in the description of both the disease evolution and the behaviour of the host population [4, 90].

Obviously, the diffusion of the disease in the host population depends crucially on the patterns of contacts between hosts. The simplest homogeneous mixing assumption, which makes many analytical results achievable, considers that individuals are identical and that each has a uniform probability of being in contact with any other individual [4, 90]. Even within this crude approximation, it is possible to highlight fundamental aspects of epidemic spreading, such as the epidemic threshold, signaling a non-equilibrium phase transition that separates an epidemic-free phase from a phase in which a finite fraction of the population is affected [90]. However, this approach neglects any non-trivial structure of the contacts, while advances in network science [125] have shown that many networks of interest have in common important features such as a strong heterogeneity in the number of connections, a large number of triads, community structures, and a low average shortest path length between individuals [24]. Spreading models have thus been adapted to complex networks, unveiling the important role of these properties [17, 131, 133]. More recently, a number of studies have also considered spreading processes on time-varying networks [72, 74, 85, 104, 166, 174], to take into account the fact that contact networks evolve on various timescales and present non-trivial temporal properties such as broad distribution of contact durations [16, 35] and burstiness [11, 74] (i.e., the

timeline of social interactions of a given individual exhibits periods of time with intense activity separated by long quiescent periods with no interactions).

All these modeling approaches consider that the propagation of the disease takes place on a substrate (the contacts between individuals) that does not depend on the disease itself. In this framework, standard containment measures consist in the immunization of individuals, in order to effectively remove them from the population and thus break propagation paths. Immunization can also (in models) be performed in a targeted way, trying to identify the most important (class of) spreaders and to suppress propagation in the most efficient possible way [37, 134]. An important point to consider however is that the structure and properties of contacts themselves can in fact be affected by the presence of the disease in the population, as individuals aware of the disease can modify their behaviour spontaneously, adopting self-protecting measures such as vaccination or mask-wearing. A number of studies have considered this issue along several directions (see Ref. [55] for a review). For instance, some works consider an adaptive evolution of the network [65] with probabilistic redirection of links between susceptible and infectious individuals, to mimic the fact that a susceptible individual might be aware of the infectious state of some of his/her neighbors, and therefore try to avoid contact with them. Such models can lead to a rich phenomenology, with first order transitions, oscillations and hysteresis phenomena. Other works introduce behavioral classes in the population, depending on the awareness to the disease [135], possibly consider that the awareness of the disease propagates on a different (static) network than the disease itself, and that being aware of the disease implies a certain level of immunity to it [64, 106]. The epidemic threshold depends then on the topology of the network on which the awareness propagates.

Alternatively, other works explore scenarios where an individual takes self-protecting measures that decrease his/her probability to be infected (such as wearing a mask or washing hands more frequently): this probability can then depend on the fraction of infectious individuals present in the whole population or among the neighbors of an individual. Different model definitions can lead to contrasting results. For instance, reducing the probability of being infected according to the instantaneous fraction of infected neighbors of an individual leads to a notable increase of the epidemic threshold and a decay of the prevalence [9]. On the other hand, in [27], the epidemic threshold stays unchanged when the infection probability is reduced according to a local epidemic incidence obtained by memorizing the past contacts with other infectious neighbors, although the prevalence is also significantly reduced in this case. Both these studies consider diseases propagating on static contact networks and local awareness effects. In contrast, refs. [94, 145] investigate the case of a temporal network in which awareness has the very strong and global effect of reducing uniformly the activity of all individuals and their numbers of contacts, either because they are infectious or because of a global knowledge of the overall incidence of the dis-

ease. Under those assumptions of a global, non-local awareness effect, both the epidemic threshold and the disease prevalence are notably affected.

Here, we consider instead the following scenario: First, individuals are connected by a time-varying network of contacts, which is more realistic than a static one; second, we use the scenario of a relatively mild disease, which does not disrupt the patterns of contacts but which leads susceptible individuals who witness the disease in other individuals to take precautionary measures. We do not assume any knowledge of the overall incidence, which is usually very difficult to know in a real epidemic, especially in real time. We consider standard models of infectious diseases and both empirical and synthetic temporal networks of contacts. We extend the concept of awareness with respect to the state of neighbors from static to temporal networks and perform extensive numerical simulations to uncover the change in the phase diagram (epidemic threshold and fraction of individuals affected by the disease) as the parameters describing the reaction of the individuals are varied.

6.2. Modelling epidemic spread in temporal networks

6.2.1. Epidemic models and epidemic threshold

We consider the paradigmatic Susceptible-Infectious-Susceptible (SIS) and Susceptible-Infectious-Recovered (SIR) models to describe the spread of a disease in a fixed population of N individuals. In the SIS model, each individual belongs to one of the following compartments: healthy and susceptible (S) or diseased and infectious (I). A susceptible individual in contact with an infectious becomes infectious at a given constant rate, while each infectious recovers from infection at another constant rate. In the SIR case, infectious individuals enter the recovered (R) compartment and cannot become infectious anymore. We consider a discrete time modeling approach, in which the contacts between individuals are given by a temporal network encoded in a time-dependent adjacency matrix $a_{ij}(t)$ taking value 1 if individuals i and j are in contact at time t, and 0 otherwise. At each time step, the probability that a susceptible individual i becomes infectious is thus given by $p_i = 1 - \prod_j [1 - \lambda\, a_{ij}(t)\, \sigma_j]$, where λ is the infection probability, and σ_j is the state of node j ($\sigma_j = 1$ if node j is infectious and 0 otherwise). We define μ as the probability that an infectious individual recovers during a time step, and we impose $\mu \ll 1$ to ensure the equivalence between the discrete time approach and a continuous-time Markov chain analysis [52]. The competition between the transmission and recovery mechanisms determines the epidemic threshold. Indeed, if λ is not large enough to compensate the recovery process (λ/μ smaller than a critical value), the epidemic outbreak will not affect a finite portion of the population, dying out rapidly. On the other hand, if λ/μ is large enough, the

spread can lead in the SIS model to a non-equilibrium stationary state, which we determine with an average over surviving runs, and in which a finite fraction of the population is in the infectious state. For the SIR model, on the other hand, the epidemic threshold is determined by the fact that the fraction $r_\infty = R_\infty/N$ of individuals in the recovered state at the end of the spread becomes finite for λ/μ larger than the threshold.

In order to numerically determine the epidemic threshold of the SIS model, we adapt the method proposed in Refs. [21, 110], which consists in measuring the lifetime and the coverage of realizations of spreading events, where the coverage is defined as the fraction of distinct nodes ever infected during the realization. Below the epidemic threshold, realizations have a finite lifetime and the coverage goes to 0 in the thermodynamic limit. Above threshold, the system in the thermodynamic limit has a finite probability to reach an endemic stationary state, with infinite lifetime and coverage going to 1, while realizations that do not reach the stationary state have a finite lifetime. The threshold is therefore found as the value of λ/μ where the average lifetime of non-endemic realizations diverges. For finite systems, one can operationally define an arbitrary maximum coverage $C > 0$ (for instance $C = 0.5$) above which a realization is considered endemic, and look for the peak in the average lifetime of non-endemic realizations as a function of λ/μ.

In the SIR model the lifetime of any realization is finite. We thus evaluate the threshold as the location of the peak of the relative variance of the fraction r_∞ of recovered individuals at the end of the process [33], i.e.,

$$\sigma_r = \frac{\sqrt{\langle r_\infty^2 \rangle - \langle r_\infty \rangle^2}}{r_\infty}. \tag{6.1}$$

6.2.2. Modeling risk perception

To model risk perception, we consider the approach proposed in Ref. [9] for static interaction networks. In this framework, each individual i is assumed to be aware of the fraction of his/her neighbors who are infectious at each time step. This awareness leads the individual to take precautionary measures that decrease its probability to become infectious upon contact. This decrease is modeled by a reduction of the transmission probability by an exponential factor: at each time step, the probability of a susceptible node i in contact with an infectious to become infectious depends on the neighborhood of i and is given by $\lambda_i(t) = \lambda_0 \exp(-J n_i(t)/k_i)$ where k_i is the number of neighbors of i, $n_i(t)$ the number of these neighbors that are in the infectious state at time t, and J is a parameter tuning the degree of awareness or amount of precautionary measures taken by individuals.

Static networks of interactions are however only a first approximation and real networks of contacts between individuals evolve on multiple timescales [16]. We

therefore consider in the present work, more realistically, that the set of neighbors of each individual i changes over time. We need thus to extend the previous concept of neighborhood awareness to take into account the history of the contacts of each individual and his/her previous encounters with infectious individuals. We consider that longer contacts with infectious individuals should have a stronger influence on a susceptible individual's awareness, and that the overall effect on any individual depends on the ratio of the time spent in contact with infectious to the total time spent in contact with other individuals. Indeed, two individuals spending a given amount of time in contact with infectious individuals may react differently depending on whether these contacts represent a large fraction of their total number of contacts or not. We moreover argue that the awareness is influenced only by recent contacts, as having encountered ill individuals in a distant past is less susceptible to lead to a change of behaviour. To model this point in a simple way, we consider that each individual has a finite memory of length ΔT and that only contacts taking place in the time window $[t - \Delta T, t[$, in which the present time t is excluded, are relevant.

We thus propose the following risk awareness change of behaviour: The probability for a susceptible individual i, in contact at time t with an infectious one, to become infectious, is given by

$$\lambda_i(t) = \lambda_0 \exp\left(-\alpha\, n_I(i)_{\Delta T}\right) \tag{6.2}$$

where $n_I(i)_{\Delta T}$ is the number of contacts with infectious individuals seen by the susceptible during the interval $[t - \Delta T, t[$, divided by the total number of contacts counted by the individual during the same time window (repeated contacts between the same individuals are also counted). α is a parameter gauging the strength of the awareness, and the case $\alpha = 0$ corresponds to the pure SIS process, in which $\lambda_i(t) = \lambda_0$ for all individuals and at all times.

6.3. Epidemic spreading on synthetic networks

6.3.1. SIS dynamics

6.3.1.1. Analytical approach

On a synthetic Activity Driven temporal network as defined in subsection 1.4.1, an infectious individual can propagate the disease only when he/she is in contact with a susceptible. As a result, the spreading results from an interplay between the recovery time scale $1/\mu$, the propagation probability λ conditioned on the existence of a contact and the multiple time scales of the network as emerging from the distribution of nodes' activity $F(a)$. Analogously to what is done for heterogeneous static networks [17, 131], it is possible to describe the spread at a mean-field level by grouping nodes in activity classes: all nodes with the same

activity a are in this approximation considered equivalent [136]. The resulting equation for the evolution of the number of infectious nodes in the class of nodes with activity a in the original AD model has been derived in Ref. [136] and reads

$$I_a^{t+1} = I_a^t - \mu\, I_a^t + \lambda\, a\, S_a^t \int \frac{I_{a'}^t}{N}\, da' + \lambda\, S_a^t \int \frac{I_{a'}^t\, a'}{N}\, da' \,. \tag{6.3}$$

where I_a and S_a are the number of infectious and susceptible nodes with activity a, verifying $N_a = S_a + I_a$.

From this equation one can show, by means of a linear stability analysis, that there is an endemic non-zero steady state if and only if $(\langle a\rangle + \sqrt{\langle a^2\rangle})\lambda/\mu > 1$ [136]. Noticing that $\langle a\rangle + \sqrt{\langle a^2\rangle}$ may be regarded as the highest statistically significant activity rate, the interpretation of this equation becomes clear: the epidemic can propagate to the whole network when the smallest time scale of relevance for the infection process is smaller than the time scale of recovery.

Let us now consider the introduction of risk awareness in the SIS dynamics on AD networks. In general, we can write for a susceptible with activity a

$$n_I(a)_{\Delta T} = \frac{\sum_{i=1}^{\Delta T}\left(a \int \frac{I_{a'}^{t-i}}{N}\, da' + \int \frac{I_{a'}^{t-i}\, a'}{N}\, da'\right)}{(a + \langle a\rangle)\, \Delta T} \,, \tag{6.4}$$

where the denominator accounts for the average number of contacts of an individual with activity a in ΔT time steps. In the steady state, where the quantities I_a become independent of t, the dependence on ΔT in Eq. (6.4) vanishes, since both the average time in contact with infectious individuals and the average total time in contact are proportional to the time window width. Introducing this expression into Eq. (6.2), we obtain

$$\lambda_a = \lambda_0 \exp\left(-\alpha\, \frac{a \int \frac{I_{a'}}{N}\, da' + \int \frac{I_{a'}\, a'}{N}\, da'}{a + \langle a\rangle}\right) , \tag{6.5}$$

which can be inserted into Eq. (6.3). Setting $\mu = 1$ without loss of generality, we obtain the steady state solution

$$\rho_a = \frac{\lambda_a(a\rho + \theta)}{1 + \lambda_a(a\rho + \theta)}, \tag{6.6}$$

where $\rho_a = I_a/N_a$ and we have defined

$$\rho = \sum_a F(a)\rho_a, \tag{6.7}$$

$$\theta = \sum_a a\, F(a)\rho_a. \tag{6.8}$$

Introducing Eqs. (6.5) and (6.6) into Eqs. (6.7) and (6.8), and expanding at second order in ρ and θ, we obtain (see appendix section C for details) the epidemic threshold

$$\lambda_c = \frac{1}{\langle a\rangle + \sqrt{\langle a^2\rangle}}. \tag{6.9}$$

Moreover, setting $\lambda_0 = \lambda_c(1+\epsilon)$ and expanding at order 1 in ϵ we obtain

$$\rho = \frac{2\epsilon}{A\alpha + B}, \tag{6.10}$$

where

$$A = \lambda_c \left\langle \frac{\frac{a^3}{\sqrt{\langle a^2\rangle}} + 3a\sqrt{\langle a^2\rangle} + \langle a^2\rangle + 3a^2}{a + \langle a\rangle} \right\rangle \tag{6.11}$$

$$B = \lambda_c^2 \left(\frac{\langle a^3\rangle}{\sqrt{\langle a^2\rangle}} + 3\langle a\rangle\sqrt{\langle a^2\rangle} + 4\langle a^2\rangle \right).$$

This indicates that, at the mean-field level, the epidemic threshold is not affected by the awareness. Nevertheless, the density of infectious individuals in the vicinity of the threshold is reduced as the awareness strength α grows.

In the case of activity driven networks with memory (ADM), no analytical approach is available for the SIS dynamics, even in the absence of awareness. The numerical investigation carried out in Ref. [170] has shown that the memory mechanism, which leads to the repetition of some contacts, reinforcing some links and yielding a broad distribution of weights, has a strong effect in the SIS model. Indeed, the repeating links help the reinfection of nodes that have already spread the disease and make the system more vulnerable to epidemics. As a result, the epidemic threshold is reduced with respect to the memory-less (AD) case. For the SIS dynamics with awareness on ADM networks, we will now resort to numerical simulations.

6.3.1.2. Numerical simulations

In order to inspect in details the effect of risk awareness on the SIS epidemic process, we perform extensive numerical simulations. Following Refs. [136, 170], we consider a distribution of nodes' activities of the form $F(a) \propto a^{-\gamma}$ for $a \in [\epsilon, 1]$,

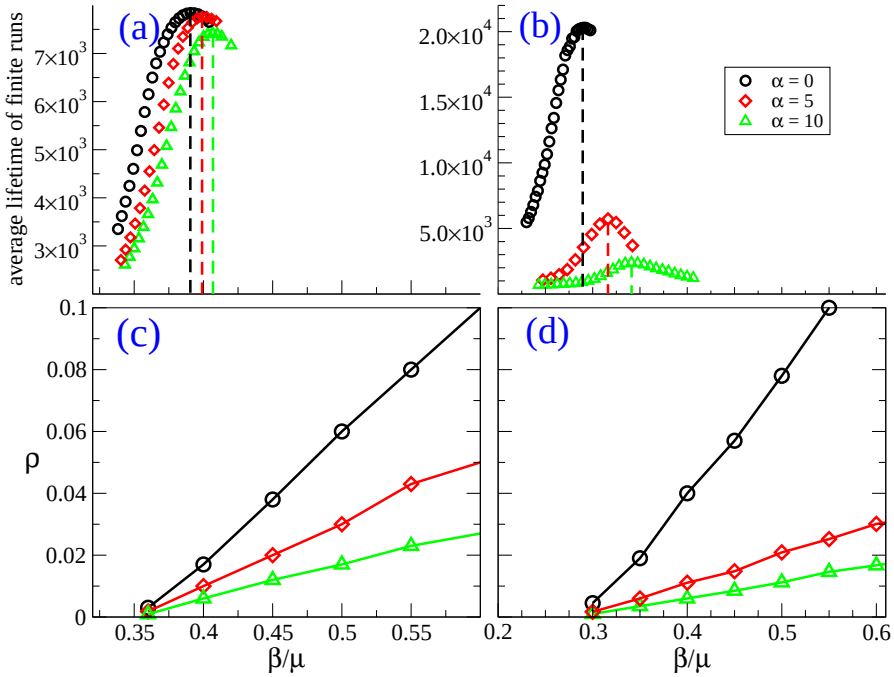

Figure 6.1.: Effect of the strength of risk awareness on the SIS spreading on AD and ADM networks with $\Delta T = \infty$. (a): average lifetime of non-endemic runs for AD network, (b): average lifetime of non-endemic runs for ADM networks, (c): Steady state fraction of infectious for AD, (d): Steady state fraction of infectious for ADM. Vertical lines in subplots (a) and (b) indicate the position of the maximum of the average lifetime. Model parameters: $\mu = 0.015$, $\gamma = 2$, $\epsilon = 10^{-3}$, $\Delta T = \infty$ and network size $N = 10^5$. Results are averaged over 1000 realizations.

where ϵ is a lower activity cut-off introduced to avoid divergences at small activity values. In all simulations we set $\epsilon = 10^{-3}$ and $\gamma = 2$. We consider networks up to a size $N = 10^5$ and a SIS process starting with a fraction $I_0/N = 0.01$ of infectious nodes chosen at random in the population. In order to take into account the connectivity of the instantaneous networks, we use as a control parameter the quantity β/μ, where $\beta = 2\langle a\rangle\lambda_0$ is the per capita rate of infection [136]. Notice that the average degree of an instantaneous network is $\langle k\rangle_t = 2\langle a\rangle$ [161]. With this definition, the critical endemic phase corresponds to

$$\frac{\beta}{\mu} \geq \frac{2\langle a\rangle}{\langle a\rangle + \sqrt{\langle a^2\rangle}}. \tag{6.12}$$

In Fig. 6.1 we first explore the effect of the strength of risk awareness, as measured by the parameter α, in the case $\Delta T = \infty$, i.e., when each agent is

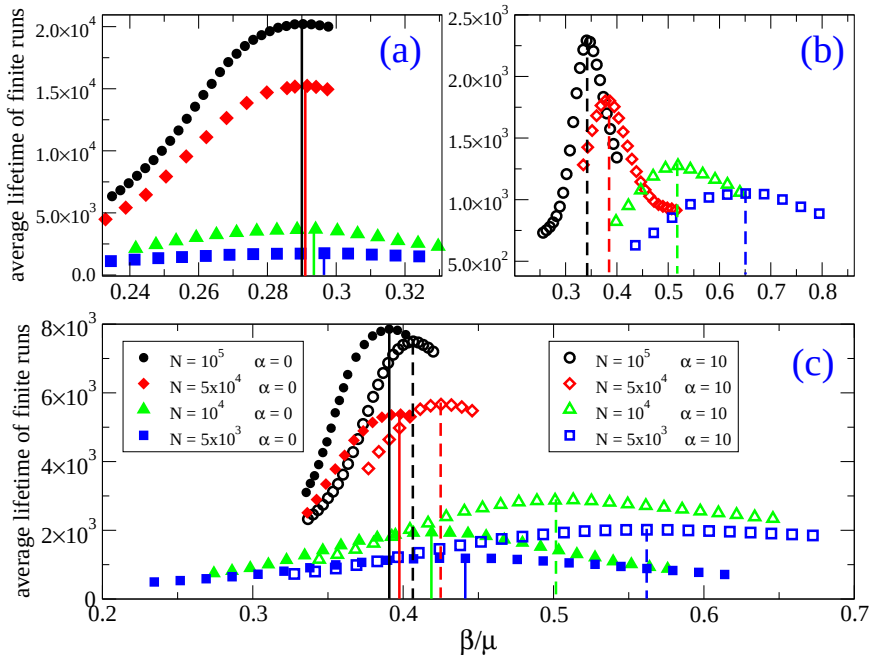

Figure 6.2.: Analysis of finite-size effects. We plot the average lifetime of non-endemic realizations of the SIS process, for different system sizes and 2 different values of α. (a): ADM networks and $\alpha = 0$. (b): ADM networks with $\alpha = 10$. (c): AD networks. Vertical lines indicate the position of the maximum of the average lifetime. Model parameters: $\mu = 0.015$, $\gamma = 2$, $\epsilon = 10^{-3}$ and $\Delta T = \infty$. Results are averaged over 1000 realizations.

influenced by the whole history of his/her past contacts, a situation in which awareness effects should be maximal. We plot the steady state average fraction of infectious nodes $\rho = \sum_a \rho_a F(a)$ as a function of β/μ for three different values of α, and evaluate the position of the effective epidemic threshold, as measured by the peak of the average lifetime of non-endemic realizations, see subsection 6.2.1. Figures 6.1c) and d) indicate that the effect of awareness in the model ($\alpha > 0$), with respect to the pure SIS model ($\alpha = 0$) is to reduce the fraction ρ of infectious individuals for all values of β/μ, and Figures 6.1a) and b) seem to indicate in addition a shift of the effective epidemic threshold to larger values. This effect is more pronounced for the ADM than for the AD networks. As this shift of the epidemic threshold is in contradiction, at least for the AD case, with the mean-field analysis of the previous paragraphs, we investigate this issue in more details in Fig. 6.2, where we show, both for the pure SIS model ($\alpha = 0$) and for a positive value of α, the average lifetime of non-endemic realizations for various system sizes. Strong finite-size effects are observed, especially for the model with awareness ($\alpha > 0$).

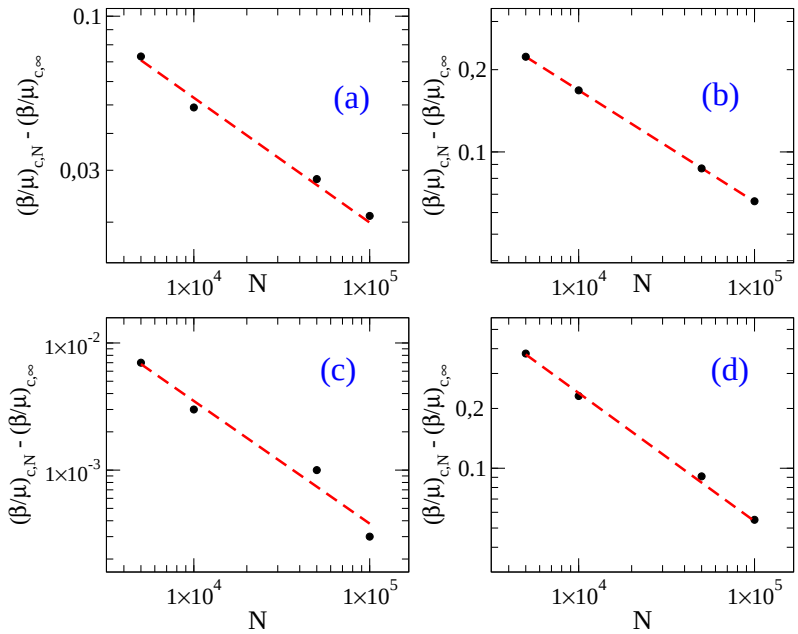

Figure 6.3.: Finite-size scaling of the epidemic threshold of the SIS process for (a): pure AD network, (b): AD network with $\alpha = 10$, (c): ADM with $\alpha = 0$ and (d): ADM with $\alpha = 10$.

In Fig. 6.3, we plot the fitting of the values of the effective threshold $(\beta/\mu)_c$ (the position of the lifetime peak) with a law of the form $(\beta/\mu)_{c,N} = (\beta/\mu)_{c,\infty} + A\,N^{-\nu}$, typical of finite-size scaling analysis [28]. In the thermodynamic limit of $(\beta/\mu)_{c,\infty} = 0.37(3)$ for the pure SIS model on AD networks, $(\beta/\mu)_{c,\infty} = 0.34(2)$ for AD with $\alpha = 10$ (SIS model with awareness), $(\beta/\mu)_{c,\infty} = 0.29(3)$ for ADM with $\alpha = 0$ (pure SIS model) and $(\beta/\mu)_{c,\infty} = 0.29(2)$ for ADM with $\alpha = 10$. We notice here that the extrapolations for $\alpha = 0$ are less accurate and thus with larger associated errors. Nevertheless, with the evidence at hand, we can conclude that, within error bars, the risk perception has no effect on the epidemic threshold in the thermodynamic limit, in agreement with the result from Eq. (6.12), that gives a theoretical threshold $(\beta/\mu)_c = 0.366$ for the AD case. It is however noteworthy that the effective epidemic threshold measured in finite systems can be quite strongly affected by the awareness mechanism, even for quite large systems, and in a particularly dramatic way for ADM networks.

We finally explore in Fig. 6.4 the effect of a varying memory length ΔT, at fixed risk awareness strength α. In both AD and ADM networks, an increasing awareness temporal window shifts the effective epidemic threshold towards larger values, up to a maximum given by $\Delta T = \infty$, when the whole system history is available. For the ADM networks, this effect is less clear because of the changing height of the maximum of the lifespan when increasing ΔT. For

AD networks, this result is apparently at odds with the mean-field analysis in which ΔT is irrelevant in the stationary state. We should notice, however, that for $\Delta T \to \infty$, the critical point is unchanged in the thermodynamic limit with respect to the pure SIS dynamics. Given that for $\Delta T \to \infty$ the effects of awareness are the strongest, we expect that a finite ΔT will not be able to change the threshold in the infinite network limit. We can thus attribute the shifts observed to pure finite size effects. Note that this effect is also seen in homogeneous AD networks with uniform activity a (data not shown), observation that we can explain as follows: when ΔT is small, the ratio of contacts with infectious $n_I(i)_{\Delta T}$ recorded by an individual i can differ significantly from the overall ratio recorded in the whole network in the same time window, which is equal to $\langle n_I(i)_{\Delta T} \rangle = \rho$ (for a uniform activity). Mathematically, we have

$$\langle \lambda_i \rangle = \lambda_0 \, \langle \exp(-\alpha \, n_I(i)_{\Delta T}) \rangle \geq \lambda_0 \, \exp(-\alpha \, \rho) \tag{6.13}$$

by concavity of the exponential function. Thus, even if locally and temporarily some individuals perceive an overestimated prevalence of the epidemics and reduce their probability of being infected accordingly, on average the reduction in the transmission rate would be larger if the ensemble average were used instead of the temporal one, and thus the epidemics is better contained in the former case. As ΔT increases, the temporal average $n_I(i)_{\Delta T}$ becomes closer to the ensemble one ρ and the effect of awareness increases. When ΔT is large enough compared to the time scale of variation of the network $1/a$, the local time recording becomes equivalent to an ensemble average, and we recover the mean-field situation.

6.3.2. SIR dynamics

6.3.2.1. Analytical approach

Following an approach similar to the case of the SIS model, the SIR model has been studied at the heterogeneous mean field level in AD networks, in terms of a set of equations for the state of nodes with activity a, which takes the form [103]

$$\begin{aligned} I_a^{t+1} &= I_a^t - \mu \, I_a^t + \lambda \, a \, (N_a - I_a^t - R_a^t) \int \frac{I_{a'}^t}{N} \, da' \\ &+ \lambda \, (N_a - I_a^t - R_a^t) \int \frac{I_{a'}^t \, a'}{N} \, da' \, , \end{aligned} \tag{6.14}$$

where N_a is the total number of nodes with activity a, and I_a and R_a are the number of nodes with activity a in the infectious and recovered states, respectively. Again, a linear stability analysis shows the presence of a threshold, which takes

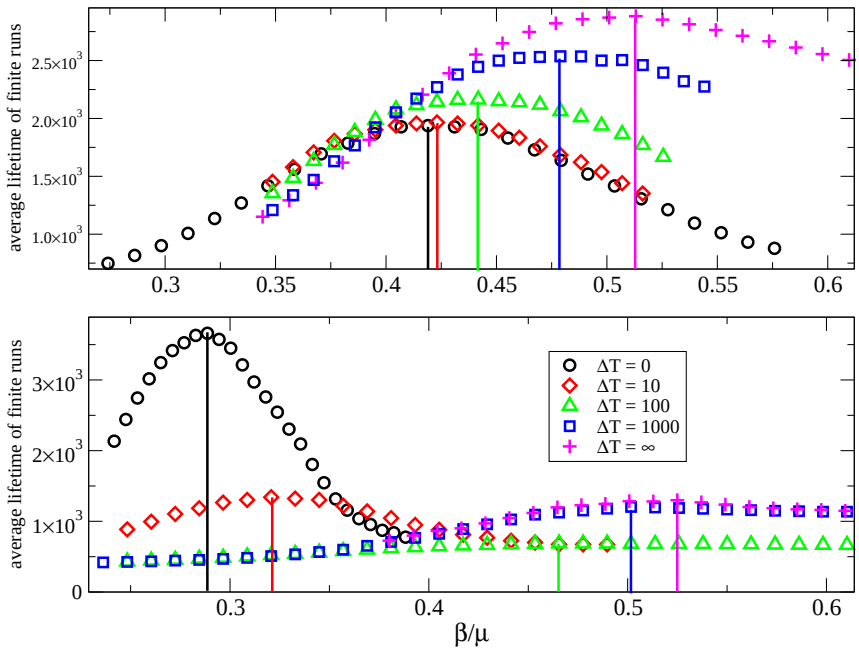

Figure 6.4.: Effect of the local risk perception with increasing memory span ΔT for the SIS spreading on AD and ADM network. (top): AD network. (bottom): ADM network. Vertical lines indicate the position of the maximum of the average lifetime. Model parameters: $\alpha = 10$, $\mu = 0.015$, $\gamma = 2$, $\epsilon = 10^{-3}$ and network size $N = 10^4$. Results are averaged over 1000 realizations.

the same form as in the SIS case:

$$\frac{\beta}{\mu} \geq \frac{2\langle a \rangle}{\langle a \rangle + \sqrt{\langle a^2 \rangle}}. \tag{6.15}$$

The same expression can be obtained by a different approach, based on the mapping of the SIR processes to bond percolation [162].

Since the SIR model lacks a steady state, we cannot apply in the general case the approach followed in the previous section. The effects of risk perception can be however treated theoretically for a homogeneous network (uniform activity) in the limit $\Delta T \to \infty$, which is defined by the effective infection probability

$$\lambda(t) = \lambda_0 \exp\left(-\frac{\alpha}{t}\int_0^t \rho(\tau)\, d\tau\right) . \tag{6.16}$$

Even this case is hard to tackle analytically, so that we consider instead a modi-

fied model defined by the infection probability

$$\lambda(t) = \lambda_0 \exp\left(-\alpha \int_0^t \rho(\tau)\, d\tau\right) . \tag{6.17}$$

In this definition the fraction of infectious seen by an individual is no longer averaged over the memory length but rather accumulated over the memory timespan, so that we expect stronger effects of the risk perception with respect to Eq. (6.15), if any. The fraction of susceptibles $s = S/N$ and the fraction of recovered $r = R/N$ in the system obey the equations

$$\frac{ds}{dt} = -\lambda_0\, \rho(t)\, s(t)\, e^{-\alpha r(t)/\mu} \tag{6.18}$$

$$\frac{dr}{dt} = \mu\rho(t) \tag{6.19}$$

where in the first equation we have used the second equation to replace $\int_0^t \rho(\tau)\, d\tau$ in $\lambda(t)$ by $(r(t) - r(0))/\mu$ (with the initial conditions $r(0) = 0$).

Setting $\mu = 1$ without loss of generality, the final average fraction of recovered individuals after the end of an outbreak is given by

$$r_\infty = 1 - s(0) \exp\left(-\frac{\lambda_0}{\alpha}(1 - e^{-\alpha r_\infty})\right) . \tag{6.20}$$

Close to the threshold, i.e., for $r_\infty \sim 0$, performing an expansion up to second order and imposing the initial condition $\rho(0) = 1 - s(0) = 0$, we obtain the asymptotic solution

$$r_\infty \simeq \frac{2}{\lambda_0(\alpha + \lambda_0)}(\lambda_0 - 1), \tag{6.21}$$

which leads to the critical infection rate $\lambda_0 = 1$. This means that, as for the SIS case, the risk perception does not affect the epidemic threshold at the mean field level, at least for a homogeneous network. The only effect of awareness is a depression of the order parameter r_∞ with α, as observed also in the SIS case. The same conclusion is expected to hold for the original model of awareness, with an infection rate of the form Eq. (6.16) as in this case the dynamics is affected to a lower extent. In analogy, for the general case of an heterogeneous AD network, with rate infection given by Eq. (6.2), we expect the effects of awareness on the epidemic threshold to be negligible at the mean-field level.

On ADM networks, the numerical analysis of the SIR model carried out in Ref. [170] has revealed a picture opposite to the SIS case. In an SIR process indeed, reinfection is not possible; as a result, repeating contacts are not useful for the diffusion of the infection. The spread is thus favoured by the more random patterns occurring in the memory-less (AD) case, which allows infectious nodes to contact a broader range of different individuals and find new susceptible ones.

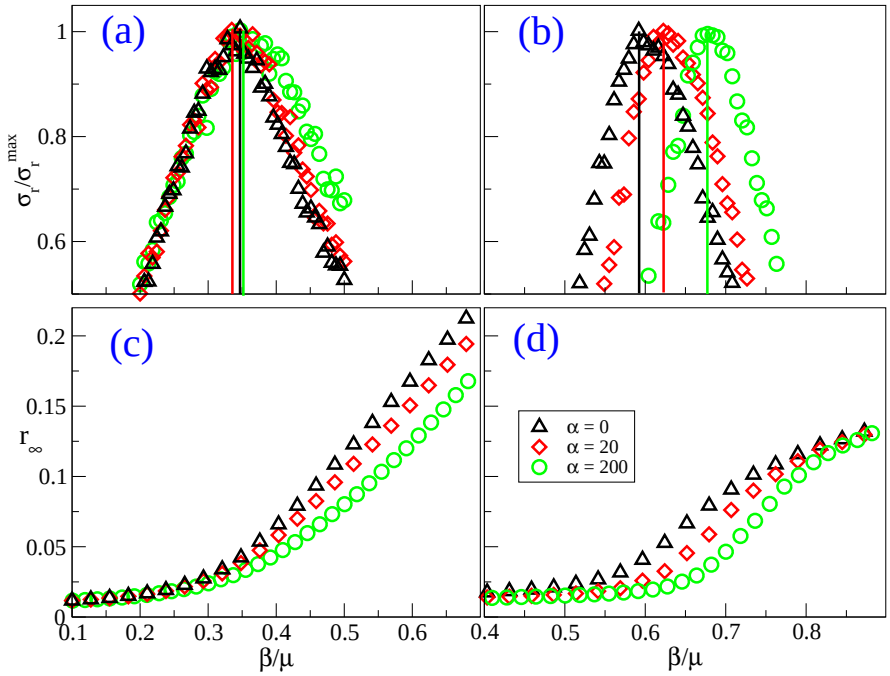

Figure 6.5.: Effect of the local risk perception on the SIR spreading on AD networks and ADM networks. We plot r_∞ and σ_r/σ_r^{max} for different values of α. (a): σ_r/σ_r^{max} on AD network, (b): σ_r/σ_r^{max} on ADM network, (c): r_∞ on AD network and (d): r_∞ on ADM network. Vertical lines in subplots (a) and (b) indicate the position of the maximum of the order parameter variance. Model parameters: $\Delta T = \infty$, $\mu = 0.015$, $\gamma = 2$, $\epsilon = 10^{-3}$ and network size $N = 10^5$. Results are averaged over 1000 realizations.

The epidemic threshold for SIR processes is hence higher in the ADM case than in the AD one [170].

6.3.2.2. Numerical simulations

To study the effects of risk perception on the dynamics of a SIR spreading process in temporal networks we resort again to numerical simulations. In Fig. 6.5 we compare the effects of the risk perception mechanism given by Eq. (6.2) for AD and ADM networks. The spread starts with a fraction $\rho_0 = I_0/N = 0.01$ of infectious nodes chosen at random in the population and the activity distribution is the same as in the SIS case. In the present simulations the memory span ΔT is infinite and we compare the results obtained for two different values of the awareness strenght α. We see that the effective epidemic threshold is increased for the ADM network, whereas it seems unchanged for the AD network and around a value of $\beta/\mu = 0.35$, an agreement with the theoretical prediction

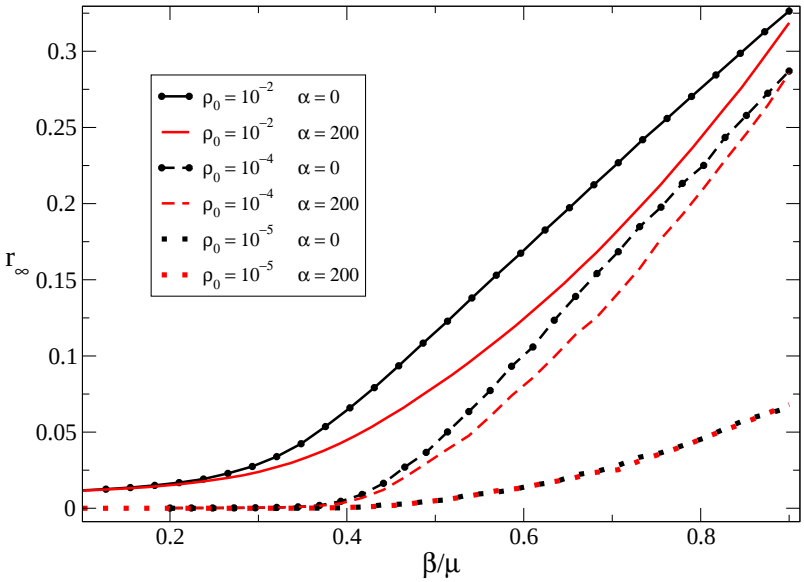

Figure 6.6.: Effect of the initial density of infectious on the SIR model on AD networks for different values of the awareness strength α and the initial density of infectious individuals ρ_0. Model parameters: $\Delta T = \infty$, $\mu = 0.015$, $\gamma = 2$, $\epsilon = 10^{-3}$ and network size $N = 10^5$. Results are averaged over 1000 realizations.

quoted in the previous section.

The SIR phase transition is rigorously defined for a vanishing initial density of infectious, i.e., in the limit $\rho(0) \to 0$ and $s(0) \to 1$, as can be seen at the mean-field level in the derivation of Eq. (6.21). In Fig. 6.6 we explore the effects of the initial density $\rho_0 = I_0/N$ of infectious individuals on the effect of awareness on AD networks. For large values of $\rho_0 = I_0/N$, the awareness ($\alpha > 0$) can significantly decrease the final epidemic size, as already observed in Fig. 6.5. This effect can be understood by the fact that, for large ρ_0, more individuals are aware already from the start of the spread and have therefore lower probabilities to be infected. At very small initial densities, on the other hand, r_∞ becomes independent of α. This is at odds with the result in Eq. (6.21), which however was obtained within an approximation that increases the effects of awareness. The milder form considered in Eq. (6.2) leads instead to an approximately unaltered threshold, and to a prevalence independent of α.

For ADM networks, Fig. 6.7 shows the variance of the order parameter for two different values of α. As in the SIS case, we see that an apparent shift of the effective epidemic threshold is obtained, but very strong finite size effects are present even at large size, especially for $\alpha > 0$. The difference between the

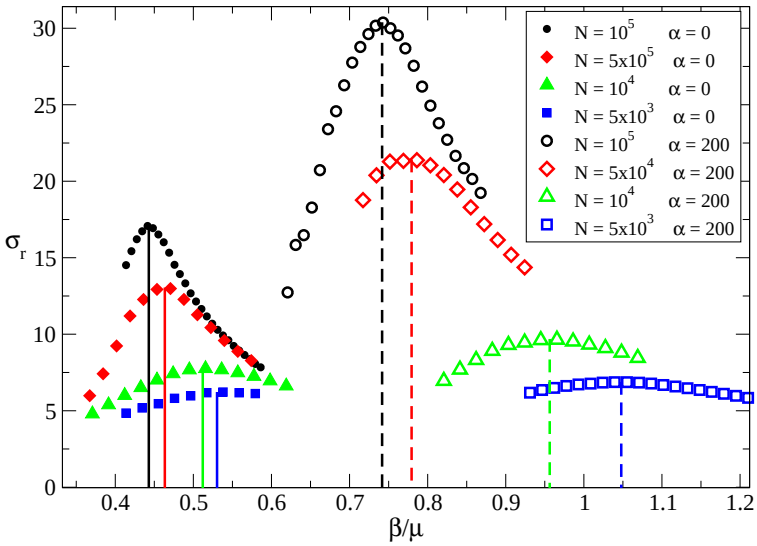

Figure 6.7.: Finite scale effects in the SIR process on ADM. we plot σ_r for different network sizes and two values of α. Vertical lines indicate the position of the maximum of the order parameter variance. Model parameters: $\rho_0 = 1/N$, $\Delta T = \infty$, $\mu = 0.005$, $\gamma = 2$, $\epsilon = 10^{-3}$. Results are averaged over 10^5 realizations.

effective thresholds at $\alpha > 0$ and $\alpha = 0$ decreases as the system size increases, but remains quite large, making it difficult to reach a clear conclusion on the infinite size limit.

6.4. Epidemic spreading on empirical social networks

As neither AD nor ADM networks display all the complex multi-scale features of real contact networks, we now turn to numerical simulations of spreading processes with and without awareness on empirical temporal contact networks, using the datasets described in section 1.3.

6.4.1. SIS dynamics

As we saw in subsection 6.3.1, the susceptibility defined to evaluate the epidemic threshold of the SIS process is subject to strong finite size effects. Since the empirical networks used in the present section are quite small, we choose to focus

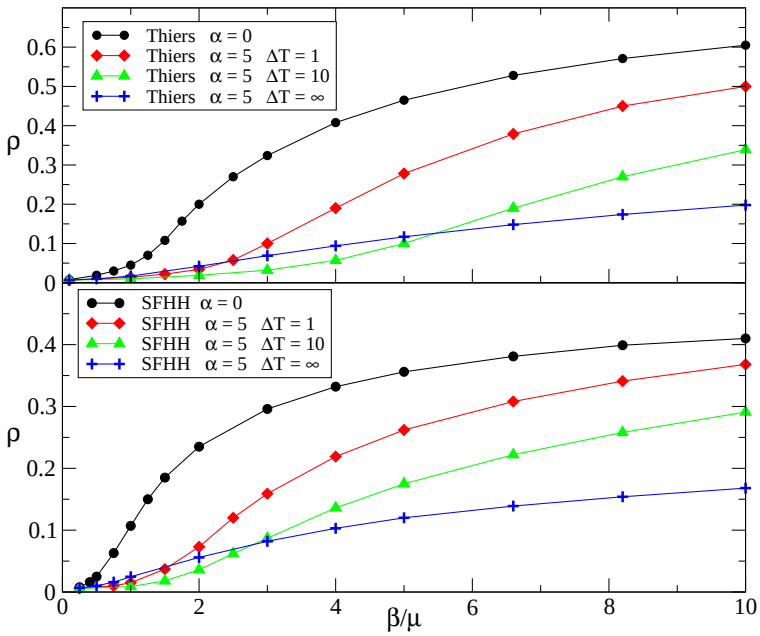

Figure 6.8.: Steady state fraction of infectious for the SIS process on both empirical networks, for 2 values of α and different values of ΔT. Model parameters: $\mu = 0.001$ for Thiers and $\mu = 0.005$ for SFHH. Results are averaged over 1000 realizations.

only on the main observable of physical interest, i.e., the average prevalence ρ in the steady state of the epidemics.

As we are interested in the influence of the structural properties of the network, we choose to skip the nights in the datasets describing the contacts between individuals, as obviously no social activity was recorded then, to avoid undesired extinction of the epidemic during those periods. In order to run simulations of the SIS spreading, we construct from the data arbitrarily long lasting periodic networks, with the period being the recording duration (once the nights have been removed). For both networks we define the average instantaneous degree $\langle k \rangle = \frac{1}{T_{data}} \sum_i \overline{k}_t$ where the sum runs over all the time steps of the data, and $\overline{k}_t$ is the average degree of the snapshot network at time t. We then define $\beta/\mu = \lambda\langle k \rangle/\mu$ as the parameter of the epidemic. For each run, a random starting time step is chosen, and a single agent in the same time step, if there is any, is defined as the seed of the infection (otherwise a new starting time is chosen).

In Fig. 6.8, we compare the curves of the prevalence ρ of the epidemics in the stationary state on both empirical networks, and for increasing values of the memory length ΔT. We can see that an important reduction of the prevalence is occurring even for $\Delta T = 1$. This is due to the presence of many contacts of

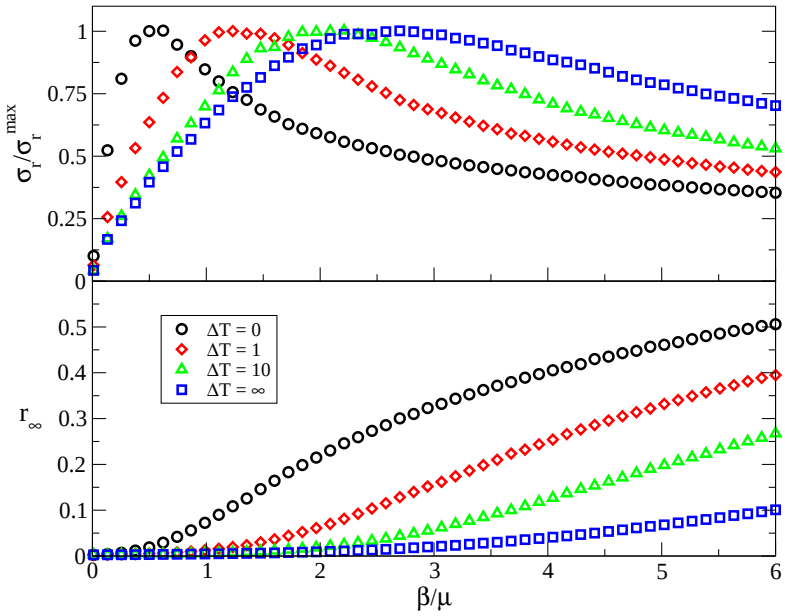

Figure 6.9.: Effect of the risk perception for different values of ΔT on the SIR spreading on SFHH network. (top): normalized standard deviation σ_r/σ_r^{max}. (bottom): order parameter r_∞. Model parameters: $\mu = 0.005$. $\alpha = 200$. Results are averaged over 10^4 realizations.

duration longer than ΔT (contrarily to the AD case): the awareness mechanism decreases the probability of contagion of all these contacts (and in particular of the contacts with very long duration, which have an important role in the propagation) as soon as $\Delta T > 1$, leading to a strong effect even in this case. At large values of the control parameter β/μ, the effect of the awareness is stronger for increasing values of the memory length ΔT, as was observed in subsection 6.3.1. At small values of β/μ on the contrary, the awareness is optimum for a finite value of ΔT, and the knowledge of the whole contact history is not the best way to contain the epidemics. While a detailed investigation of this effect lies beyond the scope of our work, preliminary investigations (not shown) seem to indicate that it is linked to the use of the periodicity introduced in the data through the repetition of the dataset.

6.4.2. SIR

In this section we study the impact of the awareness on the SIR spreading process running on the empirical networks. In particular, we study the effect of self protection on the fraction of recovered individuals r_∞ in the final state, and on the effective threshold evaluated as the peak of the relative variance of r_∞

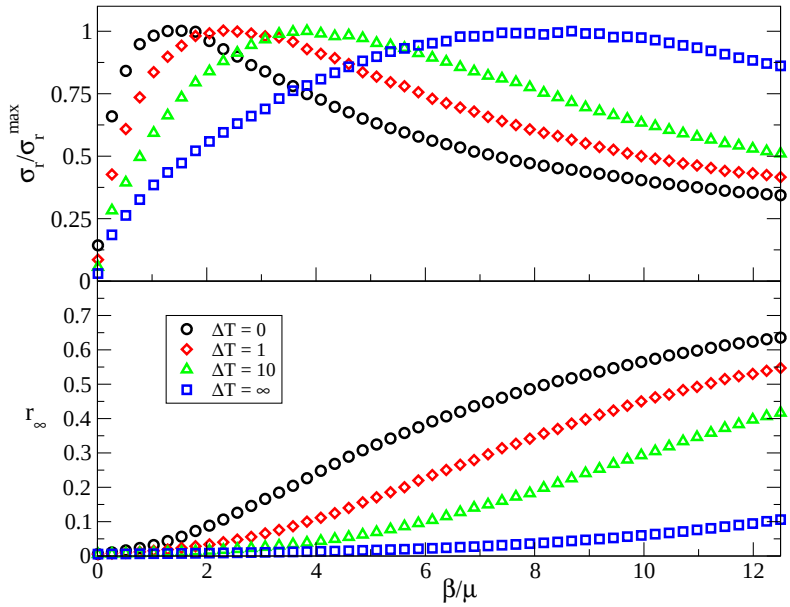

Figure 6.10.: Effect of the risk perception for different values of ΔT on the SIR spreading on the Thiers network. (top): normalized standard deviation σ_r/σ_r^{max}. (bottom): order parameter r_∞. Model parameters: $\mu = 0.001$. $\alpha = 200$. Results are averaged over 10^4 realizations.

defined in Eq. (6.1). In Fig. 6.9 and 6.10 we plot σ_r and r_∞ for different memory length ΔT, for the SFHH conference and the Thiers highschool data respectively. We first notice that a notable effect appears already for $\Delta T = 1$, similarly to the SIS process. However, we see that r_∞ is monotonously reduced as ΔT grows and that the effective threshold is shifted to higher values of β/μ, also monotonously. It is worth noticing that the timescale of the SIR process is much smaller than the one studied in the SIS process because the final state is an absorbing state free of infectious agents. The lifetime of the epidemic in this case is of the order of magnitude of the data duration, so that the periodicity introduced by the repetition of the dataset is not relevant anymore. Overall, we observe for both networks an important reduction of outbreak size when people adopt a self protecting behaviour, as well as a significant shift of the effective epidemic threshold.

6.5. Conclusion

The implementation of immunization strategies to contain the propagation of epidemic outbreaks in social networks is a task of paramount importance. In this

chapter, we have considered the effects of taking protective measures to avoid infection in the context of social temporal networks, a more faithful representation of the patterns of social contacts than often considered static structures. In this context, we have implemented a model including awareness to the propagating disease in a temporal network, extending previous approaches defined for static frameworks. In our model, susceptible individuals have a local perception of the overall disease prevalence measured as the ratio of the number of previous contacts with infectious individuals on a training window of width ΔT. An increased level of awareness induces a reduction in the probability that a susceptible individual contracts the disease via a contact with an infectious individual.

To explore the effects of disease awareness we have considered the paradigmatic SIS and SIR spreading models on both synthetic temporal networks, based in the activity driven (AD) model paradigm, and empirical face-to-face contact networks collected by the SocioPatterns collaboration. In the case of network models, we consider the original AD model, and a variation, the AD model with memory (ADM), in which a memory kernel mimics some of the non-Markovian effects observed in real social networks.

In the case of synthetic networks, analytical and numerical results hint that in AD networks without memory, the epidemic threshold on both SIS and SIR models is not changed by the presence of awareness, while the epidemic prevalence is diminished for increasing values of the parameter α gauging the strength of awareness. In the case of the ADM model (temporal network with memory effects) on the other hand, awareness seems to be able to shift the threshold to an increased value, but very strong finite size effects are present: our results are compatible with an absence of change of the epidemic threshold in the infinite size limit, while, as for the AD case, the epidemic prevalence is decreased.

In the case of empirical contact networks, we observe in all cases a strong reduction of the prevalence for different values of α and ΔT, and an apparent shift of the effective epidemic threshold. These empirical networks differ from the network models from two crucial points of view. On the one hand, they have a relatively small size. Given that important finite size effects are observed in the models, especially in the one with memory effects, one might also expect stronger effective shifts in such populations of limited size. On the other hand, AD and ADM networks lack numerous realistic features observed in real social systems. On AD and ADM networks, contacts are established with random nodes (even in the ADM case) so that the perception of the density of infectious by any node is quite homogeneous, at least in the hypothesis of a sufficiently large number of contacts recorded (i.e., at large enough times, for $a\Delta T \gg 1$). This is not the case for the empirical networks, which exhibits complex patterns such as community structures, as well as broad distributions of contact and inter-contact durations, specific time-scales (e.g., lunch breaks), correlated activity patterns, etc. [59]. This rich topological and temporal structure can lead to

strong heterogeneities in the local perception of the disease. In this respect, it would be interesting to investigate the effect of awareness in more realistic temporal network models.

Notably, the awareness mechanism, even if only local and not assuming any global knowledge of the unfolding of the epidemics, leads to a strong decrease of the prevalence and to shifts in the effective epidemic threshold even at quite large size, in systems as diverse as simple models and empirical data. Moreover, some features of empirical contact networks, such as the broad distribution of contact durations, seem to enhance this effect even for short-term memory awareness. Overall, our results indicate that it would be important to take into account awareness effects as much as possible in data-driven simulations of epidemic spread, to study the relative role of the complex properties of contact networks on these effects, and we hope this will stimulate more research into this crucial topic.

7. Voter-like model of opinion dynamics

7.1. Introduction

A wide variety of complex physical systems are concerned with the problem of an initially disordered configuration that is able to achieve an ordered state by means of local pairwise dynamical interactions. Examples of such systems range from the formation of an opinion consensus in social systems [30] to the loss of genetic diversity in evolutionary dynamics [48]. These situations, implying a competition between different alternative states diffusing among the agents, have been modelled with stochastic copying or invasion processes. In these models, each individual is endowed with a state variable and copies or imposes his/her state from or to neighbouring sites until one single state finally dominates the whole system. Among those different frameworks, the voter model [101] was introduced to schematically model the opinion spreading in human populations and has become emblematic for its simplicity and analytical tractability. In this model, the agents possess one of two discrete opinions, and at each time step an individual is chosen and adopts the opinion of a randomly chosen neighbour. On the other hand, in the context of evolutionary dynamics, the Moran process [119] considers a population of individuals belonging to different species, that reproduce generating an offspring that replaces a randomly chosen nearest neighbor. The voter and Moran models differ thus in the direction in which the state is transferred between pairs of interacting agents.

Recently, it has been acknowledged that the topology in which such ordering dynamics takes place in real systems is often far for homogeneous, and better represented in terms of heterogeneous complex networks [13, 17, 125]. This observation has led to an intense research activity in order to unveil the different properties of ordering dynamics in heterogeneous topologies [15, 17, 107, 120, 152, 156, 176], yielding a good understanding of the problem both at the numerical and analytical levels.

These studies have mainly focused on the case of *static* networks, in which nodes representing agents are connected by a set of edges, standing for pairwise possible interactions, that are fixed in time and never change. However, many networks, and in particular social ones, are dynamic in nature, given by a pattern

of connections that evolves in time. Despite their relevance, however, consensus dynamics have seldom been studied in detail in temporal topologies [53, 84, 100].

Here we contribute to fill this gap by presenting a detailed study of the voter and Moran processes on temporal networks, focusing on activity driven networks introduced in subsection 1.4.1 . We provide a full analysis of basic ordering dynamics through a heterogeneous mean-field approach that allows us to describe the dynamics of the process in the limit of a large system size, and in particular to compute the average time to reach consensus starting from a random configuration. Another quantity of interest when studying consensus or invasion processes is the so-called exit probability, defined as the probability that a single agent having a discrepant opinion among an unanimous population manages to spread his/her opinion to the whole population. In our work this quantity plays a significant role as it highlights an interesting symmetry between the voter model and the Moran process when comparing the unfolding of these processes either on static heterogeneous networks or on and the activity driven network. In particular, we show how, depending on the type of dynamics, the effect of a node's characteristics on the dynamics can be similar or drastically different when the dynamics runs on a temporal network or on the corresponding static aggregated network.

7.2. Consensus dynamics in activity driven networks with attractiveness

Throughout this chapter we use the synthetic activity driven model with attractiveness (expADA) defined in chapter 1 as a substrate for the consensus dynamics we define. The dynamics of such a network is entirely determined by the joint distribution $\eta(a, b)$ of the activity a and attractiveness b. Coupling a dynamical process with a temporal network always entails the problem of how to deal with the different time scales inherent in the process and in the evolution of the network. Here we consider the simplest case of a single time scale, imposed by the network evolution. In this way, the state of an agent can only change when s/he interacts with another agent, and is constant in the latency times between interactions. The consensus dynamics are thus defined as follows:

- We start from an initial configuration of states $s_i \in \{0, 1\}$, assigned to each agent.
- In an interval of time δt, an agent i, in state s_i, becomes active with probability $a_i \delta t$, and chooses as peer another agent j (in state s_j) with probability $\frac{b_j}{\sum_\ell b_\ell}$

- The states s_i and s_j are updated according to the chosen consensus dynamics.
- Time is updated $t \to t + \delta t$.

We consider three different variations of opinion dynamics, based on the update dynamics of the state variables. Assuming that, at given time t, agent i becomes active, and chooses agent j to start an interaction, we consider the three different updates:

1. Voter dynamics: $s_i := s_j$ (i.e., i adopts j's state).
2. Moran dynamics: $s_j := s_i$.
3. Mixed dynamics: With probability p, $s_i := s_j$; with the complementary probability $1 - p$, $s_j := s_i$.

In what follows, we consider the mixed update rule, as the voter model and the Moran process are particular cases of the latter obtained by setting $p = 1$ or $p = 0$ respectively.

7.3. Heterogeneous mean-field analysis

When agent activation is ruled by a Poisson process, it is possible to tackle the behavior of voter-like dynamics by extending the heterogeneous mean-field [17, 44] approach developed in Refs. [156, 157] to study voter dynamics on static networks. This method is based in a coarse-graining of the network, considering that the state of an agent with activity a and attractiveness b depends exclusively on those two quantities. In this way, one considers a fundamental description in terms of the fraction $\rho_{a,b}(t)$ of agents with activity strength a and attractiveness b in the state 1 at time t; in other words, $\rho_{a,b}(t)$ is the probability that a randomly chosen agent with activity a and attractiveness b is in state 1 at time t. The corresponding fraction of agents in state 0 is given by the complementary probability $1 - \rho_{a,b}(t)$. The total fraction of agents in state 1, $\rho(t)$, is given by

$$\rho(t) = \sum_{a,b} \eta(a,b)\rho_{a,b}(t). \tag{7.1}$$

To alleviate notation, we denote the pair (a, b) by the symbol h, writing thus $\rho_{a,b}(t) \equiv \rho_h(t)$.

The relevant functions defining the dynamics are the transition probabilities R_h and L_h for respectively increasing and decreasing the number of voters in state 1, among the pool of agents with activity strength a and attractiveness b, in a time interval δt. From these transition probabilities, a differential equation ruling the evolution of $\rho_h(t)$ can be derived, as well as information about the exit

probability and the average ordering time. In the dynamical rules described in the previous section, agents activate independently so that a priori multiple activations are possible during a single time step. However the use of the transition probabilities R_h and L_h relies on the implicit hypothesis that only one flip attempt may occur during a single time step, thus in order to ensure the validity of our analysis, we impose that $\langle a \rangle N \delta t \ll 1$ so that the probability of counting more than one activation during δt is almost zero. This is of course always possible as the time step δt is arbitrary.

Let us now derive the time evolution equation of the fraction $\rho_h(t)$ of agents with activity strength a and attractiveness b in state 1 at time t.

7.3.1. Evolution equation

In a single time step, the number of agents with activity strength a and attractiveness b in state 1 may either increase by one unit with probability R_h, decrease by one unit with probability L_h, or stay unchanged with probability $1 - R_h - L_h$. Thus on average the variation $\delta \rho_h$ reads

$$\delta \rho_h = (+1) \times \frac{R_h}{N_h} + (-1) \times \frac{L_h}{N_h} + 0 \times \frac{1 - R_h - L_h}{N_h}, \tag{7.2}$$

where N_h is the number of agents in the state (a, b). In the continuous time limit (for $\delta t \ll 1$) we may write

$$\frac{\partial \rho_h(t)}{\partial t} = \frac{R_h - L_h}{N_h \, \delta t}. \tag{7.3}$$

We consider the mixed process in which every agent, when activated, might either copy the state of his/her peer with probability p, or impose his/her own state to him with probability $1 - p$. The transition probabilities are thus given by

$$R_h = p \, R_h^V + (1 - p) R_h^M \tag{7.4}$$

$$L_h = p \, L_h^V + (1 - p) L_h^V, \tag{7.5}$$

where the rates L_h^X and R_h^X refer to the voter ($X = V$) and Moran ($X = M$) dynamics, respectively.

In the case of the voter dynamics, these transition probabilities take the form

$$R_h^V = N_h \, a \, \delta t \, (1 - \rho_h) \frac{\langle b \, \rho_h \rangle}{\langle b \rangle}, \tag{7.6}$$

$$L_h^V = N_h \, a \, \delta t \, \rho_h \left(1 - \frac{\langle b \, \rho_h \rangle}{\langle b \rangle} \right). \tag{7.7}$$

The origin of these expressions is easy to see. For example, in Eq. (7.6), the probability that the number of agents in state 1, activity a and attractiveness b

increases by one unit is proportional to the number of agents in this class in state 0, $N_h[1-\rho_h(t)]$, times the probability that any one of them becomes active in a time interval δt ($a\delta t$), times the probability that an active agent generates a link to an agent in state 1, thus copying the state of this last agent. The latter is the sum over all the agents i of the probability that i is chosen and is in state 1, i.e., $\sum_i \frac{b_i}{\langle b\rangle N}\, s_i = \frac{\langle b\,\rho_h\rangle}{\langle b\rangle}$ The transition probability L_h^V can be obtained by an analogous reasoning.

In the case of the Moran process, instead, the probability that in a timestep the state of node i is flipped from 1 to 0 is

$$P_i(1\to 0) = \sum_j \frac{s_i\, b_i(1-s_j)}{\langle b\rangle(N-1)} a_j \delta t = s_i\, \frac{b_i}{\langle b\rangle}\delta t(\langle a\rangle - \langle a\rho_h\rangle). \tag{7.8}$$

Indeed, the probability that the agent i is flipped from 1 to 0 while interacting with j is equal to the probability $a_j\delta t(1-s_j)$ that j becomes active and is in state 0, times the probability $\frac{s_i\, b_i}{\langle b\rangle(N-1)}$ that i is chosen among all the other agents and is in state 1. We then sum over all the agents j to obtain the total probability. Then, summing over all nodes i with activity a and attractiveness b we get

$$L_h^M = N_h\, \delta t\, \rho_h\, (\langle a\rangle - \langle a\, \rho_h\rangle)\frac{b}{\langle b\rangle}\ . \tag{7.9}$$

We obtain in a similar fashion

$$R_h^M = N_h\, \delta t\, \langle a\, \rho_h\rangle\, (1-\rho_h)\frac{b}{\langle b\rangle}. \tag{7.10}$$

From these two particular cases we deduce the time evolution equation of the fraction of nodes with activity a and attractiveness b in state 1 in the general mixed case, which is given by

$$\frac{\partial \rho_h(t)}{\partial t} = pa\left(\frac{\langle b\,\rho_h\rangle}{\langle b\rangle} - \rho_h\right) + (1-p)\langle a\rangle\frac{b}{\langle b\rangle}\left(\frac{\langle a\,\rho_h\rangle}{\langle a\rangle} - \rho_h\right). \tag{7.11}$$

7.3.2. Conservation law

In the case of the voter model on a complete static graph, the total fraction ρ of voters in state 1 is conserved by the dynamics. In our model, it is clear from the previous equation that this in not in general true. Nevertheless, we may look for a conserved quantity of the form

$$\Omega = \sum_h \lambda_h\, \rho_h, \tag{7.12}$$

where the weights λ_h are normalized as $\sum_h \lambda_h = 1$. Using Eq. (7.11), we can check that the condition $\partial\Omega/\partial t = 0$ is fulfilled if the functions λ_h satisfy the self consistent equation

$$\lambda_h = \eta(h)\,\frac{p\,b\,[\sum_{h'} a'\lambda_{h'}] + (1-p)\,a\,[\sum_{h'} b'\lambda_{h'}]}{pa\langle b\rangle + (1-p)\langle a\rangle b}, \tag{7.13}$$

where $\sum_h a\lambda_h$ and $\sum_h b\lambda_h$ are determined by the normalization of the weights λ_h (see details in appendix section D):

$$\sum_h a\lambda_h = \frac{1}{Q_p}\langle\frac{a^2}{\Delta_{h,p}}\rangle, \tag{7.14}$$

$$\sum_h b\lambda_h = \frac{\langle a\rangle}{Q_p\,\langle b\rangle}\langle\frac{b^2}{\Delta_{h,p}}\rangle, \tag{7.15}$$

where we have defined

$$\Delta_{h,p} = pa\langle b\rangle + (1-p)\langle a\rangle b \tag{7.16}$$

and

$$Q_p = p\langle\frac{a^2}{\Delta_{h,p}}\rangle\langle\frac{b}{\Delta_{h,p}}\rangle + (1-p)\frac{\langle a\rangle}{\langle b\rangle}\langle\frac{b^2}{\Delta_{h,p}}\rangle\langle\frac{a}{\Delta_{h,p}}\rangle. \tag{7.17}$$

Notice that this last quantity depends only on p.

7.3.3. Exit probability

As in the case of the standard voter model [95], the presence of a conservation law allows us to estimate directly the exit probability E for a single agent with state 1 in a population of agents with state 0, i.e., the probability that all agents finally adopt the state 1. Indeed, the final state with all voters in state 1, corresponding to $\Omega = 1$, takes place with probability E (by definition), while the final state with all voters in state 0, with $\Omega = 0$, happens with probability $1 - E$. The conservation of Ω implies that $\Omega(t = 0) = E \times 1 + (1 - E) \times 0$, from where we immediately obtain

$$E = \sum_h \lambda_h\,\rho_h(0), \tag{7.18}$$

which depends exclusively on the initial state in which the system is prepared. For the particular initial conditions consisting of a single voter with variables $h = (a, b)$, i.e., activity a and attractiveness b, in state 1 in a background of voters in state 0, we have that $\rho_{h'}(0) = \delta_{h',h}\,N_h^{-1}$, which leads to an exit probability

$$E_{a,b} = \frac{\lambda(a,b)}{N\eta(a,b)}, \tag{7.19}$$

which, using Eq. (7.13) can be more explicitly expressed as

$$E_{a,b} = \frac{1}{NQ_p} \frac{pb\langle \frac{a^2}{\Delta_{h,p}} \rangle + (1-p)a\frac{\langle a \rangle}{\langle b \rangle}\langle \frac{b^2}{\Delta_{h,p}} \rangle}{pa\langle b \rangle + (1-p)b\langle a \rangle}. \tag{7.20}$$

Interestingly, this exit probability is a function of the ratio $\frac{a}{b}$ only.

7.3.4. Average consensus time

In order to compute the consensus time we can follow [156, 157] and apply a one-step calculation to write down the recursion relation for the time $T[\{\rho_h\}]$ to reach consensus starting from a configuration $\{\rho_h\}$:

$$\begin{aligned} T[\{\rho_h\}] &= \delta t + \left(1 - \sum_h (R_h + L_h)\right) T[\{\rho_h\}] \\ &\quad + \sum_h \left(R_h T[\{\rho_{h'}, \rho_h + 1/N_h\}] + L_h T[\{\rho_{h'}, \rho_h - 1/N_h\}] \right) \end{aligned} \tag{7.21}$$

where the notation $\{\rho_{h'}, \rho_h \pm 1/N_h\}$ denotes a modification of the configuration $\{\rho_h\}$ by the flip of one agent of variables h (either from state 0 to the state 1, for the $+$ case, or vice-versa for the $-$ case).

This equation essentially amounts to consider that the consensus time for a given configuration is equal to the consensus time at the configuration obtained after a transition taking place in a time δt, weighted by the corresponding transition probabilities, plus δt. Expanding Eq. (7.21) at second order in $1/N_h$ we obtain the backward Kolmogorov equation [57]

$$\sum_h v_h \frac{\partial T}{\partial \rho_h} + \sum_h D_h \frac{\partial^2 T}{\partial \rho_h^2} = -1, \tag{7.22}$$

where

$$v_h = pa\left(\frac{\langle b\,\rho_h \rangle}{\langle b \rangle} - \rho_h\right) + (1-p)\langle a \rangle \frac{b}{\langle b \rangle}\left(\frac{\langle a\,\rho_h \rangle}{\langle a \rangle} - \rho_h\right) \tag{7.23}$$

and

$$\begin{aligned} D_h &= \frac{pa}{2N_h}\left(\frac{\langle b\,\rho_h \rangle}{\langle b \rangle} + \rho_h - 2\,\frac{\langle b\,\rho_h \rangle}{\langle b \rangle}\rho_h\right) \\ &\quad + \frac{(1-p)\langle a \rangle b}{2\langle b \rangle N_h}\left(\frac{\langle a\,\rho_h \rangle}{\langle a \rangle} + \rho_h - 2\,\frac{\langle a\,\rho_h \rangle}{\langle a \rangle}\rho_h\right) \end{aligned} \tag{7.24}$$

are the drift and diffusion coefficients, respectively [57]. After a transient time depending on the distribution $\eta(a, b)$, the system reaches a steady state where

$\rho_h = \Omega$, $\forall h$. Then we may drop the drift term in Eq. (7.22), and, considering Eq. (7.12), change variable from ρ_h to Ω [156, 157]

$$\frac{\partial T}{\partial \rho_h} = \lambda_h \frac{\partial T}{\partial \Omega}. \tag{7.25}$$

Substituting into Eq. (7.22) and simplifying (see details in appendix section D), we finally obtain

$$\Omega(1-\Omega)\frac{\partial^2 T}{\partial \Omega^2} = \frac{-N\langle b\rangle}{\left(\sum_h a\lambda_h\right)\left(\sum_h b\lambda_h\right)}. \tag{7.26}$$

This last equation can be directly integrated, yielding the consensus time

$$T = \tau\frac{N}{\langle a\rangle}\left((1-\Omega)\ln\frac{1}{1-\Omega} + \Omega\ln\frac{1}{\Omega}\right), \tag{7.27}$$

where we defined the characteristic adimensional consensus time

$$\tau = \frac{\langle a\rangle\langle b\rangle}{\left(\sum_h a\lambda_h\right)\left(\sum_h b\lambda_h\right)}. \tag{7.28}$$

The model is then entirely solved in terms of the previous expressions for the consensus time and the exit probability. These expressions are however quite intricate and it is quite insightful to study particular cases of interest, for given forms of the distribution of the activity and attractiveness $\eta(a,b)$ and particular values of the mixing probability p. We present this analysis in the following Section.

7.4. Particular cases

7.4.1. p = 1/2

From the definition of $\Delta_{h,p}$ in Eq. (7.16), one obtains, by multiplying this equation respectively by $a/\Delta_{h,p}$ and $b/\Delta_{h,p}$ and averaging,

$$\langle b\rangle = p\langle\frac{ab}{\Delta_{h,p}}\rangle\langle b\rangle + (1-p)\langle\frac{b^2}{\Delta_{h,p}}\rangle\langle a\rangle, \tag{7.29}$$

$$\langle a\rangle = p\langle\frac{a^2}{\Delta_{h,p}}\rangle\langle b\rangle + (1-p)\langle\frac{ab}{\Delta_{h,p}}\rangle\langle a\rangle. \tag{7.30}$$

Thus for $p = 1/2$, one obtains, eliminating $\langle ab/\Delta_{h,p}\rangle$ between these two equations,

$$\frac{\langle a\rangle}{\langle b\rangle}\langle\frac{b^2}{\Delta_{h,p}}\rangle = \frac{\langle b\rangle}{\langle a\rangle}\langle\frac{a^2}{\Delta_{h,p}}\rangle, \tag{7.31}$$

and Eq. (7.17) becomes

$$\begin{aligned} Q_{1/2} &= \frac{1}{2}\langle\frac{b^2}{\Delta_{h,p}}\rangle\frac{\langle a\rangle}{\langle b\rangle}\left(\langle\frac{a}{\Delta_{h,p}}\rangle+\langle\frac{b}{\Delta_{h,p}}\rangle\frac{\langle a\rangle}{\langle b\rangle}\right) \\ &= \langle\frac{b^2}{\Delta_{h,p}}\rangle\frac{\langle a\rangle}{\langle b\rangle^2} = \frac{\langle 1\rangle}{\langle a\rangle}\langle\frac{a^2}{\Delta_{h,p}}\rangle. \end{aligned} \tag{7.32}$$

From here, it follows that $\sum_h a\,\lambda_h = \langle a\rangle$ and $\sum_h b\,\lambda_h = \langle b\rangle$, which finally implies that $\lambda_h = \eta_h$ and $\tau = 1$.

In this case, the dynamics becomes identical to the standard link update dynamics of the voter model [169], and it is totally independent on a and b (in terms of the number of flip attempts) because the probability that the total number of voters in state 1 is increased during an update attempt is exactly compensated by the probability that this same number is decreased.

7.4.2. Pure voter model

The voter model, corresponding to $p = 1$, leads in Eq. (7.13) to

$$\lambda(a,b) = \eta(a,b)\frac{b\,a^{-1}}{\langle b\,a^{-1}\rangle}\ . \tag{7.33}$$

We also obtain $\Delta_{h,p} = a\langle b\rangle$ and $Q_1 = \langle a\rangle\langle ba^{-1}\rangle/\langle b\rangle^2$, leading for the consensus time in Eq. (7.28) to the simple form:

$$\tau = \langle a\rangle\frac{\langle b\,a^{-1}\rangle^2}{\langle b^2a^{-1}\rangle} \tag{7.34}$$

The exit probability is also straightforward to derive from Eq. (7.19):

$$E_{a,b} = \frac{b\,a^{-1}}{N\langle b\,a^{-1}\rangle}. \tag{7.35}$$

7.4.3. Moran process

The Moran process corresponds to $p = 0$, then Eq. (7.13) reduces to

$$\lambda(a,b) = \eta(a,b)\frac{a\,b^{-1}}{\langle a\,b^{-1}\rangle}, \tag{7.36}$$

leading, with $\Delta_{h,p} = b\langle a\rangle$ and $Q_0 = \langle ab^{-1}\rangle/\langle a\rangle$, from Eq. (7.28) to

$$\tau = \langle b\rangle\frac{\langle a\,b^{-1}\rangle^2}{\langle a^2b^{-1}\rangle}. \tag{7.37}$$

The exit probability reads in this case

$$E_{a,b} = \frac{a\, b^{-1}}{N\langle a\, b^{-1}\rangle}. \tag{7.38}$$

It is noteworthy that the results for the Moran process are obtained from the ones of the voter model by simply exchanging a and b. In fact, we see from Eq. (7.13) that the dynamics of the mixed process is the same as the dynamics of the symmetrical process (i.e. with $p \leftarrow 1-p$) upon exchanging a and b. This is intuitively clear if we examine the process from a stochastic point of view: at each update attempt, the node i is chosen at random with probability $\frac{a_i}{\langle a\rangle}$, according to the Gillespie procedure [60], and the node j with probability $\frac{b_j}{\langle b\rangle}$. Besides, changing p into $1-p$ is equivalent to reversing the roles of i and j, which has no effect if a and b are exchanged. This is however valid only when the time is measured as the number of update attempts, the physical time being multiplied by $\frac{\langle a\rangle}{\langle b\rangle}$ when swapping a and b.

7.4.4. Pure Activity Driven Networks

The original activity driven network model [137] does not consider a heterogeneous attractiveness, and this corresponds to a joint distribution $\eta(a,b) = F(a)\delta_{b,b_0}$, where $F(a)$ is the activity distribution and $b = b_0$, constant. In this case we have $Q_p = \dfrac{\langle a\rangle}{b_0}\langle\, [pa + (1-p)\langle a\rangle]^{-1}\rangle$, and the characteristic consensus time reads

$$\tau = \frac{\langle a\rangle^2\langle\, [pa + (1-p)\langle a\rangle]^{-1}\rangle}{\langle a^2\, [pa + (1-p)\langle a\rangle]^{-1}\rangle}, \tag{7.39}$$

while the exit probability is given by

$$E_a = \frac{1}{N}\frac{p\frac{\langle a\rangle}{\tau} + (1-p)a}{pa + (1-p)\langle a\rangle}. \tag{7.40}$$

In order to study the behavior of the consensus time, in Fig. 7.1 we plot the analytical evaluation of τ, Eq. (7.39), for a normalized activity distribution with a power-law form, as empirically observed in Ref. [137],

$$F(a) = \frac{1-\gamma}{1-\epsilon^{1-\gamma}}a^{-\gamma}, \quad a \in [\epsilon, 1]. \tag{7.41}$$

where ϵ is the minimum activity in the system, imposed in order to avoid divergences in the normalization and moments of $F(a)$. From Fig. 7.1 we see that the consensus time has a minimum around $\gamma = 2$ for the Moran process ($p = 0$) and a maximum around $\gamma = 1$ for the voter model ($p = 1$). Note that by virtue of the symmetry property discussed above, the dynamics of the pure attractiveness

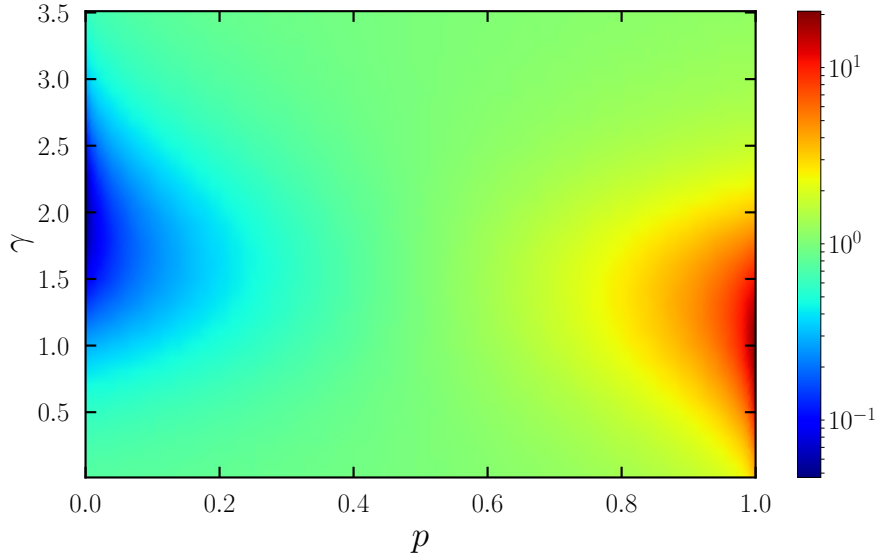

Figure 7.1.: Characteristic consensus time τ for the dynamics on a pure activity driven network, i.e., fixed attractivity $b = b_0$, and a distribution of activities $F(a)$ given by Eq. (7.41), as a function of p and of the exponent γ of the distribution F. $\epsilon = 10^{-3}$.

model (setting $a_i = a_0, \forall i$), taking the same distribution F for b and imposing $a_0 = b_0$, is the same upon exchanging p by $1 - p$. In particular, the consensus time is obtained by reversing the p axis in Fig. 7.1.

7.4.5. Independent activity and attractiveness

In the case where a and b are drawn independently from the same distribution F, we have $\eta(a, b) = F(a)F(b)$. In Fig. 7.2 we plot the characteristic consensus time τ as a function of p and γ for F given by Eq. (7.41). For this particular form of the distribution $\eta(a, b)$ (and in general for any symmetric joint distribution such that $\eta(a, b) = \eta(b, a)$), the dynamics remains the same when changing p into $1 - p$ because exchanging a and b has no effect. This is clearly observed in Fig. 7.2. Additionally, we see that both the voter model and the Moran process have a minimum consensus time for $\gamma \simeq 2.25$ and a maximum consensus time for $\gamma = 0.75$, respectively.

7.4.6. Strongly correlated activity and attractiveness

As we previously mentioned, the weight function λ_h is the product of η_h and a function of the ratio $\frac{a}{b}$. This fact straightforwardly implies that, in the maximally correlated case $\eta(a, b) = F(a)\delta_{a,b}$, where $a = b$ for every agent, the dynamics is the same as in a fully connected static network, i.e. the average density $\rho = \langle \rho_h \rangle$

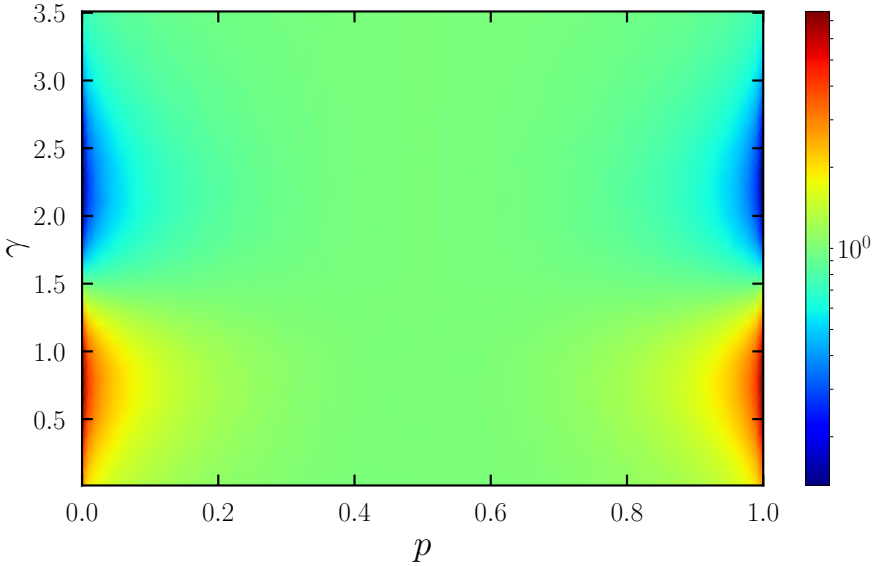

Figure 7.2.: Characteristic consensus time τ as a function of γ and p in the case $\eta(a,b) = F(a)F(b)$, with F given by Eq. (7.41) and $\epsilon = 10^{-3}$.

of voters in state 1 is conserved, the reduced consensus time τ is equal to 1, and the exit probability is homogeneous and equals $1/N$.

7.4.7. Discussion

The results obtained above relate the average consensus time and the exit probability with the moments of the joint distribution $\eta(a,b)$ and the value of the activity a and the attractiveness b of the initial invading voter. Remarkably, when we compare these results with the ones obtained in the case of static networks with a given degree distribution $P(k)$ [156, 157] we observe interesting symmetries between voter and Moran dynamics.

This symmetry is of particular interest when we consider the pure activity driven network (setting $b = 1$). Let us consider for instance the invasion exit probability, Eqs. (7.35) and (7.38). In the case of the voter model, this exit probability is inversely proportional to the activity of the node with initial state 1 ($E_a^{voter} \propto 1/a$), while for the Moran process, it is proportional to the activity ($E_a^{Moran} \propto a$). This can be understood by the fact that an active node will often change state in the voter model, by contacting other nodes, while in the Moran process it will often spread his/her state towards the other nodes contacted.

These results have to be compared with the result for the voter and Moran processes in static networks, in which the exit probability for a single node of degree k with state 1 is $E_k^{\text{voter}} \sim k$ for the voter and $E_k^{\text{Moran}} \sim k^{-1}$ for the Moran process [156, 157]. Intuitively indeed, in the case of static networks, in the voter model high degree nodes are chosen to be copied with high probability [45],

implying that they are very efficient spreaders of their own state to the rest of the network. Hence, the larger k, the higher the exit probability. In the case of the Moran process, by applying the same argument, high degree nodes are prone to often change state by adopting the state of a neighbor [156, 157], and hence the exit probability decreases with the degree.

Let us now recall that, for a pure activity driven network, the aggregated degree of a node with activity a takes the value $\bar{k}_a(t) \simeq (a + \langle a \rangle)t$ at time t: nodes with high activity tend to have large integrated degree [137, 160]. Putting this in relation with the behavior of the exit probability as a function of activity in temporal networks and of degree in static networks, we thus obtain that the dynamics on the temporal activity driven network yields a completely different and opposite result when compared with the dynamics on the static, integrated network counterpart: High activity nodes are more prone to spread under Moran dynamics, while low activity nodes are more prone under voter dynamics.

This symmetry voter-Moran between pure activity driven networks and their integrated counterpart occurs as well at the level of the average consensus time when we measure it as a function of the update attempts. Considering that a randomly chosen node becomes active with average probability $\langle a \rangle$, we have that, as a function of updated attempts, the convergence time is $\bar{T}_N \equiv \langle a \rangle T_N$. We have thus, for homogeneous initial conditions ($\Omega = 1/2$),

$$\bar{T}_N^{\text{voter}} = N\langle a \rangle \langle a^{-1} \rangle \ln 2, \quad \bar{T}_N^{\text{Moran}} = N\frac{\langle a \rangle^2}{\langle a^2 \rangle} \ln 2. \tag{7.42}$$

Comparing with the results for static networks [156, 157],

$$\bar{T}_N^{\text{Moran}} = N\langle k \rangle \langle k^{-1} \rangle \ln 2, \quad \bar{T}_N^{\text{voter}} = N\frac{\langle k \rangle^2}{\langle k^2 \rangle} \ln 2, \tag{7.43}$$

we observe that the formulas for voter and Moran dynamics are indeed mirror images, with the activity distribution a in the temporal representation substituted by the degree distribution in the integrated representation.

Let us now consider instead the pure attractiveness temporal network model (setting $a = 1$). In that case, the exit probability is proportional to the attractiveness for the voter model, $E_b^{voter} \propto b$, while for the Moran process, it is inversely proportional to the attractiveness, $E_b^{Moran} \propto 1/b$. Moreover, the integrated degree of a node with attractiveness b is $\bar{k}_b(t) \sim \frac{b}{\langle b \rangle} t$. Here therefore, we have the same kind of behavior on the temporal and corresponding integrated static network when making an equivalence between attractiveness in the temporal network and degree in the static network. This equivalence between a static network with a degree distribution $P(k)$ and a pure attractiveness temporal network with the same distribution $P(b)$ is also obtained by looking at the consensus time measured as the number of update attempts.

7.5. Numerical results

In order to check the analytical predictions made above, we have performed simulations of the mixed process defined earlier on activity driven networks with attractiveness, choosing a marginal activity distribution following a power-law, Eq. (7.41), similar to the distribution observed empirically in some real networks [137]. We have performed simulations for network sizes $N = 10^2$, 10^3 and 10^4, averaging over 10^3 realizations.

In Fig. 7.3 we plot the reduced consensus time τ as a function of γ for three different values of the network size and three different dynamics: voter and Moran processes on a pure activity driven network, and voter model on an activity driven network with attractiveness with a and b independently and equally distributed $\eta(a, b) = F(a)F(b)$. The curves are compared to the theoretical value given in Eq. (7.28). We see that for $N = 10^4$ the dynamics already matches well the expected behaviour in the infinite size limit. We deduce that our heterogeneous mean-field analysis captures efficiently the opinion dynamics on the activity driven network with attractiveness.

7.6. Asymptotic behaviour

In Figs. 7.1-7.3, we see that the consensus time presents minima and maxima when γ varies. To investigate this point in more details, we analyse the asymptotic behaviour of the moments of the distribution $F(a)$ when ϵ tends to zero. For an activity distributed with Eq. (7.41), the moments of a take the form

$$\langle a^n \rangle = \frac{1-\gamma}{n+1-\gamma} \frac{1-\epsilon^{1+n-\gamma}}{1-\epsilon^{1-\gamma}}. \tag{7.44}$$

The dynamics of the voter and Moran processes on pure activity driven network and on activity driven network with equally and independently distributed a and b depends on the moments $\langle a^{-1} \rangle$, $\langle a \rangle$ and $\langle a^2 \rangle$ only. The asymptotic behaviour of these three quantities for $\epsilon \to 0$ are summarized in Tables 7.1 and 7.2, along with the resulting behaviour of the consensus time in the case with a and b independently and equally distributed and $p = 1$ (or equivalently $p = 0$), for which

$$\tau = \frac{\langle a \rangle^3 \langle a^- 1 \rangle}{\langle a^2 \rangle}. \tag{7.45}$$

We observe that for $0 < \gamma < 1.5$ the consensus time in Eq. (7.45) diverges when ϵ goes to zero, and tends instead to zero for $1.5 < \gamma < 3$. We also recover the fact that the fastest consensus is reached for $\gamma = 2$ and the slowest for $\gamma = 1$ and that for $0 < \gamma < 3$ the consensus time exhibits a symmetry with respect to the axis $\gamma = 1.5 : \tau(\gamma) = \frac{1}{\tau(3-\gamma)}$. Finally, for $\gamma \gg 3$, the heterogeneity of the distribution of

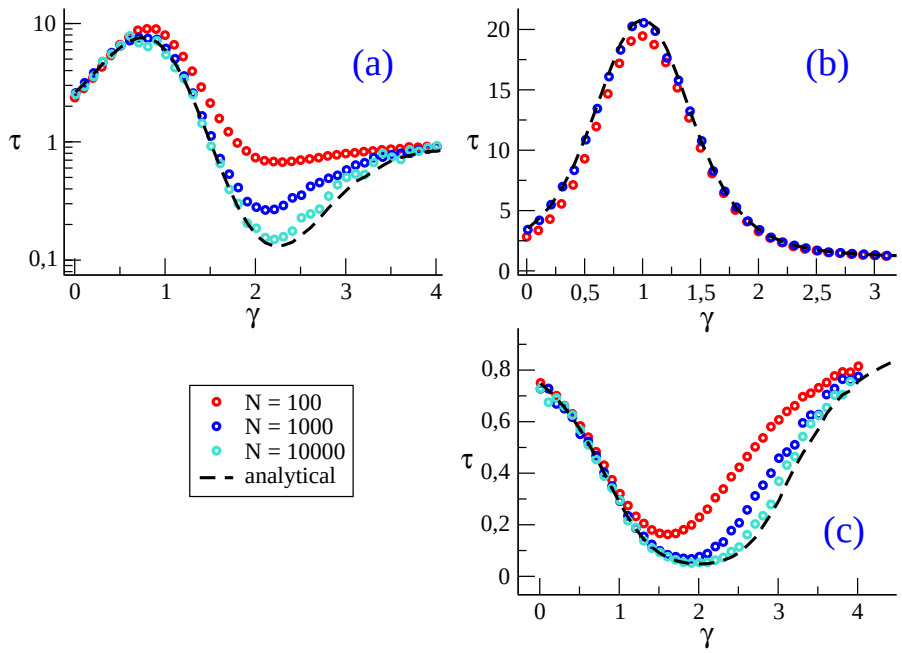

Figure 7.3.: Voter-like dynamics in temporal activity driven networks with attractiveness. Reduced consensus time as a function of γ for different values of the network size N, for an activity distribution $F(a)$ given by Eq. (7.41) with $\epsilon = 10^{-3}$. (a): Voter and Moran processes (equivalent) for $\eta(a, b) = F(a)F(b)$. (b): Voter model on pure AD network ($b = 1$). (c): Moran process on pure AD network ($b = 1$). In each case, the dashed line corresponds to the analytical expression given by Eq. (7.28).

a is no longer significant, so that the dynamics is that of a fully connected static network. In Fig. 7.4 we plot the reduced consensus time for the voter dynamics on a network with independent activity and attractiveness as obtained by direct numerical simulations of a voter model on a temporal network, compared with the analytical predictions of Eq. (7.45), for various values of ϵ and $N = 10^4$. The simulations confirm the predicted asymptotic behaviour of τ when ϵ tends to zero. We also observe stronger finite size effects when epsilon tends to zero due to a poorer sampling of the activity distribution given by Eq. (7.41).

7.7. Conclusions

In this chapter, we have studied in detail the properties of consensus processes mixing the voter and Moran models update rules, on temporal network models based on the activity driven paradigm. Through a heterogeneous mean-field approach, we have derived the evolution equation of the average density of voters

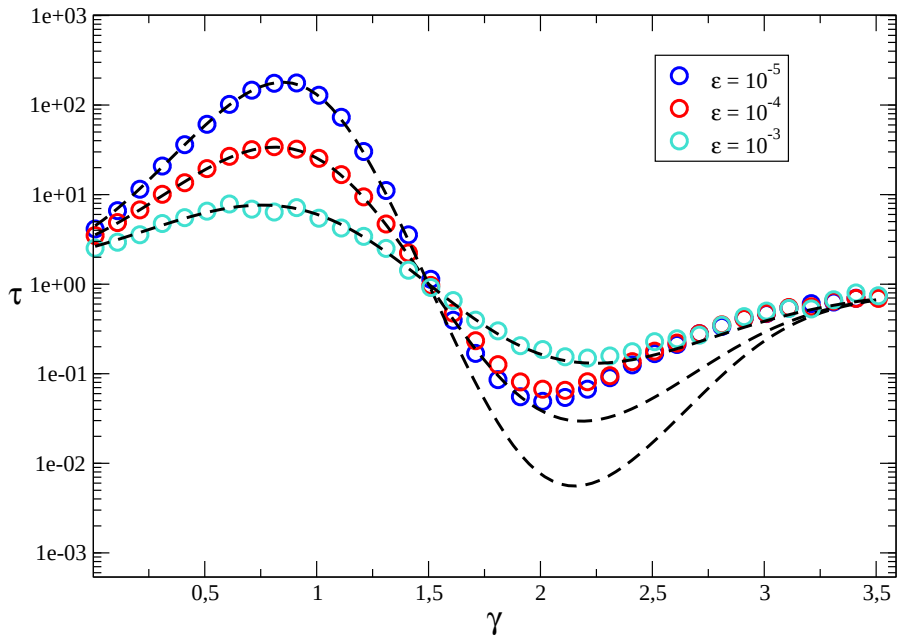

Figure 7.4.: Voter dynamics in temporal networks with independent and equally distributed activity and attractiveness. Consensus time τ as a function of γ for activity and attractiveness distributed according to Eq. (7.41) and different values of ϵ. The analytical expression given by Eq. (7.45) is shown in dashed lines. The numerical simulations are performed with network size $N = 10^4$.

in state 1 with activity a and attractiveness b. This has allowed us to identify a conserved quantity of the dynamics, and subsequently to compute the average time to reach consensus and the probability that a single agent with a discrepant opinion among an otherwise unanimous population spreads his/her opinion to the whole network, called the exit probability. Surprising results arise from the study of particular cases of the distribution of the parameters a and b. When the attractiveness is taken to be proportional to the activity a, the dynamics is the same as if the copying process were running on a static complete graph. The average activity $\langle a \rangle$ determines the time scale of the dynamics, but otherwise the precise distribution of activity among the agents is no longer relevant. This holds for all values of the probability p determining the state update rule, and in particular for the voter model ($p = 1$) and the Moran process ($p = 0$). The same behaviour happens when $p = 1/2$, regardless of the distribution $\eta(a, b)$ of activity and attractiveness: surprisingly, the exit probability is equal to $1/N$ and does not depend of the parameters of the initial invading node.

Interestingly, when the activity and the attractiveness are independent and equally distributed, the dynamics is unchanged when replacing p by $1 - p$. In fact, it appears that by construction, when the time is counted as the number of

γ	$]0,1[$	$]1,2[$	$]2,3[$	>3
$\langle a^{-1}\rangle$	$\mathcal{O}(\epsilon^{-\gamma})$	$\mathcal{O}(\epsilon^{-1})$	$\mathcal{O}(\epsilon^{-1})$	$\mathcal{O}(\epsilon^{-1})$
$\langle a\rangle$	$\mathcal{O}(1)$	$\mathcal{O}(\epsilon^{\gamma-1})$	$\mathcal{O}(\epsilon)$	$\mathcal{O}(\epsilon)$
$\langle a^2\rangle$	$\mathcal{O}(1)$	$\mathcal{O}(\epsilon^{\gamma-1})$	$\mathcal{O}(\epsilon^{\gamma-1})$	$\mathcal{O}(\epsilon^2)$
τ	$\mathcal{O}(\epsilon^{-\gamma})$	$\mathcal{O}(\epsilon^{2\gamma-3})$	$\mathcal{O}(\epsilon^{3-\gamma})$	$\mathcal{O}(1)$

Table 7.1.: Asymptotic behaviour of the moments of the distribution $F(a)$ defined in Eq. (7.41), and resulting asymptotic behaviour of the reduced consensus time τ given by Eq. (7.45) when ϵ tends to zero, as a function of the exponent γ. For $\gamma = 0, 1, 2, 3$, logarithmic corrections are present, given in Table 7.2.

γ	0	1	2	3
$\langle a^{-1}\rangle$	$-\ln\epsilon$	$-(\epsilon\ln\epsilon)^{-1}$	$(2\epsilon)^{-1}$	$\frac{2}{3}\epsilon^{-1}$
$\langle a\rangle$	$1/2$	$-(\ln\epsilon)^{-1}$	$-\epsilon\ln\epsilon$	2ϵ
$\langle a^2\rangle$	$1/3$	$-(2\ln\epsilon)^{-1}$	ϵ	$-2\epsilon^2\ln\epsilon$
τ	$-\frac{3}{8}\ln\epsilon$	$-2\epsilon^{-1}(\ln\epsilon)^{-3}$	$-\frac{1}{2}\epsilon(\ln\epsilon)^3$	$-\frac{8}{3}(\ln\epsilon)^{-1}$

Table 7.2.: Asymptotic behaviour of the moments of the distribution $F(a)$ defined in Eq. (7.41), and resulting asymptotic behaviour of the reduced consensus time τ given by Eq. (7.45) when ϵ tends to zero, for the specific cases $\gamma = 0, 1, 2, 3$.

update attempts, exchanging a and b on all the nodes is equivalent to replace p by $1-p$ in the update rule. One of our main results lies in the observation that the voter model and the Moran process on a pure activity driven network (setting $b = 1$ for all nodes) are in some sense mirror images of their static network counterparts. Indeed, the dynamics of the voter model on an activity driven network with a distribution $F(a)$ is the same as the Moran dynamics running on top of a static network with a degree distribution $P(k) = F(k)$. The same holds for the Moran process on the activity driven network and the voter model on the static network. This implies that the apparently appealing operation consisting in considering an activity driven network and its integrated counterpart as similar substrates for this kind of opinion dynamics process would be misleading, despite the fact that the degree distribution of the integrated network is practically equal to the activity distribution of the temporal network [137]. On the contrary, a pure attractiveness temporal network (setting $a = 1$ for all nodes) and its integrated counterpart are equivalent substrates for the voter and Moran processes. It would be very interesting to check whether similar conclusions hold for other consensus formation processes with more complex update rules like the majority rule process. Our results will hopefully motivate further research in this direction.

8. Random Walks on non-Markovian temporal networks

8.1. Introduction

The exploration and navigation of complex networks represent a challenging scientific problem with a large number of practical applications. The most emblematic example is the World Wide Web (WWW), a colossal database which however acquires a practical interest only if one is able to efficiently locate a specific desired information. These searching processes and the related algorithms in large-scale networks are clearly related to the paradigmatic random walk process diffusing on a given topology [108]. Indeed, the simplest strategy to explore a network is to select a node, to follow randomly one of the departing links to probe one of its neighbours, and to iterate this process until the requested information is found or a satisfying knowledge of the network connectivity is obtained. It is clear that random walks lie at the core of this strategy, and in order to properly implement the search and navigation of a network an accurate knowledge of this process is necessary.

Heterogeneous topologies of complex networks [125] can dramatically impact the properties of dynamical processes running on top of them [17, 44]. Moreover, such dynamical effects, originally studied within the static networks framework, may take an even more complex turn when one considers the inherent time-varying nature of many real networks [73]. Most notably, the burstiness observed in the temporal patterns of social contact networks may further complicate the picture, causing for example an important slowing down in the dynamics of epidemic spreading, diffusion or synchronization processes [83, 92, 175]. Random walks are of course no exception to this state of facts, and one expects noticeable differences with respect to static networks when a time-varying substrate is considered [138, 143]. Particularly noteworthy in this sense is the analysis of the random walk process in activity driven networks. Indeed, the inquiry of the random walk in this class of models, focusing on steady state quantities, reveals striking differences induced by a time-varying topology, with respect to a static one. In particular, the steady state probability for a walker to

be hosted by a node with activity a is inversely proportional to a plus a constant contribution from all the other nodes [138]. On static uncorrelated networks on the other hand, this large time visiting probability is proportional to the degree k of the node [17]. Recalling that for activity driven networks, there is a linear relation between the activity of a node and its degree in the static time-aggregated counterpart, we deduce that the unfolding of a random walk process on a time-varying network yields a totally different result as compared to the outcome of the same process running on top of the static counterpart of the graph, pointing out once more the limits of the static representation of temporal networks.

In this chapter, we naturally extend these investigations by analysing a random walk process on a PLAD0 network, appropriate to investigate the effects of the empirically observed burstiness of social activity. We observe dramatical changes with respect to the activity driven network framework, depending on the exponent α of the waiting time distribution.

8.2. Random walks on non-Markovian activity driven networks

We suppose that the nodes activate according to renewal processes with waiting time distributions $\psi_i(t)$, which can take any form, including a non-Markovian one $\psi_i(t) \sim t^{-\alpha-1}$. The dynamics of a random walk on non-Markovian activity driven networks is defined as follows: A walker arriving at a node j at time t remains on it until an edge is created joining i and other node j at a subsequent time $t' > t$. We consider that the internal clock of the host node is not reset at the walker's arrival, thus defining a *node-centric passive random walk* [108]. The walker then jumps instantaneously to node j and waits there until an edge departing from it is created. To simplify calculations, here we will focus on *directed random walks*: a walker can leave node i only when i becomes active and creates an edge pointing at another node [138]. Once the walker has arrived to node i, it must wait there until i creates a new connection. The dynamics of directed random walks under these restrictions is particularly easy to implement in continuous time and can be directly mapped to a continuous time random walk (CTRW) on a fully connected network in which each node i has a different distribution of waiting times $\psi_i(t)$ [181].

We can obtain information on the time evolution of the random walk by solving it in Laplace space, applying techniques of CTRW and renewal processes [40, 181]. It is important to notice that, although the fundamental quantity defining the dynamics of the network is the inter-event time distribution $\psi_c(t)$, when mapping to an directed CTRW, the relevant quantity is the forward waiting time distribution $h_c(t', t)$, defined as the probability that a walker arriving on a node

with activity c at time t' will be trapped for a time t before escaping from the node. We suppose, for the sake of simplicity, that all the nodes are synchronized at time $t = -t_a < 0$ (i.e., the internal clock of all nodes is reset to zero at time $-t_a$) and that the random walk starts at time $t = 0$ from a node with activity c_0, chosen for gen- erality with probability $H(c_0)$.

To proceed, let us define $P(c, t|c_0)$ as the probability that a walker is at a node with activity c at time t , provided it started its walk at time $t = 0$ on a node with activity c_0. The probability that the walker is at c in time t, independently of its starting point, will thus be

$$P(c, t) = \sum_{c_0} H(c_0)P(c, t|c_0). \tag{8.1}$$

Where H is the initial distribution of the walkers' hosts activity, possibly distinct from η. Let us define also the probability $\Phi_n(c, t|c_0)$ that a walker starting at c_0 has performed n hops at time t, landing at the last hop at a node c. These two probabilities are related by

$$P(c, t|c_0) = \sum_{n=0}^{\infty} \Phi_n(c, t|c_0). \tag{8.2}$$

We obviously have

$$\Phi_0(c, t|c_0) = \tilde{h}_{c_0}(t_a, t)\delta_{c,c_0} \tag{8.3}$$

where $\delta_{c,c'}$ is the Kronecker symbol and we have defined

$$\tilde{h}_c(t_a + t', t - t') = \int_{t-t'}^{\infty} h_c(t_a + t', \tau)\, d\tau \tag{8.4}$$

as the probability that a walker arriving at time t' on a node c has not jumped at time t. To calculate $\Phi_n(c, t|c_0)$ for $n \geq 1$ we make use of a self-consistent condition. Defining $\Psi_n(t|c_0)$ as the probability that the n-th jump of a walker starting at c_0 takes place exactly at time t, we can write

$$\Phi_n(c, t|c_0) = \int_0^t \Psi_n(t'|c_0)\eta(c)\tilde{h}_c(t_a + t', t - t')\, dt'. \tag{8.5}$$

This equation simply expresses the sum of the probabilities of the events in which the walker performs its n-th jump at any time t', arrives in this jump at a node c, given by the probability $\eta(c)$, and rests at that node c for a time larger than $t - t'$. To compute $\Psi_n(t|c_0)$ we apply another self-consistent condition, namely

$$\Psi_n(t|c_0) = \sum_{c'} \int_0^t \Psi_{n-1}(t'|c_0)\eta(c')h_{c'}(t_a + t', t - t')\, dt'. \tag{8.6}$$

This equation implies the $(n - 1)$-th jump taking place at time t', and leading

to a node c', with probability $\eta(c')$, and the last jump taking place, from c', at time $t - t'$. The expression is averaged over all possible values of the activity c' of the intermediate step. The form of Eq. (8.5) and Eq. (8.6) suggests passing to Laplace space to obtain a closed solution. However, the general case is not solvable because of the dependency of the forward waiting time distribution h_c on the epoch of arrival t'. From now on we will suppose that this dependency vanishes, i.e. that $h_c(t_a + t', t - t') = h_c(t - t')$, and in the next sections we will study particular cases for which this condition is fulfilled. Then in the Laplace space we can write Eq. (8.5) as

$$\Phi_n(c, s|c_0) = \eta(c)\Psi_n(s|c_0)\tilde{h}_c(s). \tag{8.7}$$

Eq. (8.6) is also simplified in Laplace space,

$$\Psi_n(s|c_0) = \sum_{c'} \eta(c')\Psi_{n-1}(s|c_0)h_{c'}(s). \tag{8.8}$$

The ensuing iterative equation can be easily solved, yielding

$$\Psi_n(s|c_0) = \left[\sum_{c'} \eta(c')h_{c'}(s)\right]^{n-1} \Psi_1(s|c_0). \tag{8.9}$$

Considering that $\Psi_1(t|c_0) = h_{c_0}(t)$, we can combine Eqs. (8.9) and (8.7) to obtain

$$\Phi_n(c, s|c_0) = \eta(c)\tilde{h}_c(s) \left[\sum_{c'} \eta(c')h_{c'}(s)\right]^{n-1} h_{c_0}(s), \tag{8.10}$$

valid for $n \geq 1$. Combining this last result with Eqs. (8.1), (8.2), and (8.3) , expressed in Laplace space, we obtain the final solution

$$\begin{aligned} P(c, s) &= \sum_{c_0} H(c_0) \sum_{n=0}^{\infty} \Phi_n(c, s|c_0) \\ &= \sum_{c_0} H(c_0)\tilde{h}_{c_0}(s)\delta_{c,c_0} + \eta(c)\tilde{h}_c(s) \sum_{c_0} H(c_0)h_{c_0}(s) \sum_{n=1}^{\infty} \left[\sum_{c'} \eta(c')h_{c'}(s)\right]^{n-1} \\ &= H(c)\tilde{h}_c(s) + \frac{\eta(c)\tilde{h}_c(s) \sum_{c_0} H(c_0)h_{c_0}(s)}{1 - \sum_{c'} \eta(c')h_{c'}(s)}. \end{aligned} \tag{8.11}$$

8.3. Random walk on a PLAD0 network

8.3.1. Random walk on a network with finite average individual interevent time

Let's focus on a NoPAD network with an inter-event time distribution

$$\psi_c(t) = \alpha c(ct+1)^{-(1+\alpha)}, \qquad 1 < \alpha < 2 \tag{8.12}$$

Then for an infinitely aged network, i.e. for $t_a \to +\infty$ the forward recurrence time no longer depends on the ageing time and one has [40]

$$h_c(t) = \frac{1}{\bar{\tau}_c} \int_t^\infty \psi_c(u) du \tag{8.13}$$

where $\bar{\tau}_c = \frac{1}{c(\alpha-1)}$ is the average waiting time between two activations of a node with activity c. In the Laplace space, by virtue of the Tauberian theorem n°1, we can write

$$\psi_c(s) \simeq 1 - \bar{\tau}_c\, s + \frac{\Gamma(2-\alpha)}{\alpha-1}\, c^{-\alpha}\, s^\alpha + o(s^\alpha) \tag{8.14}$$

$$h_c(s) = \frac{1-\psi_c(s)}{\bar{\tau}_c\, s} \simeq 1 - \Gamma(2-\alpha) c^{-(\alpha-1)}\, s^{\alpha-1} + o(s^{\alpha-1}) \tag{8.15}$$

$$\tilde{h}_c(s) = \frac{1-h_c(s)}{s} \simeq \Gamma(2-\alpha) c^{-(\alpha-1)}\, s^{\alpha-2} + o(s^{\alpha-2}) \tag{8.16}$$

Which, combined with (8.11) gives,

$$P(c,s) \simeq \frac{\eta(c) c^{-(\alpha-1)}}{s\langle c^{-(\alpha-1)}\rangle} + o\left(\frac{1}{s}\right) \tag{8.17}$$

so that at large t one finally obtains

$$P(c,t) \simeq \frac{\eta(c) c^{-(\alpha-1)}}{\langle c^{-(\alpha-1)}\rangle} + o(1) \tag{8.18}$$

In order to confirm this result, we perform numerical simulations of the directed random walk on an infinitely aged network with an inter-event time distribution given by Eq. (8.12) and power-law distributed activity $\eta(c) \propto c^{-\gamma}$, where the activity takes values in the interval $[\epsilon, 1]$. For $\alpha > 1$ and $t_a \to \infty$, the distribution of the waiting time between two hops of a walker at a node with activity c reads

$$h_c(t) = (\alpha-1) c\, (ct+1)^{-\alpha}. \tag{8.19}$$

It is worth noting that this distribution is the same as the distribution ψ_c of the inter-event time between two activations of a node with activity c, upon replacing α by $\alpha - 1$. This means that the directed random walk on a network

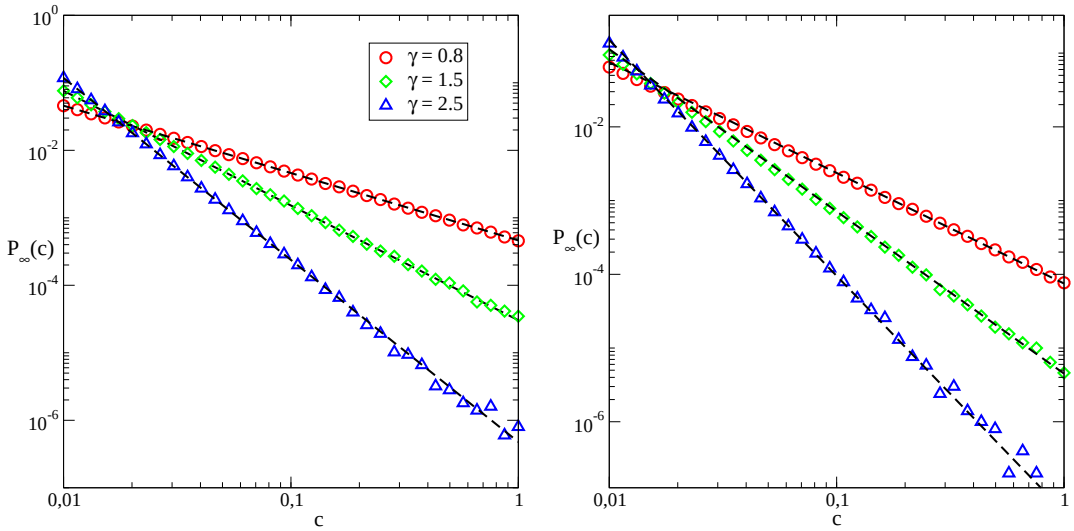

Figure 8.1.: Directed random walk on an infinitely aged network with waiting time distribution of the form Eq. (8.12), for different values of the exponent γ of the activity distribution. Left panel: $\alpha = 1.2$. Right panel $\alpha = 1.7$. The black dashed lines correspond to the analytical result of Eq. (8.18). Number of walkers $N_1 = 5.10^6$, $t = 10^6$ and $\epsilon = 10^{-2}$.

parametrized by $\{\psi, \alpha, \eta, t_a = \infty\}$ is equivalent to a reset directed random walk (i.e. where the nodes are reset when a walker arrives on them, the waiting time until the next activation being counted from the epoch of arrival) parametrized by $\{\psi, \alpha - 1, \eta\}$. This allows us to simplify the numerical analysis, as in the reset random walk framework there is no aging and the links dynamics prior to the beginning of the walkers dynamics is not relevant. On Fig. 8.1 we plot the steady state probability for two different values of α and three different values of γ along with the expected result of Eq. (8.18). We observe a perfect agreement between the simulations and the analytical prediction.

Interestingly, when taking the limit $\alpha \to 2$ in Eq. (8.18), we recover the result established for Poissonian Activity Driven networks, i.e. that $P(c, \infty) = \eta(c)c^{-1}/\langle c^{-1}\rangle$. Besides, for values of $\alpha > 2$, corresponding to a distribution of inter-event times with finite first and second moments, the latter result obviously still holds and the dynamics is the same as that of a random walk running on top of a Poissonian activity driven network. In the literature, the continuous time random walks are generally defined in terms of edge-centric processes [68, 108]. Within this framework the "slowest" dynamics that has been considered is that of an active random walk with power-law waiting time distribution between two link activations with infinite first moment [126]. However, we saw that this scenario is closely related to a particular case of our model, obtained for an infinitely aged network with inter-event time distributed according to Eq. (8.12)

and $1 < \alpha < 2$. In this sense, if we investigate the behaviour of our model for values of $\alpha < 1$, we explore an even slower dynamics that cannot be considered in the context of active random walks. In the next section we will focus on those values of the parameter α.

8.3.2. Network with infinite average individual interevent time

In this section we consider a waiting time distribution ψ of the form (8.12) but with $0 < \alpha < 1$, which implies that the average time between two activations of an agent with activity c is infinite. For such values of α, the dependency of the forward waiting time distribution on the aging time cannot be eliminated even in the limit of strongly aged networks, so that the equations derived in the previous section do not seem to be solvable in a first analysis, in the sense that the use of the Laplace transform does not yield any substantial simplification. Nevertheless, some insight may be given concerning the dynamics of the random walk starting on a strongly aged network. Let us recall the expression of the double Laplace transform of the forward waiting time distribution

$$h_c(u,s) = \frac{1}{1-\psi_c(u)} \frac{\psi_c(u) - \psi_c(s)}{s-u} \tag{8.20}$$

In the hypothesis of a strongly aged network, i.e. for $c\,t_a \gg 1$, corresponding to $\frac{u}{c} \ll 1$, we may write, by virtue of a the Tauberian theorem n°1

$$\psi_c(u) \simeq 1 - (u/c)^\alpha\,\Gamma_{1-\alpha} + o(u^\alpha) \tag{8.21}$$

which, inserted into the expression of the forward waiting time distribution gives

$$h_c(u,s) \simeq \begin{cases} \dfrac{1}{\Gamma_{1-\alpha}} \left(\dfrac{c}{u}\right)^\alpha \dfrac{1-\psi_c(s)}{s} & \text{for } u \ll s \\[2ex] \dfrac{1}{u} - \dfrac{s^\alpha}{u^{\alpha+1}} & \text{for } u \gg s \end{cases} \tag{8.22}$$

we recognize the Laplace transform $(1-\psi_c(s))/s$ of the survival probability $\tilde{\psi}_c(t)$ defined in section 2.4. Using the Tauberian theorem n°2 we derive

$$h_c(t_a,t) \simeq \begin{cases} c\,(c\,t_a)^{\alpha-1}\,\dfrac{sin\pi\alpha}{\pi}\,\tilde{\psi}_c(t) & \text{for } t \ll t_a \\[2ex] t_a^\alpha\,\dfrac{sin\pi\alpha}{\pi}\,t^{-\alpha-1} & \text{for } t \gg t_a \end{cases} \tag{8.23}$$

Given Eq. (8.12) one has $\tilde{\psi}_c(t) = (ct+1)^{-\alpha}$, so that the behaviour of $h_c(t_a, t)$ splits into three different regimes

$$h_c(t_a,t) \simeq \begin{cases} c\,(c\,t_a)^{\alpha-1}\,\dfrac{sin\pi\alpha}{\pi}\,\tilde{\psi}_c(t) & \text{for } c\,t \ll 1 \\ t_a^{\alpha-1}\,\dfrac{sin\pi\alpha}{\pi}\,t^{-\alpha} & \text{for } 1 \ll c\,t \ll c\,t_a \\ t_a^{\alpha}\,\dfrac{sin\pi\alpha}{\pi}\,t^{-\alpha-1} & \text{for } t \gg t_a \end{cases} \tag{8.24}$$

Surprisingly, at large times, i.e. $ct \gg 1$, the forward waiting time distribution is independent of c. Besides, the tail of the distribution is proportional to $t_a^{\alpha}\,t^{-\alpha-1}$, so that the probability that the forward waiting time is greater than t_a is constant and does not depend on t_a. This means that the interval $[t_a, +\infty[$ carries a constant probability weight although its size decreases when t_a grows. This, along with the fact that the total weight is constant and equal to 1 because h_c is normalized, implies that the weight carried in a time window $[0, t_0]$ tends to zero when t_a tends to infinity. In fact, one could argue that the weights calculated from Eq. (8.24) are not exact because they neglect higher order corrections (in particular the distribution in Eq. (8.24) is not normalized). The reasoning is thus true under the implicit assumption that the weights calculated from Eq. (8.24) and carried in the intervals $[0, t_0]$ and $[t_0, +\infty[$ are proportional to their corresponding real weights, which is not guaranteed. On Fig. 8.2(b) we compare the ratio of the real weights $\left[\tilde{h}_c(t_a, 0) - \tilde{h}_c(t_a, t_0)\right] / \tilde{h}_c(t_a, t_0)$, evaluated from a numerical simulation and the ratio evaluated from Eq. (8.24), whose dominant order, with the conditions $1 \ll ct_0 \ll ct_a$, is equal to $\alpha(t_0/t_a)^{1-\alpha}$. We observe a good agreement between the simulations and the analytical estimation, which allows us to make the following reasoning: let us consider a network of size N with waiting time distribution given by Eq. (8.12) with $\alpha < 1$, and an arbitrary activity distribution $\eta(c)$ excluding zero-valued activities. Then there exists a node with a minimum activity $c_{\min} > 0$, and also a time t_0, such that $c_{\min}\,t_0 \gg 1$. Then if the nodes are synchronized at $t = -t_a$ with $t_a \gg t_0$ and we start an directed random walk dynamics at time $t = 0$, the probability that the time t_1 at which the walkers escape from their first hosts is greater than t_0 is almost equal to 1. This holds a fortiori for all the following waiting times of the walker occurring at times $t = t_2, t_3, ..., t_k$ because t_k is extracted from the distribution $h_c(t_a + t_{k-1}, \tau)$. Besides, the conditional probability that $t_1 = \tau$ given that $t_1 \geq t_0$ is independent of c as we see from Eq. (8.24), which means that all the hops for all the walkers are performed with waiting times that practically do not depend on the activity of the hosts.

As a result, after its first jump, the probability that a walker is at a node of activity c is constant and equal to $\eta(c)$. In other words, if the initial distribution

of the walkers is $H(c)$, the probability $P(c,t)$ that the walker is at a node with activity c at time t is equal to $\eta(c)$ if the walker has escaped from its first host and $H(c)$ otherwise, i.e.

$$P(c,t) \simeq H(c)\tilde{h}_c(t_a,t) + \eta(c)(1-\tilde{h}_c(t_a,t)) \tag{8.25}$$

In order to test the validity of this expression, we perform numerical simulations of the directed random walk on a network of size $N = 9.10^4$ where the activity is three-valued: $c = 0.1, 1$ or 10. We consider the simple case for which the probability that a node i has activity c_i is constant and equal to $1/3$ for each of the three possible values of c. The $N_1 = 10^6$ walkers are initially hosted by nodes with activity equal to $c = 10$, i.e. $H(c) = \delta_{c,10}$, and the age of the network is $t_a = 10^3$. The probability $\tilde{h}_c$ is evaluated numerically. On Fig. 8.2, panels (a_1), (a_2) and (a_3) corresponding to $\alpha = 0.2$ and $\alpha = 0.5$ and $\alpha = 0.7$ respectively, we plot the probabilities $[P(c=10,t) - 1/3]/2$, $1/3 - P(c=1,t)$ and $1/3 - P(c=0.1,t)$ along with their expected value $\tilde{h}_{c=1}(t_a,t)/3$ (this last curve is in fact evaluated with an independent numerical simulation). For $\alpha = 0.2$ we observe that the result stated in Eq. (8.25) perfectly fits the simulations, for $\alpha = 0.5$ the fit is not very accurate at large times and for $\alpha = 0.7$ the curves take negative values at large times, at odds with the expected power-law decay, so that the plot is made with a linear vertical axis. The reason why the fit is less accurate for values of α close to 1 is clear if we observe the panel (b) of the figure, which allows us to evaluate the accuracy of the hypothesis we made, stating that the probability that the forward waiting time is less than $t_0 = 10^3$ is almost zero at large t_a. We see that for a network of age $t_a = 10^3$, this probability is even larger than the complementary probability that the waiting time is larger than t_0.

For values of α close to 1, the substrate network needs to be strongly aged in order for the random walk to be correctly described by Eq. (8.25). On the other hand at those values of α the nodes are more active, which renders numerical simulations very costly at large t_a. Although additional simulations would be required to further establish the relevancy of Eq. (8.25), we are confident that finer simulations would corroborate our result.

8.4. Conclusion

In this chapter we have investigated the temporal relaxation of the random walk process on the class of generalized activity driven temporal networks. We have focused in particular in the case of directed random walks, in which a walker can only leave a node when the latter becomes active and creates an outgoing link to another node chosen uniformly at random. As the waiting time between the walker's arrival at a node and the next activation of the node corresponds to the forward waiting time of the renewal process ruling the node's dynam-

ics, the fully passive random walk process we defined is subject to aging effects. In the case of power-law distributions of the holding times with finite first moment, we derive an exact expression, in the Laplace domain, of the probability to find the walker at a node with activity c, for a random walk taking place on a equilibrium (infinitely aged) network. The ensuing steady state probability is subsequently expressed explicitly, and checked with numerical simulations. For infinite average waiting times of the agents, we surprisingly observe that a random walk starting after a large enough time t_a since the beginning of the network dynamics (at which all the nodes are synchronized), will "feel" a network with homogeneous activity, so that the probability that a walker is at a node of activity c is equal to $\eta(c)$ in the large time limit. This result is straightforwardly extended to arbitrary aging times t_a (including non-aged networks $t_a = 0$) because after a transient regime of duration t', the forward waiting time distribution $h_c(t_a + t', \tau)$ will meet the conditions expressed earlier and the system is in the same situation as before, i.e. evolving as if the network was homogeneous. Interestingly, this result is recovered taking the limit $\alpha \to 1$ in the equation Eq. (8.18) of the previous section, providing additional evidence of its relevance.

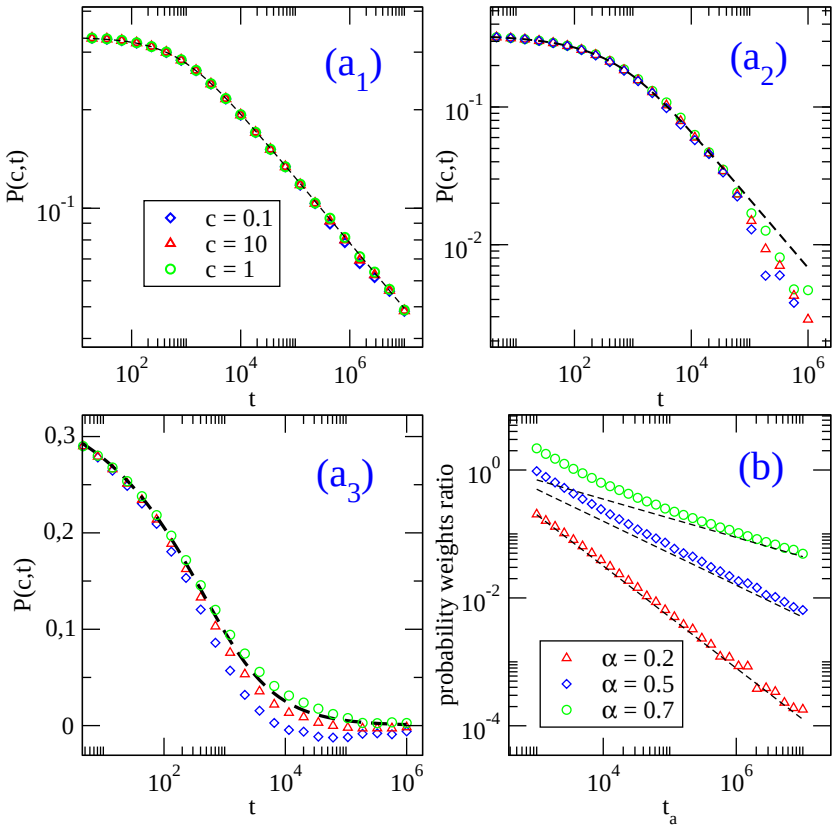

Figure 8.2.: Random walk dynamics on an aged network with three-valued activity and infinite average waiting time. $\eta(c) = 1/3$ and $H(c) = \delta_{c,10}$. In the panels $(\mathrm{a}_{1,2,3})$ we plot the probability of presence $P(c,t)$ as a function of time: $[P(c=10,t) - 1/3]/2$, $1/3 - P(c=1,t)$ and $1/3 - P(c = 0.1, t)$. (a_1): $\alpha = 0.2$. (a_2): $\alpha = 0.5$. (a_3): $\alpha = 0.7$. The behaviour predicted by Eq. (8.25) is plotted in dashed lines. Network size $N = 9.10^4$, number of walkers $N_1 = 10^6$ and aging time $t_a = 10^3$. (b): Ratios $\left[\tilde{h}_c(t_a,0) - \tilde{h}_c(t_a,t_0)\right] / \tilde{h}_c(t_a,t_0)$ as a function of t_a, obtained from numerical simulations. The asymptotes $\alpha(t_0/t_a)^{1-\alpha}$ calculated from Eq. (8.24) are plotted in dashed lines. Reference time $t_0 = 10^3$ and $c = 1$.

Conclusion

The ever increasing availability of large datasets in social science motivated intense scientific investigations that revealed complex patterns of interactions in human dynamics, such as heterogeneity and burstiness of social contacts. These recently uncovered temporal features of social interactions call for a renewed effort in the analysis and modeling of empirical time-vaying networks. I hope to have contributed to pursue this program with the doctoral investigation presented in this manuscript, focusing on a twofold objective: the modeling of dynamical social systems and the study of the impact of non-Markovian substrates on dynamical processes running on top of them. The following is a general summary of the overall content of the manuscript, including perspectives for future work. For more detailed considerations the reader should examine the concluding sections of each chapter.

Firstly, in chapter 1 we defined the basic concepts of the static networks formalism, and we extended some of them to include the temporal evolution of the network. Besides, we also presented the main statistical properties of two real social contact networks, recorded by the SocioPatterns collaboration, the most emblematic of which is the burstiness of human social behaviour, revealed by the heavy tailed distributions of the holding times between consecutive interactions. This fundamental trait of human dynamics motivates the modelling effort presented afterwards, and which constitutes a keystone of my doctoral investigation. Indeed we consider the activity driven network model (expAD0), which defines the nodes in terms of their fundamental rate, or activity, at which they engage into social interaction, and generalize it to arbitrary distributions of the holding times between successive activations of the agents, and in particular the power-law form observed in real temporal social networks. We also consider two pairing mechanisms that go beyond the simplistic assumption of the original activity driven model, for which peers are chosen uniformly at random in the network. The reinforcement rule mimics the empirically observed existence of strong and weak ties among the agents, by setting a different probability for an agent to choose a peer inside or outside the circle of previously encountered neighbours. The introduction of such local memory kernels implies non-Markovian dynamical effects, and is used extensively in chapter 6. We also consider a pairing rule based on the concept of social attractiveness, i.e. the idea that some people are intrinsically socially attractive (due to their status for

example) are more likely to make people connect to them.

In chapter 2, we provide a full mathematical description of the generalized activity driven network with attractiveness (GADA), by means of a mapping of the model onto the class of hidden variables networks. The topological properties of the integrated network, and in particular the degree distribution and the degree-degree correlations are explicitly computed in the case of power-law waiting time distributions with a homogeneous attractiveness (PLAD0 network). Most interestingly, the degree distribution is power-law tailed, and indicates an intimate connection between the scale-free nature of static social networks, and two main characteristics of social temporal networks, namely a power-law distributed waiting time, and a power-law form of the heterogeneity distribution. This connection is quantified in a simple identity relating the three exponents. The generalized activity driven framework constitutes a minimal model of temporal networks with long tailed inter-event time distribution. As such, it has a wide potential to serve as a synthetic controlled environment to check both numerically and analytically several properties of these networks, and in particular the effect of the non-Markovianity on dynamical processes, in much the same way as the configuration model has played this role for static networks. Moreover, due to its simple definition, it can be easily modified to take into account, among others, the finite duration of the social contacts, and the temporal correlations of the individual patterns of activations.

In chapter 3, we studied the connectivity properties of the time-integrated networks emerging from the dynamics of the GAD0 model. As the network grows, a giant cluster spanning a finite fraction of the total size of the network emerges at some time T_p, defining the temporal percolation transition of the network. Applying the branching matrix formalism [62, 162], we derive a general criterion defining implicitly the percolation time and depending on the average and average square number of activations of the agents in the network. This criterion successfully relates the percolation phenomenon, which depends on the connectivity properties of the whole network, to local quantities only, regardless of who is connected to whom. We check the validity of this criterion for a PLAD0 network, and for the particular case of a Levy distribution of the waiting times. This criterion remains a priori valid, although no numerical experiments were conducted to verify it, in the case where the activation pattern of an agent follows a general counting process characterized by the distribution of the number of events counted in a time window $[0, t]$, i.e. when the holding times are not necessarily independently distributed, thus allowing for temporal correlations. Our criterion appears to be a crucial result for the study of the percolation on temporal networks, and we hope that this framework will help understanding how dynamical processes, and in particular epidemic spreading, unfold on time-varying networks.

In the context of empirical inquiry of social networks, an observer has often access to an aggregated static version of a network only. Then in order to infer

the actual contacts sequence that originated the network, a simple assumption, widespread in the literature, is that of a contact pattern following a Poissonian process, and more specifically a description in terms of activity driven temporal networks. In chapter 4 we investigate such a *poissonization* procedure, and in particular we gauge the error made in the estimation of the percolation threshold with this method. When the network under scrutiny is a PLAD0 network, we provide an expression of the estimated percolation time, i.e. the percolation time of the inferred activity driven network, as a function of the average number and average square number of activations in the original network counted in the interval $[0, T]$. Two major observations arise from our study. Firstly, the traditional classification opposing bursty and Poissonian-like behaviour is not entirely relevant, as revealed by the fact that the ratio between the poissonized percolation threshold and the original threshold depends on the early behaviour of the inter-event time distribution of the original network. Secondly, mapping a bursty network with infinite average waiting time onto an activity driven network leads to a dramatic error in the evaluation of the time of birth of a giant connected component in the network. Indeed, in this case the threshold trivially tends to infinity when the observational time T tends to infinity because the activity of the agents of the poissonized network vanishes as T grows. To sum up, our analysis goes along the same lines as what is found in the literature, indicating that the Poissonian model fails to capture the essential ingredients of the network's dynamics, and leads to a misleading picture of the unfolding of dynamical processes running on top of it.

In chapter 5, we analysed a renewal process for which the average holding time between consecutive events is infinite. For such a process, the number of events counted within a time window of fixed length strongly depends on the specific instant at which the observation starts. This statistical effect is called aging of the process. Being structured upon parallel renewal processes of the agents, the generalized activity driven model developed in this thesis is obviously subject to such aging effects. Distinguishing between the strongly aged and the slightly aged regime, we provide effective expressions of the degree distribution of the time-integrated aged PLAD0 network, as a function of the corresponding non-aged degree distribution, i.e. integrated throughout a time window of same length t. Besides, we investigate the percolation of an aged time-integrated GAD0 network. The general criterion derived in chapter 3 giving implicitly the threshold T_p is still valid for aged networks and in the strongly aged regime we derive an explicit asymptotic expression for the percolation time as a function of the aging time. The resulting expression is confirmed by numerical analysis. In a third part, we discuss the poissonization procedure presented in the previous chapter in the presence of aging. It turns out that the main picture of the poissonization method thus remains the same as in the non-aged case, i.e. that assuming a Poissonian dynamics to explain a given time-integrated network structure may lead to a dramatic error in the evaluation of the real percolation

threshold of the network. To sum up, aging effects are inherent to the generalized activity driven model we developed, and affect the structural and connectivity properties of the corresponding time-aggregated network, and subsequently any dynamical process unfolding on top of it.

In chapter 6, we investigated the effects of the individual risk perception of a disease propagating on social temporal networks. In our model, susceptible individuals have a local perception of the overall disease prevalence measured as the ratio of the number of previous contacts with infectious individuals on a training window of width ΔT. An increased level of awareness then induces a reduction in the probability to get infected via a contact with an infectious individual. We have considered the paradigmatic SIS and SIR spreading models on expAD0 networks with random pairing rule, and with the reinforcement pairing rule (expADM), in which the memory kernel mimics some of the non-Markovian effects observed in real social networks. A similar study is conducted for the empirical face-to-face contact networks collected by the SocioPatterns collaboration presented in the first chapter. For both synthetic networks, analytical and numerical results hint that the epidemic threshold on both SIS and SIR models is not changed by the presence of awareness, but very strong finite size effects are present: the effective threshold is increased with the level of awareness, while the epidemic prevalence is substantially decreased. In the case of empirical contact networks, we observe in all cases a similar strong reduction of the prevalence and an apparent shift of the effective epidemic threshold. Notably, the awareness mechanism, even if only local and not assuming any global knowledge of the unfolding of the epidemics, leads to a strong decrease of the prevalence and to shifts in the effective epidemic threshold even at quite large size, in systems as diverse as simple models and empirical data. Moreover, some features of empirical contact networks, such as the broad distribution of contact durations, seem to enhance this effect even for short-term memory awareness. To confirm this statement, we envision to study the risk perception on larger empirical networks, as well as on the GAD model, which exhibits some of the non-Markovian effects observed in empirical networks.

In chapter 7, we have studied in detail the properties of consensus processes mixing the voter and Moran models update rules, on expADA networks. Through a heterogeneous mean-field approach, we derived the average time to reach consensus and the probability that a single agent with a discrepant opinion among an otherwise unanimous population spreads his/her opinion to the whole network, called the exit probability. One of our main results lies in the observation that the voter model and the Moran process on a pure activity driven network (setting $b = 1$ for all nodes) are in some sense mirror images of their static network counterparts. Indeed, the dynamics of the voter model on an activity driven network with a distribution $F(a)$ is the same as the Moran dynamics running on top of a static network with a degree distribution $P(k) = F(k)$. The same holds for the Moran process on the activity driven network and the voter model on the

static network. This implies that the apparently appealing operation consisting in considering an activity driven network and its integrated counterpart as similar substrates for this kind of opinion dynamics process would be misleading, despite the fact that the degree distribution of the integrated network is practically equal to the activity distribution of the temporal network [137]. On the contrary, a pure attractiveness temporal network (setting $a = 1$ for all nodes) and and its integrated counterpart are equivalent substrates for the voter and Moran processes. It would be very interesting to check whether similar conclusions hold for other consensus formation processes with more complex update rules like the majority rule process. Moreover, using the GAD model as a substrate for this voter-like process, in order to take into account the bursty nature of human social behaviour, constitutes in our view an interesting guideline for further research in this direction.

Finally, in chapter 8 we investigated the unfolding of a random walk process on GAD0 networks. We have focused in particular in the case of directed and fully passive random walks, in which a walker does not alter the internal clock of his/her hosts, and can only leave a node when the latter becomes active and creates an outgoing link to another node chosen uniformly at random. In the case of power-law distributions of the holding times with finite first moment, we derive, for infinitely aged networks, the steady state probability for a walker to be at a node with activity c and confirm the result with numerical simulations. For infinite average waiting times of the agents, we surprisingly observe that a random walk starting after a large enough time t_a since the beginning of the network dynamics (at which all the nodes are synchronized), will "feel" a network with homogeneous activity, so that the probability that a walker is at a node of activity c is equal to $\eta(c)$ in the large time limit. This result is straightforwardly extended to arbitrary aging times t_a (including non-aged networks $t_a = 0$) because after a transient regime of duration t', the forward waiting time distribution $h_c(t_a + t', \tau)$ will meet the conditions expressed earlier and the system is in the same situation as before, i.e. evolving as if the network was homogeneous. Interestingly, this result is recovered taking the limit $\alpha \to 1$ in the equation Eq. (8.18) of the previous section, providing additional evidence of its relevance.

The investigation of non-Markovian effects on temporal network is still in its infancy. In this thesis we have proposed a relatively simple model that allows to evaluate the impact of non-Markovian contact sequences on different dynamical processes running on top of the network, providing new insights into the field of social temporal networks. We hope that our work will motivate further efforts in that direction, taking the models to more realistic levels, and possibly bridging with other field of research involving dynamical networked systems.

Bibliography

[1] Bonnie A. Nardi and Steve Whittaker. "The Place of Face-to-Face Communication in Distributed Work". In: (2001), pp. 83–110 (cit. on p. 21).

[2] Lada A. Adamic and Natalie Glance. "The Political Blogosphere and the 2004 U.S. Election: Divided They Blog". In: *Proceedings of the 3rd International Workshop on Link Discovery*. LinkKDD '05. Chicago, Illinois: ACM, 2005, pp. 36–43. ISBN: 1-59593-215-1. DOI: 10.1145/1134271.1134277. URL: http://doi.acm.org/10.1145/1134271.1134277 (cit. on p. 21).

[3] O. Al Hammal, H. Chaté, I. Dornic, et al. "Langevin description of critical phenomena with two symmetric absorbing states". In: *Phys. Rev. Lett.* 94 (2005), p. 230601 (cit. on p. 15).

[4] Roy M. Anderson and Robert McCredie May. *Infectious diseases of humans: dynamics and control*. Oxford, New York: Oxford University Press, 1991 (cit. on p. 80).

[5] T. Antal, S. Redner, and V. Sood. "Evolutionary Dynamics on Degree-Heterogeneous Graphs". In: *Phys. Rev. Lett.* 96 (2006), p. 188104 (cit. on p. 15).

[6] H. Arrow, J.E. McGrath, and J.L. Berdahl. *Small Groups as Complex Systems: Formation, Coordination, Development, and Adaptation*. SAGE Publications, 2000. ISBN: 9780803972308. URL: https://books.google.fr/books?id=_UhbhVvGeQQC (cit. on p. 21).

[7] Susan Athey, Emilio Calvano, and Saumitra Jha. *A Theory of Community Formation and Social Hierarchy*. CSEF Working Papers. Centre for Studies in Economics and Finance (CSEF), University of Naples, Italy, 2016. URL: https://EconPapers.repec.org/RePEc:sef:csefwp:451 (cit. on p. 26).

[8] Ellison Nicole B., Steinfield Charles, and Lampe Cliff. "The Benefits of Facebook "Friends:" Social Capital and College Students' Use of Online Social Network Sites". In: *Journal of Computer-Mediated Communication* 12.4 (), pp. 1143–1168. DOI: 10.1111/j.1083-6101.2007.00367.x. eprint: https://onlinelibrary.wiley.com/doi/pdf/10.1111/j.1083-6101.2007.00367.x. URL: https://onlinelibrary.wiley.com/doi/abs/10.1111/j.1083-6101.2007.00367.x (cit. on p. 21).

[9] F. Bagnoli, P. Lio, and L. Sguanci. "Risk perception in epidemic modeling". In: *Phys Rev E* 76 (2007), p. 061904 (cit. on pp. 81, 83).

[10] Paolo Bajardi, Alain Barrat, Fabrizio Natale, et al. "Dynamical Patterns of Cattle Trade Movements". In: *PLoS ONE* 6.5 (May 2011), e19869. DOI: 10.1371/journal.pone.0019869 (cit. on p. 15).

[11] A.-L. Barabàsi. "The origin of bursts and heavy tails in human dynamics". In: *Nature* 435 (2005), p. 207 (cit. on pp. 15, 80).

[12] A.L. Barabási. *Bursts: the hidden patterns behind everything we do, from your e-mail to bloody crusades*. Plume, 2011. URL: https://books.google.fr/books?id=4pfZswEACAAJ (cit. on p. 21).

[13] Albert-László Barabási and R. Albert. "Emergence of scaling in random networks". In: *Science* 286 (1999), pp. 509–512 (cit. on pp. 14, 23, 28, 101).

[14] Eli Barkai and Yuan-Chung Cheng. "Aging continuous time random walks". en. In: *J. Chem. Phys.* 118.14 (2003), p. 6167. ISSN: 00219606. DOI: 10.1063/1.1559676. URL: http://scitation.aip.org/content/aip/journal/jcp/118/14/10.1063/1.1559676 (cit. on pp. 15, 69).

[15] Andrea Baronchelli, Claudio Castellano, and Romualdo Pastor-Satorras. "Voter models on weighted networks". In: *Phys. Rev. E* 83 (2011), p. 066117 (cit. on p. 101).

[16] A. Barrat, C. Cattuto, A. E. Tozzi, et al. "Measuring contact patterns with wearable sensors: methods, data characteristics and applications to data-driven simulations of infectious diseases". In: *Clinical Microbiology and Infection* 20.1 (2014), pp. 10–16 (cit. on pp. 80, 83).

[17] Alain Barrat, Marc Barthelemy, and Alessandro Vespignani. *Dynamical processes on complex networks*. Cambridge University Press (Cambridge), 2008 (cit. on pp. 14, 16, 46, 80, 84, 101, 103, 118, 119).

[18] N.H. Bingham and R.A. Doney. "Asymptotic properties of supercritical branching processes I: The Galton-Watson process". In: *Advances in Applied Probability* 112 (1974), pp. 489–524 (cit. on p. 153).

[19] W.R. BION. *Experiences in Groups AND OTHER PAPERS*. 1961. URL: https://books.google.fr/books?id=OmYLQq47k6cC (cit. on p. 21).

[20] Marián Boguñá and Romualdo Pastor-Satorras. "Class of correlated random networks with hidden variables". In: *Phys. Rev. E* 68 (2003), p. 036112 (cit. on pp. 25, 30, 31, 33, 34).

[21] M. Boguñá, C. Castellano, and R. Pastor-Satorras. "Nature of the Epidemic Threshold for the Susceptible-Infected-Susceptible Dynamics in Networks". In: *Phys. Rev. Lett.* 111 (2013), p. 068701 (cit. on p. 83).

[22] D. Brockmann, L. Hufnagel, and T. Geisel. "The scaling laws of human travel". In: *Nature* 439 (2006), 462 EP –. URL: http://dx.doi.org/10.1038/nature04292 (cit. on p. 21).

[23] W. Van den Broeck, C. Cattuto, A. Barrat, et al. "The Live Social Semantics application: a platform for integrating face-to-face presence with on-line social networking". In: *2010 8th IEEE International Conference on Pervasive Computing and Communications Workshops (PERCOM Workshops)*. 2010, pp. 226–231. DOI: 10.1109/PERCOMW.2010.5470665 (cit. on p. 23).

[24] G. Caldarelli. *Scale-Free Networks: Complex Webs in Nature and Technology*. Oxford: Oxford University Press, 2007 (cit. on p. 80).

[25] G. Caldarelli, A. Capocci, P. De Los Rios, et al. "Scale-Free Networks from Varying Vertex Intrinsic Fitness". In: *Phys. Rev. Lett.* 89 (25 2002), p. 258702. DOI: 10.1103/PhysRevLett.89.258702. URL: http://link.aps.org/doi/10.1103/PhysRevLett.89.258702 (cit. on pp. 25, 31).

[26] D S Callaway, M E Newman, S H Strogatz, et al. "Network robustness and fragility: percolation on random graphs." In: *Physical review letters* 85.25 (Dec. 2000), pp. 5468–71. ISSN: 0031-9007. URL: http://www.ncbi.nlm.nih.gov/pubmed/11136023 (cit. on pp. 45, 46).

[27] Cao, Lang. "Infection dynamics in structured populations with disease awareness based on neighborhood contact history". In: *Eur. Phys. J. B* 87.10 (2014), p. 225. DOI: 10.1140/epjb/e2014-50422-8. URL: http://dx.doi.org/10.1140/epjb/e2014-50422-8 (cit. on p. 81).

[28] J. L. Cardy, ed. *Finite Size Scaling*. Vol. 2. Current Physics-Sources and Comments. Amsterdam: North Holland, 1988 (cit. on p. 89).

[29] Daniel P. Carpenter, Kevin M. Esterling, and David M. J. Lazer. "Friends, Brokers, and Transitivity: Who Informs Whom in Washington Politics?" In: *The Journal of Politics* 66.1 (2004), pp. 224–246. ISSN: 00223816, 14682508. URL: http://www.jstor.org/stable/10.1046/j.1468-2508.2004.00149.x (cit. on p. 21).

[30] C. Castellano, S. Fortunato, and V. Loreto. "Statistical physics of social dynamics". In: *Rev. Mod. Phys.* 81 (2009), pp. 591–646 (cit. on p. 101).

[31] C. Castellano, V. Loreto, A. Barrat, et al. "Comparison of Voter and Glauber dynamics on networks". In: *Phys. Rev. E* 71 (2005), p. 066107 (cit. on p. 15).

[32] Claudio Castellano and Romualdo Pastor-Satorras. "Thresholds for Epidemic Spreading in Networks". In: *Phys. Rev. Lett.* 105 (21 2010), p. 218701. DOI: 10.1103/PhysRevLett.105.218701 (cit. on p. 17).

[33] Claudio Castellano and Romualdo Pastor-Satorras. "On the numerical study of percolation and epidemic critical properties in networks". In: *Eur. Phys. J. B* 89.11 (2016), p. 243. DOI: 10.1140/epjb/e2016-60953-5. URL: https://doi.org/10.1140/epjb/e2016-60953-5 (cit. on p. 83).

[34] Ciro Cattuto, Wouter Van den Broeck, Alain Barrat, et al. "Dynamics of Person-to-Person Interactions from Distributed RFID Sensor Networks". In: *PLoS ONE* 5 (2010), e11596 (cit. on pp. 15, 19, 21, 56).

[35] Ciro Cattuto, Wouter Van den Broeck, Alain Barrat, et al. "Dynamics of Person-to-Person Interactions from Distributed RFID Sensor Networks". In: *PLoS ONE* 5.7 (2010), e11596. DOI: 10.1371/journal.pone.0011596. (Visited on 01/03/2016) (cit. on p. 80).

[36] Damon Centola. "The Spread of Behavior in an Online Social Network Experiment". In: *Science* 329.5996 (2010), pp. 1194–1197 (cit. on p. 21).

[37] R. Cohen, S. Havlin, and D. ben Avraham. "Efficient Immunization Strategies for Computer Networks and Populations". In: *Phys. Rev. Lett.* 91 (2003), p. 247901 (cit. on p. 81).

[38] E.R. Colman and D. Vukadinovic. In: *Phys. Rev. E* 92 (2015), p. 012817 (cit. on p. 26).

[39] Álvaro Corral. "Long-Term Clustering, Scaling, and Universality in the Temporal Occurrence of Earthquakes". In: *Physical Review Letters* 92 (Mar. 2004), pp. 108501+. DOI: 10.1103/physrevlett.92.108501. URL: http://dx.doi.org/10.1103/physrevlett.92.108501 (cit. on p. 15).

[40] D. R. Cox. *Renewal Theory*. London: Methuen, 1967 (cit. on pp. 26, 35, 44, 119, 122).

[41] Andrea Cuttone, Sune Lehmann, and Jakob Eg Larsen. "A Mobile Personal Informatics System with Interactive Visualizations of Mobility and Social Interactions". In: *Proceedings of the 1st ACM International Workshop on Personal Data Meets Distributed Multimedia*. PDM '13. Barcelona, Spain: ACM, 2013, pp. 27–30. ISBN: 978-1-4503-2397-0. DOI: 10.1145/2509352.2509397. URL: http://doi.acm.org/10.1145/2509352.2509397 (cit. on p. 21).

[42] G. Doherty-Sneddon, A.H. Anderson, C. O'Malley, et al. "Face-to-face and video mediated communication: a comparison of dialogue structure and task performance". In: *Journal of Experimental Psychology: Applied* 3.2 (1997), pp. 105–125. URL: http://eprints.gla.ac.uk/30075/ (cit. on p. 21).

[43] S. N. Dorogovtsev. *Lectures on complex networks*. Oxford Master Series in Physics. Oxford: Oxford University Press, 2010 (cit. on p. 14).

[44] S. N. Dorogovtsev, A. V. Goltsev, and J .F. F. Mendes. "Critical phenomena in complex networks". In: *Rev. Mod. Phys.* 80 (2008), pp. 1275–1335 (cit. on pp. 14, 103, 118).

[45] S. N. Dorogovtsev and J. F. F. Mendes. "Evolution of networks". In: *Advances in Physics* 51 (2002), pp. 1079–1187 (cit. on p. 112).

[46] S. N. Dorogovtsev and J. F. F. Mendes. *Evolution of networks: From biological nets to the Internet and WWW*. Oxford: Oxford University Press, 2003 (cit. on p. 23).

[47] S. N. Dorogovtsev, J. F. F. Mendes, and A. N. Samukhin. "Structure of growing networks with preferential linking". In: *Phys. Rev. Lett.* 85 (2000), pp. 4633–4636 (cit. on p. 23).

[48] B. Drossel. "Biological evolution and statistical physics". In: *Advances in Physics* 50.2 (2001), pp. 209–295 (cit. on p. 101).

[49] Nathan Eagle, Alex (Sandy) Pentland, and David Lazer. "Inferring friendship network structure by using mobile phone data". In: *Proceedings of the National Academy of Sciences* 106.36 (2009), pp. 15274–15278. ISSN: 0027-8424. DOI: 10.1073/pnas.0900282106. eprint: http://www.pnas.org/content/106/36/15274.full.pdf. URL: http://www.pnas.org/content/106/36/15274 (cit. on p. 21).

[50] Nathan Eagle and Alex (Sandy) Pentland. "Reality Mining: Sensing Complex Social Systems". In: *Personal Ubiquitous Comput.* 10.4 (2006), pp. 255–268. ISSN: 1617-4909. DOI: 10.1007/s00779-005-0046-3. URL: http://dx.doi.org/10.1007/s00779-005-0046-3 (cit. on p. 21).

[51] P. Erdös and P. Rényi. "On random graphs". In: *Publicationes Mathematicae* 6 (1959), pp. 290–297 (cit. on p. 23).

[52] Peter G. Fennell, Sergey Melnik, and James P. Gleeson. "Limitations of discrete-time approaches to continuous-time contagion dynamics". In: *Phys. Rev. E* 94 (5 2016), p. 052125. DOI: 10.1103/PhysRevE.94.052125. URL: https://link.aps.org/doi/10.1103/PhysRevE.94.052125 (cit. on p. 82).

[53] J. Fernández-Gracia, V. M. Eguíluz, and Maxi San Miguel. "Update rules and interevent time distributions: Slow ordering versus no ordering in the voter model". In: *Phys. Rev. E* 84.1 (2011), p. 015103. ISSN: 1539-3755. DOI: 10.1103/PhysRevE.84.015103. URL: http://link.aps.org/doi/10.1103/PhysRevE.84.015103 (cit. on p. 102).

[54] Julie Fournet and Alain Barrat. "Contact Patterns among High School Students". In: *PLOS ONE* 9.9 (Sept. 2014), pp. 1–17. DOI: 10.1371/journal.pone.0107878 (cit. on p. 22).

[55] S. Funk, M. Salathé, and V.A.A. Jansen. "Modelling the influence of human behaviour on the spread of infectious diseases: a review". In: *J R Soc Interface* 7 (2010), pp. 1247–1256 (cit. on p. 81).

[56] F. R. Gantmacher. *The Theory of Matrices*. Vol. II. New York: Chelsea Publishing Company, 1959 (cit. on p. 47).

[57] C. Gardiner. *Stochastic Methods: A Handbook for the Natural and Social Sciences*. 4th. Berlin: Springer-Verlag, 2010 (cit. on p. 107).

[58] Aurelien Gautreau, Alain Barrat, and Marc Barthélemy. "Microdynamics in stationary complex networks". In: *Proceedings of the National Academy of Sciences* 106.22 (2009), pp. 8847–8852. ISSN: 0027-8424. DOI: 10.1073/pnas.0811113106. eprint: http://www.pnas.org/content/106/22/8847.full.pdf. URL: http://www.pnas.org/content/106/22/8847 (cit. on p. 24).

[59] Laetitia Gauvin, André Panisson, and Ciro Cattuto. "Detecting the community structure and activity patterns of temporal networks: a non-negative tensor factorization approach". In: *PLoS ONE* 9.1 (2014) (cit. on pp. 56, 99).

[60] Daniel T. Gillespie. "Exact stochastic simulation of coupled chemical reactions". In: *The journal of physical chemistry* 81.25 (1977), pp. 2340–2361. URL: http://pubs.acs.org/doi/abs/10.1021/j100540a008 (visited on 04/25/2013) (cit. on p. 110).

[61] C. Godrèche and J.M. Luck. "Statistics of the occupation time of renewal processes". In: *Journal of Statistical Physics* 104 (2001), pp. 711–731 (cit. on pp. 40, 61, 69).

[62] A. V. Goltsev, S. N. Dorogovtsev, and J. F. F. Mendes. "Percolation on correlated networks". In: *Phys. Rev. E* 78 (5 2008), p. 051105. DOI: 10.1103/PhysRevE.78.051105. URL: http://link.aps.org/doi/10.1103/PhysRevE.78.051105 (cit. on pp. 47, 55, 130).

[63] Marta C. Gonzalez, Cesar A. Hidalgo, and Albert-Laszlo Barabasi. "Understanding individual human mobility patterns". In: *Nature* 453.7196 (June 2008), pp. 779–782 (cit. on pp. 15, 21).

[64] Clara Granell, Sergio Gómez, and Alex Arenas. "Dynamical Interplay between Awareness and Epidemic Spreading in Multiplex Networks". In: *Physical Review Letters* 111.12 (Sept. 2013), p. 128701. ISSN: 0031-9007. DOI: 10.1103/PhysRevLett.111.128701 (cit. on p. 81).

[65] Thilo Gross and Bernd Blasius. "Adaptive coevolutionary networks: a review". In: *Journal of The Royal Society Interface* 5.20 (2008), pp. 259–271. ISSN: 1742-5689. DOI: 10.1098/rsif.2007.1229 (cit. on p. 81).

[66] Alison L. Hill, David G. Rand, Martin A. Nowak, et al. "Infectious Disease Modeling of Social Contagion in Networks". In: *PLoS Comput Biol* 6.11 (Nov. 2010), e1000968– (cit. on p. 20).

[67] Scott A. Hill and Dan Braha. "Dynamic model of time-dependent complex networks". In: *Phys. Rev. E* 82 (4 2010), p. 046105. DOI: 10.1103/PhysRevE.82.046105. URL: https://link.aps.org/doi/10.1103/PhysRevE.82.046105 (cit. on p. 24).

[68] Till Hoffmann, Mason A. Porter, and Renaud Lambiotte. "Generalized master equations for non-Poisson dynamics on networks". In: *Physical Review E* 86.4 (Oct. 2012), p. 046102. (Visited on 10/01/2013) (cit. on pp. 15, 123).

[69] P. Holme. In: *PLoS Comput Biol* 9 (2013), e1003142 (cit. on p. 26).

[70] "Temporal networks". In: ed. by P. Holme and J. Saramäki. Berlin: Springer, 2013 (cit. on pp. 14, 15, 19, 20, 22, 24).

[71] Petter Holme. "Network reachability of real-world contact sequences". In: *Phys. Rev. E* 71 (4 2005), p. 046119 (cit. on pp. 15, 24).

[72] Petter Holme. "Modern temporal network theory: a colloquium". In: *The European Physical Journal B* 88.9 (2015), p. 234. ISSN: 1434-6036. DOI: 10.1140/epjb/e2015-60657-4 (cit. on p. 80).

[73] Petter Holme and Jari Saramäki. "Temporal networks". In: *Physics Reports* 519 (2012), pp. 97–125 (cit. on pp. 56, 118).

[74] Petter Holme and Jari Saramäki. "Temporal networks". In: *Physics Reports* 519.3 (2012), pp. 97 –125. ISSN: 0370-1573. DOI: http://dx.doi.org/10.1016/j.physrep.2012.03.001. URL: http://www.sciencedirect.com/science/article/pii/S0370157312000841 (cit. on p. 80).

[75] Bernardo Huberman, Daniel Romero, and Fang Wu. "Social networks that matter: Twitter under the microscope". In: *First Monday* 14.1 (2008). ISSN: 13960466. DOI: 10.5210/fm.v14i1.2317. URL: http://firstmonday.org/ojs/index.php/fm/article/view/2317 (cit. on p. 21).

[76] Pan Hui, Augustin Chaintreau, James Scott, et al. "Pocket switched networks and human mobility in conference environments". In: *WDTN '05: Proceedings of the 2005 ACM SIGCOMM workshop on Delay-tolerant networking*. Philadelphia, Pennsylvania, USA: ACM, 2005, pp. 244–251. ISBN: 1-59593-026-4. DOI: http://doi.acm.org/10.1145/1080139.1080142 (cit. on pp. 15, 24).

[77] José Iribarren and Esteban Moro. "Impact of Human Activity Patterns on the Dynamics of Information Diffusion". In: *Physical Review Letters* 103.3 (July 2009), p. 038702. ISSN: 0031-9007. DOI: 10.1103/PhysRevLett.103.038702. URL: http://link.aps.org/doi/10.1103/PhysRevLett.103.038702 (cit. on p. 56).

[78] Lorenzo Isella, Juliette Stehlé, Alain Barrat, et al. "What's in a crowd? Analysis of face-to-face behavioral networks". In: *J. Theor. Biol* 271 (2011), p. 166 (cit. on pp. 15, 20, 23).

[79] M. Jackson. *Social and Economic Networks*. Princeton: Princeton University Press, 2010 (cit. on pp. 21, 30).

[80] Howard E. Jensen. "Interaction Process Analysis: A Method for the Study of Small Groups." In: *Social Forces* 29.3 (1951), pp. 329–330. DOI: 10.2307/2572427. eprint: /oup/backfile/content_public/journal/sf/29/3/10.2307/2572427/2/29-3-329.pdf. URL: http://dx.doi.org/10.2307/2572427 (cit. on p. 21).

[81] Hang-Hyun Jo, Márton Karsai, János Kertész, et al. "Circadian pattern and burstiness in mobile phone communication". In: *New Journal of Physics* 14.1 (2012), p. 013055. URL: http://stacks.iop.org/1367-2630/14/i=1/a=013055 (cit. on p. 15).

[82] Hang-Hyun Jo, Raj Kumar Pan, and Kimmo Kaski. "Emergence of Bursts and Communities in Evolving Weighted Networks". In: *PLoS ONE* 6 (2011), e22687 (cit. on p. 15).

[83] Hang-Hyun Jo, Juan I. Perotti, Kimmo Kaski, et al. "Analytically Solvable Model of Spreading Dynamics with Non-Poissonian Processes". In: *Phys. Rev. X* 4 (1 2014), p. 011041 (cit. on p. 118).

[84] Fariba Karimi and Petter Holme. "Threshold model of cascades in empirical temporal networks". In: *Physica A: Statistical Mechanics and its Applications* 392.16 (Aug. 2013), pp. 3476–3483. ISSN: 03784371. DOI: 10.1016/j.physa.2013.03.050. URL: http://linkinghub.elsevier.com/retrieve/pii/S0378437113002835 (cit. on p. 102).

[85] M. Karsai, M. Kivelä, R. K. Pan, et al. "Small but slow world: How network topology and burstiness slow down spreading". In: *Phys. Rev. E* 83 (2 2011), p. 025102. DOI: 10.1103/PhysRevE.83.025102. URL: http://link.aps.org/doi/10.1103/PhysRevE.83.025102 (cit. on pp. 15, 80).

[86] M. Karsai, M. Kivelä, R. K. Pan, et al. "Small but slow world: How network topology and burstiness slow down spreading". In: *Phys. Rev. E* 83 (2011), p. 025102 (cit. on pp. 28, 56).

[87] Márton Karsai, Kimmo Kaski, Albert-László Barabási, et al. "Universal features of correlated bursty behaviour". In: *Scientific Reports* 2 (2012). Article, 397 EP –. URL: http://dx.doi.org/10.1038/srep00397 (cit. on p. 16).

[88] Márton Karsai, Nicola Perra, and Alessandro Vespignani. "Time varying networks and the weakness of strong ties." In: *Sci Rep* 4 (2014), p. 4001. DOI: 10.1038/srep04001 (cit. on pp. 24, 56).

[89] Márton Karsai, Nicola Perra, and Alessandro Vespignani. "Time varying networks and the weakness of strong ties". In: *Scientific Reports* 4 (2014), 4001 EP –. URL: http://dx.doi.org/10.1038/srep04001 (cit. on p. 28).

[90] Matthew James Keeling and Pejman Rohani. *Modeling Infectious Diseases in Humans and Animals*. Princeton: Princeton University Press, 2008 (cit. on p. 80).

[91] Takehito Kemuriyama, Hiroyuki Ohta, Yoshiaki Sato, et al. "A power-law distribution of inter-spike intervals in renal sympathetic nerve activity in salt-sensitive hypertension-induced chronic heart failure". In: *Biosystems* 101.2 (2010), pp. 144–147. DOI: 10.1016/j.biosystems.2010.06.002. URL: http://dx.doi.org/10.1016/j.biosystems.2010.06.002 (cit. on p. 16).

[92] M. Kivela, R. Kumar Pan, K. Kaski, et al. "Multiscale Analysis of Spreading in a Large Communication Network". In: *J. Stat. Mech.* (2012), P03005 (cit. on pp. 15, 118).

[93] J. Klafter and I.M. Sokolov. *First Steps in Random Walks: From Tools to Applications*. Oxford: Oxford University Press, 2011 (cit. on pp. 32, 40, 53).

[94] Bhushan Kotnis and Joy Kuri. "Stochastic analysis of epidemics on adaptive time varying networks". In: *Phys. Rev. E* 87 (6 2013), p. 062810. DOI: 10.1103/PhysRevE.87.062810. URL: http://link.aps.org/doi/10.1103/PhysRevE.87.062810 (cit. on p. 81).

[95] P.L Krapivsky, S. Redner, and E. Ben-Naim. *A Kinetic View of Statistical Physics*. Cambridge: Cambridge University Press, 2010 (cit. on p. 106).

[96] Gautier Krings, Márton Karsai, Sebastian Bernhardsson, et al. "Effects of time window size and placement on the structure of an aggregated communication network". In: *EPJ Data Science* 1.4 (2012), pp. 1–16 (cit. on p. 20).

[97] Haewoon Kwak, Changhyun Lee, Hosung Park, et al. "What is Twitter, a Social Network or a News Media?" In: *Proceedings of the 19th International Conference on World Wide Web*. WWW '10. Raleigh, North Carolina, USA: ACM, 2010, pp. 591–600. ISBN: 978-1-60558-799-8. DOI: 10.1145/1772690.1772751. URL: http://doi.acm.org/10.1145/1772690.1772751 (cit. on p. 21).

[98] David Lazer. "Networks in Political Science: Back to the Future". In: *PS: Political Science and Politics* 44.1 (2011), 61–68. DOI: 10.1017/S1049096510001873 (cit. on p. 21).

[99] B. Lepri, J. Staiano, G. Rigato, et al. "The SocioMetric Badges Corpus: A Multilevel Behavioral Dataset for Social Behavior in Complex Organizations". In: *2012 International Conference on Privacy, Security, Risk and Trust and 2012 International Confernece on Social Computing*. 2012, pp. 623–628. DOI: 10.1109/SocialCom-PASSAT.2012.71 (cit. on p. 21).

[100] Mingwu Li and Harry Dankowicz. "Impact of temporal network structures on the speed of consensus formation in opinion dynamics". In: *arXiv preprint arXiv:1804.03525* (2018) (cit. on p. 102).

[101] T. M. Liggett. *Interacting Particle Systems*. New York: Springer-Verlag, 1985 (cit. on p. 101).

[102] Fredrik Liljeros, Christofer R. Edling, Luís A. Nunes Amaral, et al. "The web of human sexual contacts". en. In: *Nature* 411.6840 (June 2001), pp. 907–908. ISSN: 0028-0836. DOI: 10.1038/35082140. URL: http://www.nature.com/nature/journal/v411/n6840/full/411907a0.html (visited on 03/14/2013) (cit. on pp. 14, 21).

[103] Suyu Liu, Nicola Perra, Márton Karsai, et al. "Controlling Contagion Processes in Activity Driven Networks". In: *Physical Review Letters* 112.11 (2014), p. 118702. ISSN: 0031-9007. DOI: 10.1103/PhysRevLett.112.118702. URL: http://arxiv.org/abs/1309.7031http://www.arxiv.org/pdf/1309.7031.pdfhttp://link.aps.org/doi/10.1103/PhysRevLett.112.118702 (cit. on pp. 25, 90).

[104] Anna Machens, Francesco Gesualdo, Caterina Rizzo, et al. "An infectious disease model on empirical networks of human contact: bridging the gap between dynamic network data and contact matrices". In: *BMC Infectious Diseases* 13.1 (2013), p. 185. ISSN: 1471-2334. DOI: 10.1186/1471-2334-13-185. URL: http://www.biomedcentral.com/1471-2334/13/185 (cit. on pp. 56, 80).

[105] A.V. Mantzaris and D.J. Higham. In: *Eur. J. Appl. Math.* 23 (2012), p. 659 (cit. on p. 26).

[106] Emanuele Massaro and Franco Bagnoli. "Epidemic spreading and risk perception in multiplex networks: A self-organized percolation method". In: *Phys. Rev. E* 90 (5 2014), p. 052817. DOI: 10.1103/PhysRevE.90.052817. URL: http://link.aps.org/doi/10.1103/PhysRevE.90.052817 (cit. on p. 81).

[107] Naoki Masuda, N. Gibert, and S. Redner. "Heterogeneous voter models". In: *Phys. Rev. E* 82.1 (2010), p. 010103. DOI: 10.1103/PhysRevE.82.010103 (cit. on p. 101).

[108] Naoki Masuda, Mason A. Porter, and Renaud Lambiotte. "Random walks and diffusion on networks". In: *Physics Reports* 716-717 (2017). Random walks and diffusion on networks, pp. 1 –58. ISSN: 0370-1573. DOI: https://doi.org/10.1016/j.physrep.2017.07.007. URL: http://www.sciencedirect.com/science/article/pii/S0370157317302946 (cit. on pp. 76, 118, 119, 123).

[109] Angélica Sousa da Mata and Romualdo Pastor-Satorras. "Slow relaxation dynamics and aging in random walks on activity driven temporal networks". English. In: *The European Physical Journal B* 88.2, 12 (2015). ISSN: 1434-6028 (cit. on pp. 15, 25).

[110] Angélica S. Mata, Marian Boguñá, Claudio Castellano, et al. "Lifespan method as a tool to study criticality in absorbing-state phase transitions". In: *Phys. Rev. E* 91 (5 2015), p. 052117. DOI: 10.1103/PhysRevE.91.052117 (cit. on p. 83).

[111] Matúš Medo, Giulio Cimini, and Stanislao Gualdi. "Temporal Effects in the Growth of Networks". en. In: *Physical Review Letters* 107.23 (Dec. 2011). ISSN: 0031-9007, 1079-7114. (Visited on 01/19/2015) (cit. on p. 79).

[112] Giovanna Miritello, Esteban Moro, and Rubén Lara. "Dynamical strength of social ties in information spreading". In: *Phys. Rev. E* 83 (4 2011), p. 045102. DOI: 10.1103/PhysRevE.83.045102. URL: http://link.aps.org/doi/10.1103/PhysRevE.83.045102 (cit. on pp. 15, 56).

[113] Delia Mocanu, Andrea Baronchelli, Nicola Perra, et al. "The Twitter of Babel: Mapping World Languages through Microblogging Platforms". In: *PLOS ONE* 8.4 (2013), pp. 1–9. DOI: 10.1371/journal.pone.0061981. URL: https://doi.org/10.1371/journal.pone.0061981 (cit. on p. 21).

[114] Antoine Moinet, Romualdo Pastor-Satorras, and Alain Barrat. "Effect of risk perception on epidemic spreading in temporal networks". In: *Phys. Rev. E* 97 (1 2018), p. 012313. DOI: 10.1103/PhysRevE.97.012313. URL: https://link.aps.org/doi/10.1103/PhysRevE.97.012313 (cit. on p. 13).

[115] Antoine Moinet, Michele Starnini, and Romualdo Pastor-Satorras. "Burstiness and Aging in Social Temporal Networks". In: *Phys. Rev. Lett.* 114 (10 2015), p. 108701. DOI: 10.1103/PhysRevLett.114.108701. URL: http://link.aps.org/doi/10.1103/PhysRevLett.114.108701 (cit. on pp. 13, 43).

[116] Antoine Moinet, Michele Starnini, and Romualdo Pastor-Satorras. "Aging and percolation dynamics in a Non-Poissonian temporal network model". In: *Phys. Rev. E* 94 (2 2016), p. 022316. DOI: 10.1103/PhysRevE.94.022316. URL: https://link.aps.org/doi/10.1103/PhysRevE.94.022316 (cit. on p. 13).

[117] M. Molloy and B. Reed. "A critical point for random graphs with a given degree sequence". In: *Random Struct. Algorithms* 6 (1995), p. 161 (cit. on pp. 23, 42, 46).

[118] James Moody. "The Importance of Relationship Timing for Diffusion*". In: *Social Forces* 81.1 (2002), pp. 25–56. DOI: 10.1353/sof.2002.0056. eprint: /oup/backfile/content_public/journal/sf/81/1/10.1353_sof.2002.0056/2/81-1-25.pdf. URL: http://dx.doi.org/10.1353/sof.2002.0056 (cit. on p. 22).

[119] P.A.P. Moran. *The Statistical Processes of Evolutionary Theory*. Oxford: Clarendon Press, 1962 (cit. on p. 101).

[120] Moretti, P., Liu, S.Y., Baronchelli, A., et al. "Heterogenous mean-field analysis of a generalized voter-like model on networks". In: *Eur. Phys. J. B* 85.3 (2012), p. 88 (cit. on p. 101).

[121] M. Newman. "Spread of epidemic disease on networks". In: *Phys. Rev. E* 66 (July 2002), p. 016128 (cit. on p. 45).

[122] M. E. J. Newman. "The structure of scientific collaboration networks". In: *Proc. Natl. Acad. Sci. USA* 98 (2001), pp. 404–409 (cit. on pp. 14, 19).

[123] M. E. J. Newman. "Assortative Mixing in Networks". In: *Phys. Rev. Lett.* 89 (2002), p. 208701. DOI: 10.1103/PhysRevLett.89.208701 (cit. on p. 18).

[124] M. E. J. Newman. "The structure and function of complex networks". In: *SIAM Review* 45 (2003), pp. 167–256 (cit. on pp. 16, 45, 46).

[125] M. E. J. Newman. *Networks: An introduction*. Oxford: Oxford University Press, 2010 (cit. on pp. 14, 34, 37, 80, 101, 118).

[126] Sarah de Nigris, Anthony Hastir, and Renaud Lambiotte. "Burstiness and fractional diffusion on complex networks". In: *The European Physical Journal B* 89.5 (2016), p. 114. ISSN: 1434-6036. DOI: 10.1140/epjb/e2016-60947-3. URL: https://doi.org/10.1140/epjb/e2016-60947-3 (cit. on p. 123).

[127] Joao Gama Oliveira and Albert-Laszlo Barabasi. "Human dynamics: Darwin and Einstein correspondence patterns". In: *Nature* 437.7063 (Oct. 2005), pp. 1251–1251 (cit. on p. 15).

[128] J.-P. Onnela, J. Saramäki, J. Hyvönen, et al. "Structure and tie strengths in mobile communication networks". In: *Proceedings of the National Academy of Sciences* 104.18 (2007), pp. 7332–7336. DOI: 10.1073/pnas.0610245104 (cit. on pp. 15, 20, 56).

[129] André Panisson, Alain Barrat, Ciro Cattuto, et al. "On the dynamics of human proximity for data diffusion in ad-hoc networks". In: *Ad Hoc Networks* 10.8 (2012). Special Issue on Social-Based Routing in Mobile and Delay-Tolerant Networks, pp. 1532 –1543. ISSN: 1570-8705. DOI: https://doi.org/10.1016/j.adhoc.2011.06.003. URL: http://www.sciencedirect.com/science/article/pii/S1570870511001272 (cit. on p. 23).

[130] R. Parshani, M. Dickison, R. Cohen, et al. "Dynamic networks and directed percolation". In: *EPL (Europhysics Letters)* 90.3 (2010), p. 38004. URL: http://stacks.iop.org/0295-5075/90/i=3/a=38004 (cit. on p. 15).

[131] R. Pastor-Satorras, C. Castellano, P. Van Mieghem, et al. "Epidemic processes in complex networks." In: *Rev. Mod. Phys.* 87.3 (2015), p. 925 (cit. on pp. 80, 84).

[132] R. Pastor-Satorras, A. Vázquez, and A. Vespignani. "Dynamical and correlation properties of the Internet". In: *Phys. Rev. Lett.* 87 (2001), p. 258701 (cit. on pp. 31, 32, 47).

[133] R. Pastor-Satorras and A. Vespignani. "Epidemic spreading in scale-free networks". In: *Phys. Rev. Lett.* 86 (2001), pp. 3200–3203 (cit. on p. 80).

[134] R. Pastor-Satorras and A. Vespignani. "Immunization of complex networks". In: *Phys. Rev. E* 65 (2002), p. 036104 (cit. on p. 81).

[135] N Perra, D Balcan, B Gonçalves, et al. "Towards a Characterization of Behavior-Disease Models". In: *PLoS ONE* 6 (2011), e23084 (cit. on p. 81).

[136] N Perra, B Gonçalves, R Pastor-Satorras, et al. "Activity driven modeling of time varying networks." In: *Scientific reports* 2 (2012), p. 469 (cit. on pp. 15, 24, 25, 40, 41, 64, 85–87).

[137] N. Perra, B. Gonçalves, R. Pastor-Satorras, et al. "Activity driven modeling of time varying networks". In: *Scientific Reports* 2 (2012), srep00469 (cit. on pp. 40, 43, 110, 113, 114, 117, 133).

[138] Nicola Perra, Andrea Baronchelli, Delia Mocanu, et al. "Random walks and search in time-varying networks". In: *Physical Review Letters* 109.23 (2012), p. 238701. (Visited on 01/28/2013) (cit. on pp. 15, 25, 118, 119).

[139] Iacopo Pozzana, Kaiyuan Sun, and Nicola Perra. "Epidemic spreading on activity-driven networks with attractiveness". In: *Phys. Rev. E* 96 (4 2017), p. 042310. DOI: 10.1103/PhysRevE.96.042310. URL: https://link.aps.org/doi/10.1103/PhysRevE.96.042310 (cit. on p. 26).

[140] Tobias Preis, Helen Susannah Moat, and H. Eugene Stanley. "Quantifying Trading Behavior in Financial Markets Using Google Trends". In: *Scientific Reports* 3 (2013). Article, 1684 EP –. URL: http://dx.doi.org/10.1038/srep01684 (cit. on p. 21).

[141] Filippo Radicchi, Andrea Baronchelli, and Luís A. N. Amaral. "Rationality, Irrationality and Escalating Behavior in Lowest Unique Bid Auctions". In: *PLOS ONE* 7.1 (2012), pp. 1–8. DOI: 10.1371/journal.pone.0029910. URL: https://doi.org/10.1371/journal.pone.0029910 (cit. on p. 21).

[142] Erzsébet Ravasz and Albert-László Barabási. "Hierarchical organization in complex networks". In: *Physical Review E* 67.2 (Feb. 2003), p. 026112. DOI: 10.1103/PhysRevE.67.026112. URL: http://link.aps.org/doi/10.1103/PhysRevE.67.026112 (visited on 03/04/2013) (cit. on p. 32).

[143] Bruno Ribeiro, Nicola Perra, and Andrea Baronchelli. "Quantifying the effect of temporal resolution on time-varying networks". In: *Scientific Reports* 3 (Oct. 2013), p. 3006. ISSN: 2045-2322. DOI: 10.1038/srep03006. (Visited on 10/25/2013) (cit. on pp. 20, 118).

[144] John Riordan. "Moment Recurrence Relations for Binomial, Poisson and Hypergeometric Frequency Distributions". In: *Ann. Math. Statist.* 8.2 (1937), pp. 103–111. DOI: 10.1214/aoms/1177732430. URL: https://doi.org/10.1214/aoms/1177732430 (cit. on p. 36).

[145] Alessandro Rizzo, Mattia Frasca, and Maurizio Porfiri. "Effect of individual behavior on epidemic spreading in activity-driven networks". In: *Phys. Rev. E* 90 (4 2014), p. 042801. DOI: 10.1103/PhysRevE.90.042801. URL: http://link.aps.org/doi/10.1103/PhysRevE.90.042801 (cit. on p. 81).

[146] Luis E. C. Rocha, Fredrik Liljeros, and Petter Holme. "Simulated Epidemics in an Empirical Spatiotemporal Network of 50,185 Sexual Contacts". In: *PLoS Comput Biol* 7.3 (Mar. 2011), e1001109. DOI: 10.1371/journal.pcbi.1001109 (cit. on p. 15).

[147] Martin Rosvall, Alcides V. Esquivel, Andrea Lancichinetti, et al. "Memory in network flows and its effects on spreading dynamics and community detection". In: *Nature Communications* 5 (2014). Article, 4630 EP –. URL: http://dx.doi.org/10.1038/ncomms5630 (cit. on p. 56).

[148] Marcel Salathé, Maria Kazandjieva, Jung Woo Lee, et al. "A high-resolution human contact network for infectious disease transmission". In: *Proceedings of the National Academy of Sciences* 107.51 (2010), pp. 22020–22025. ISSN: 0027-8424. DOI: 10.1073/pnas.1009094108. eprint: http://www.pnas.org/content/107/51/22020.full.pdf. URL: http://www.pnas.org/content/107/51/22020 (cit. on p. 21).

[149] A. Scherrer, P. Borgnat, E. Fleury, et al. "Description and Simulation of Dynamic Mobility Networks". In: *Comput. Netw.* 52.15 (2008), pp. 2842–2858. ISSN: 1389-1286. DOI: 10.1016/j.comnet.2008.06.007. URL: http://dx.doi.org/10.1016/j.comnet.2008.06.007 (cit. on p. 24).

[150] Ingo Scholtes, Nicolas Wider, René Pfitzner, et al. "Causality-driven slowdown and speed-up of diffusion in non-Markovian temporal networks". In: *Nature Communications* 5 (2014). Article, 5024 EP –. URL: http://dx.doi.org/10.1038/ncomms6024 (cit. on p. 56).

[151] Johannes H.P. Schulz, Eli Barkai, and Ralf Metzler. "Aging renewal theory and application to random walks". In: *Physical Review X* 4 (2014), p. 011028 (cit. on pp. 40, 52, 68–70, 75).

[152] M Ángeles Serrano, Konstantin Klemm, Federico Vazquez, et al. "Conservation laws for voter-like models on random directed networks". In: *Journal of Statistical Mechanics: Theory and Experiment* 2009.10 (2009), P10024 (cit. on p. 101).

[153] *SocioPatterns Dataset: High school dynamic contact networks*. www.sociopatterns.org/datasets/high-school-dynamic-contact-networks. Accessed 13 Feb 2017 (cit. on p. 22).

[154] Bo Söderberg. "General formalism for inhomogeneous random graphs". In: *Physical Review E* 66.6 (2002) (cit. on pp. 25, 31).

[155] Chaoming Song, Tal Koren, Pu Wang, et al. "Modelling the scaling properties of human mobility". In: *Nature Physics* 6.10 (Sept. 2010), pp. 818–823. ISSN: 1745-2473. DOI: 10.1038/nphys1760. URL: http://dx.doi.org/10.1038/nphys1760 (cit. on p. 15).

[156] V. Sood, T. Antal, and S. Redner. "Voter models on heterogeneous networks". In: *Phys. Rev. E* 77 (2008), p. 041121 (cit. on pp. 101, 103, 107, 108, 112, 113).

[157] V. Sood and S. Redner. "Voter Model on Heterogeneous Graphs". In: *Phys. Rev. Lett.* 94.17 (2005), p. 178701. DOI: 10.1103/PhysRevLett.94.178701 (cit. on pp. 103, 107, 108, 112, 113).

[158] Michele Starnini, Andrea Baronchelli, and Romualdo Pastor-Satorras. "Modeling Human Dynamics of Face-to-Face Interaction Networks". In: *Phys. Rev. Lett.* 110.16 (2013), p. 168701. DOI: 10.1103/PhysRevLett.110.168701. URL: http://link.aps.org/doi/10.1103/PhysRevLett.110.168701http://prl.aps.org/pdf/PRL/v110/i16/e168701 (cit. on pp. 15, 26, 28).

[159] Michele Starnini, Anna Machens, Ciro Cattuto, et al. "Immunization strategies for epidemic processes in time-varying contact networks". In: *Journal of Theoretical Biology* 337.0 (2013), pp. 89 –100. ISSN: 0022-5193. DOI: http://dx.doi.org/10.1016/j.jtbi.2013.07.004. URL: http://www.sciencedirect.com/science/article/pii/S0022519313003251 (cit. on p. 15).

[160] Michele Starnini and Romualdo Pastor-Satorras. "Topological properties of a time-integrated activity-driven network". In: *Physical Review E* 87.6 (June 2013), p. 062807. (Visited on 09/27/2013) (cit. on pp. 25, 35, 113).

[161] Michele Starnini and Romualdo Pastor-Satorras. "Topological properties of a time-integrated activity-driven network". In: *Phys. Rev. E* 87 (6 2013), p. 062807. DOI: 10.1103/PhysRevE.87.062807. URL: http://link.aps.org/doi/10.1103/PhysRevE.87.062807 (cit. on p. 87).

[162] Michele Starnini and Romualdo Pastor-Satorras. "Temporal percolation in activity-driven networks". en. In: *Physical Review E* 89.3 (2014), p. 032807. ISSN: 1539-3755, 1550-2376. DOI: 10.1103/PhysRevE.89.032807. URL: http://link.aps.org/doi/10.1103/PhysRevE.89.032807 (cit. on pp. 25, 46–48, 55, 66, 91, 130).

[163] D. Stauffer and A. Aharony. *Introduction to Percolation Theory*. 2nd. London: Taylor & Francis, 1994 (cit. on pp. 45, 48, 55).

[164] Juliette Stehlé, Alain Barrat, and Ginestra Bianconi. "Dynamical and bursty interactions in social networks". In: *Phys. Rev. E* 81 (2010), p. 035101 (cit. on p. 15).

[165] Juliette Stehle, Nicolas Voirin, Alain Barrat, et al. "Simulation of an SEIR infectious disease model on the dynamic contact network of conference attendees". In: *BMC Medicine* 9.87 (2011) (cit. on pp. 15, 24).

[166] Juliette Stehlé, Nicolas Voirin, Alain Barrat, et al. "Simulation of an SEIR infectious disease model on the dynamic contact network of conference attendees". In: *BMC Medicine* 9 (2011), p. 87. ISSN: 1741-7015. DOI: 10.1186/1741-7015-9-87 (cit. on pp. 22, 80).

[167] Juliette Stehlé, Nicolas Voirin, Alain Barrat, et al. "High-Resolution Measurements of Face-to-Face Contact Patterns in a Primary School". In: *PLOS ONE* 6.8 (2011), pp. 1–13. DOI: 10.1371/journal.pone.0023176. URL: https://doi.org/10.1371/journal.pone.0023176 (cit. on p. 23).

[168] Michael Storper and Anthony J. Venables. "Buzz: face-to-face contact and the urban economy". In: *Journal of Economic Geography* 4.4 (2004), pp. 351–370. DOI: 10.1093/jnlecg/lbh027. eprint: /oup/backfile/content_public/journal/joeg/4/4/10.1093/jnlecg/lbh027/3/lbh027.pdf. URL: http://dx.doi.org/10.1093/jnlecg/lbh027 (cit. on p. 21).

[169] K. Suchecki, V. M. Eguíluz, and M. San Miguel. "Conservation laws for the voter model in complex networks". In: *Europhys. Lett.* 69.2 (2005), pp. 228–234 (cit. on p. 109).

[170] K. Sun, A. Baronchelli, and N. Perra. "Contrasting effects of strong ties on SIR and SIS processes in temporal networks". In: *Eur. Phys. J. B* 88 (2015), p. 326 (cit. on pp. 86, 92, 93).

[171] Yuri Takhteyev, Anatoliy Gruzd, and Barry Wellman. "Geography of Twitter networks". In: *Social Networks* 34.1 (2012). Capturing Context: Integrating Spatial and Social Network Analyses, pp. 73 –81. ISSN: 0378-8733. DOI: https://doi.org/10.1016/j.socnet.2011.05.006. URL: http://www.sciencedirect.com/science/article/pii/S0378873311000359 (cit. on p. 21).

[172] J. Tang, S. Scellato, M. Musolesi, et al. "Small-world behavior in time-varying graphs". In: *Phys. Rev. E* 81 (5 2010), p. 055101. DOI: 10.1103/PhysRevE.81.055101. URL: http://link.aps.org/doi/10.1103/PhysRevE.81.055101 (cit. on pp. 15, 24).

[173] *The SocioPatterns project*. URL: http://www.sociopatterns.org/ (cit. on pp. 15, 21).

[174] Eugenio Valdano, Luca Ferreri, Chiara Poletto, et al. "Analytical Computation of the Epidemic Threshold on Temporal Networks". In: *Phys. Rev. X* 5 (2 2015), p. 021005 (cit. on p. 80).

[175] Alexei Vazquez, Balázs Rácz, András Lukács, et al. "Impact of Non-Poissonian Activity Patterns on Spreading Processes". In: *Phys. Rev. Lett.* 98 (15 2007), p. 158702. DOI: 10.1103/PhysRevLett.98.158702 (cit. on pp. 15, 56, 118).

[176] Federico Vazquez and Víctor M Eguíluz. "Analytical solution of the voter model on uncorrelated networks". In: *New Journal of Physics* 10.6 (2008), p. 063011 (cit. on p. 101).

[177] Christian L. Vestergaard, Mathieu Génois, and Alain Barrat. “How memory generates heterogeneous dynamics in temporal networks”. In: *Phys. Rev. E* 90 (4 2014), p. 042805 (cit. on p. 26).

[178] Yang Wang, Deepayan Chakrabarti, Chenxi Wang, et al. “Epidemic Spreading in Real Networks: An Eigenvalue Viewpoint”. In: *22nd International Symposium on Reliable Distributed Systems (SRDS’03)*. Los Alamitos, CA, USA: IEEE Computer Society, 2003, pp. 25–34 (cit. on p. 17).

[179] S. Wasserman and K. Faust. *Social Network Analysis: Methods and Applications*. Cambridge: Cambridge University Press, 1994 (cit. on p. 14).

[180] D. J. Watts and S. H. Strogatz. “Collective dynamics of ‘small-world’ networks”. In: *Nature* 393 (1998), pp. 440–442 (cit. on p. 32).

[181] George H. Weiss. *Aspects and Applications of the Random Walk*. Amsterdam: North-Holland Publishing Co., 1994 (cit. on p. 119).

[182] M. S. Wheatland, P. A. Sturrock, and J. M. McTiernan. “The Waiting-Time Distribution of Solar Flare Hard X-Ray Bursts”. In: *The Astrophysical Journal* 509.1 (1998), p. 448. URL: http://stacks.iop.org/0004-637X/509/i=1/a=448 (cit. on p. 16).

[183] Kun Zhao, Juliette Stehlé, Ginestra Bianconi, et al. “Social network dynamics of face-to-face interactions”. In: *Phys. Rev. E* 83 (2011), p. 056109 (cit. on pp. 15, 24).

[184] Han Zhu, Xinran Wang, and Jian-Yang Zhu. “Effect of aging on network structure”. en. In: *Physical Review E* 68.5 (Nov. 2003). (Visited on 01/19/2015) (cit. on p. 79).

APPENDIX

A. Tauberian theorems

A proof of these theorems can be found in Ref. [18]

A.1. Tauberian theorem n°1

Consider the probability density function $f : \mathbb{R}^+ \longrightarrow \mathbb{R}^+$ of a non-negative continuous random variable t. By definition f is normalized $\int_0^\infty f(t)dt = 1$. We suppose that f is power-law tailed, i.e. $\exists\, A > 0$, $f(t) \underset{\infty}{=} A\, t^{-1-\alpha} + o(t^{-1-\alpha})$. Then for $\alpha \in \mathbb{R}^+ \backslash \mathbb{N}$ the following holds

$$F(s) \underset{0}{=} \sum_{k=0}^{\lfloor \alpha \rfloor} \mu_k \frac{(-s)^k}{k!} + A\Gamma(-\alpha)s^\alpha + o(s^\alpha) \tag{.26}$$

where F is the Laplace transform of f, $\mu_k = \int_0^\infty t^k f(t)dt$, $\lfloor \cdot \rfloor$ is the floor function and Γ is the gamma function.

A.2. Tauberian theorem n°2

Consider the probability density function $f : \mathbb{R}^+ \longrightarrow \mathbb{R}^+$ of a non-negative continuous random variable t. For $\lambda > -1$ and $A > 0$ the following holds

$$f(t) \underset{\infty}{=} A\, t^\lambda + o(t^\lambda) \Leftrightarrow F(s) \underset{0}{=} \frac{A\Gamma(1+\lambda)}{s^{\lambda+1}} + o(s^{-1-\lambda}) \tag{.27}$$

where F is the Laplace transform of f.

B. Taylor series expansions of the average and average square number of counted events for a renewal process with arbitrary inter-event time distribution

Suppose a renewal process with inter-event time $\psi(t)$, starting at $t = 0$. We demonstrate that the Taylor expansion of the average number of renewals counted in the interval $[0, t]$ reads

$$\overline{r}(t) \underset{0}{\simeq} \sum_{n=1}^{q} \alpha_n \, t^n \tag{.28}$$

where $\alpha_1 = \psi(0)$ and

$$\alpha_n = \frac{1}{n!} \left(tr(F_n D_n) + \psi(0)^n \right), \quad n \geqslant 2 \tag{.29}$$

with F_n and D_n being two matrices of size $n-1$ such that

$$F_{n,ij} = \begin{cases} \binom{i}{j} \psi(0)^{i-j} & \text{for } j \leqslant i \leqslant n-j \\ 0 & \text{otherwise} \end{cases} \tag{.30}$$

the indices running from 1 to $n-1$, and

$$D_n = \begin{pmatrix} (M_n^0 A_n)^T \\ (M_n A_n)^T \\ \vdots \\ (M_n^{n-2} A_n)^T \end{pmatrix} \tag{.31}$$

where we used the intermediate matrix

$$M_n = \begin{pmatrix} 0 & \psi'(0) & \psi''(0) & \cdots & \psi^{(n-2)}(0) \\ \vdots & & & & \vdots \\ & & & & \psi''(0) \\ & & & & \psi'(0) \\ 0 & & & & 0 \end{pmatrix} \tag{.32}$$

and the column vector

$$A_n = \begin{pmatrix} \psi^{(n-1)}(0) \\ \vdots \\ \psi'(0) \end{pmatrix} \tag{.33}$$

The T exponent represent the matrix transposition operator and tr is the trace operator i.e. the sum of the diagonal elements of a matrix.

Additionally, we prove that the average square number of renewals reads

$$\overline{r^2}(t) \underset{0}{\simeq} \sum_{n=1}^{q} \beta_n t^n \tag{.34}$$

where $\beta_1 = \psi(0)$, $\beta_2 = \alpha_2 + \psi(0)^2$ and

$$\beta_n = \alpha_n + \frac{2}{n!}\left(tr(G_n D_{n-1}) + (n-1)\psi(0)^n\right), \quad n \geqslant 3 \tag{.35}$$

with G_n being a matrix of size $n-2$ such that

$$G_n = \begin{pmatrix} L_2 \\ 2L_3 \\ \vdots \\ (n-2)L_{n-1} \end{pmatrix} \tag{.36}$$

where L_k is the kth line of the matrix F_n with the last column previously removed.

B.1. Proof

The distribution of the number of renewals is expressed in the Laplace domain as (see the derivation in section 2.4)

$$\chi_s(r|\psi) = \psi(s)^r \frac{1-\psi(s)}{s}, \tag{.37}$$

Then using the partial derivation ∂_ψ we derive the average number of renewals $\overline{r}(s) = \sum_r r\, \chi_s(r|\psi)$

$$\begin{aligned} \overline{r}(s) &= \frac{\psi(s)}{s(1-\psi(s))} \\ &= \frac{1}{s}\sum_{k=1}^{\infty} \psi(s)^k \end{aligned} \tag{.38}$$

In the time domain, this reads

$$\overline{r}(t) = \sum_{k=1}^{\infty} \int_0^t du\, g_k(u) \tag{.39}$$

where $g_k = \psi * \psi * ... * \psi$ is the convolution of ψ with itself repeated k times. Now we perform a Taylor expansion of this expression at order q

$$\overline{r}(t) = \sum_{k=1}^{\infty} \sum_{n=1}^{q} \frac{d^{n-1}}{dt^{n-1}} g_k(0)\, \frac{t^n}{n!} \tag{.40}$$

from which we identify $\alpha_0 = 0$ and

$$\alpha_n = \frac{1}{n!} \sum_{k=1}^{\infty} \frac{d^{n-1}}{dt^{n-1}} g_k(0), \quad n \geqslant 1 \tag{.41}$$

By definition, one has for $k \geqslant 1$

$$g_{k+1}(t) = \int_0^t \psi(t-u) g_k(u) du \tag{.42}$$

From which we deduce, for $m \geqslant 1$

$$\frac{d^m}{dt^m} g_{k+1}(t) = \int_0^t \frac{d^m \psi}{dt^m}(t-u) g_k(u) du + \sum_{\ell=0}^{m-1} \frac{d^\ell \psi}{dt^\ell}(0)\, \frac{d^{m-1-\ell}}{dt^{m-1-\ell}} g_k(t) \tag{.43}$$

Then at $t = 0$ we write

$$\frac{d^m}{dt^m} g_{k+1}(0) = \sum_{\ell=0}^{m-1} \frac{d^\ell \psi}{dt^\ell}(0)\, \frac{d^{m-1-\ell}}{dt^{m-1-\ell}} g_k(0) \tag{.44}$$

with a straightforward recurrence, we deduce that for $n \geqslant 1$

$$\frac{d^{n-1}}{dt^{n-1}} g_k(0) = 0, \quad \forall\, k \geqslant n+1 \tag{.45}$$

so that the expression of α_n reduces to

$$\alpha_n = \frac{1}{n!}\sum_{k=1}^{n}\frac{d^{n-1}}{dt^{n-1}}g_k(0), \quad n \geqslant 1 \tag{.46}$$

and the Eq.(.44) reduces to

$$\frac{d^m}{dt^m}g_{k+1}(0) = \sum_{\ell=k-1}^{m-1}\psi^{(m-1-\ell)}(0)\,\frac{d^\ell}{dt^\ell}g_k(0) \tag{.47}$$

we see that

$$\frac{d^k}{dt^k}g_{k+1}(0) = \psi(0)^{k+1} \tag{.48}$$

and after computing the first terms of the sequence $d_t^{n+1+k}g_{n+1}(0)$ with n fixed we look for a general term of the form

$$d_t^{n+1+k}g_{n+1}(0) = \sum_{j=0}^{k}\psi(0)^{n-j}\binom{n+1}{j+1}a_{j,k+1} \tag{.49}$$

where $\binom{n+1}{j+1}$ is the binomial coefficient with the convention $\binom{n+1}{j+1} = 0$ for $j > n$. Then using Eq.(.47) we write, for $n \geqslant 2$

$$\begin{aligned}
d_t^{n+1+k}g_{n+1}(0) &= \sum_{\ell=n-1}^{n+k}\psi^{(n+k-\ell)}(0)\,\frac{d^\ell}{dt^\ell}g_n(0) \\
&= \left(\sum_{j=0}^{k}\sum_{\ell=j}^{k}\psi(0)^{n-1-j}\psi^{(k-\ell)}(0)\binom{n}{j+1}a_{j,\ell+1}\right) + \psi(0)^n\psi^{(k+1)}(0) \\
&= \left(\sum_{j=0}^{k-1}\sum_{\ell=j}^{k-1}\psi(0)^{n-1-j}\psi^{(k-\ell)}(0)\binom{n}{j+1}a_{j,\ell+1}\right) + \sum_{j=0}^{k}\psi(0)^{n-j}\binom{n}{j+1}a_{j,k+1} \\
&\quad +\psi(0)^n\psi^{(k+1)}(0)
\end{aligned} \tag{.50}$$

from which we identify

$$\begin{aligned}
\binom{n+1}{j+1}a_{j,k+1} &= \binom{n}{j+1}a_{j,k+1} + \sum_{\ell=j-1}^{k-1}\binom{n}{j}\psi^{(k-\ell)}(0)a_{j-1,\ell+1} \quad \text{for } j \geqslant 1 \\
\binom{n+1}{1}a_{0,k+1} &= \psi^{(k+1)}(0) + \binom{n}{1}a_{0,k+1} \quad \text{for } j = 0
\end{aligned} \tag{.51}$$

which finally implies

$$a_{j,k+1} = \sum_{\ell=j-1}^{k-1} \psi^{(k-\ell)}(0) a_{j-1,\ell+1} \quad \text{for } j \geqslant 1 \tag{.52}$$

and $a_{0,k+1} = \psi^{(k+1)}(0)$. This can be put under the matricial form $B_j = M_{k+2}^j A_{k+2}$ where we defined the column vector

$$B_j = \begin{pmatrix} a_{j,k+1} \\ a_{j,k} \\ \vdots \\ a_{j,1} \end{pmatrix} \tag{.53}$$

Now we can write

$$\alpha_n = \frac{1}{n!} \left(\sum_{k=0}^{n-2} d_t^{n-1} g_{k+1}(0) \quad + \quad \psi(0)^n \right) \tag{.54}$$

and

$$\sum_{k=0}^{n-2} d_t^{n-1} g_{k+1}(0) = \sum_{k=1}^{n-1} \sum_{j=1}^{n-k-1} \psi(0)^{k-j} \binom{k}{j} a_{j-1,n-k} \tag{.55}$$

which can be put under the matricial form $tr(F_n D_n)$.

The average square number of renewals $\overline{r^2}(s) = \sum_r r^2 \, \chi_s(r|\psi)$ reads (using again ∂_ψ^2)

$$\begin{aligned} \overline{r^2}(s) &= \overline{r}(s) + \frac{2\psi(s)^2}{s(1-\psi(s))^2} && (.56) \\ &= \overline{r}(s) + \frac{2}{s} \sum_{n=1}^{\infty} n \, g_{n+1}(s) && (.57) \end{aligned}$$

from which we identify, in the time domain,

$$\begin{aligned} \beta_n &= \alpha_n + \frac{2}{n!} \sum_{k=1}^{n-1} k \frac{d^{n-1}}{dt^{n-1}} g_{k+1}(0) \quad \text{for } n \geqslant 3 \\ &= \alpha_n + \frac{2}{n!} \left((n-1)\psi(0)^n + \sum_{k=1}^{n-2} k \frac{d^{n-1}}{dt^{n-1}} g_{k+1}(0) \right) \\ &= \alpha_n + \frac{2}{n!} \left(tr(G_n D_{n-1}) + (n-1)\psi(0)^n \right) && (.58) \end{aligned}$$

B.2. Power-law renewal process

We can explicit the coefficients of the expansions when $\psi_c(t) = \alpha\, c(ct+1)^{-1-\alpha}$. Indeed, in this case we straightforwardly prove that

$$\psi_c^{(n)}(0) = (-1)^n\, c^{n+1} \prod_{k=0}^{n} (\alpha + k)\ , \quad \forall n \geqslant 0 \tag{.59}$$

For reasons of dimensional consistency of the series expansions, we expect the coefficients α_n and β_n to be proportional to c^n, which means that without loss of generality we may set $c = 1$. The coefficients are then functions of the exponent α only, and may be readily computed with the formulas (.28) and (.34). In the following we provide a simple *Octave* program which calculates the coefficients α_n and β_n until an arbitrary large order q for a given value of α and prints the resulting $\overline{r}(t)$ and $\overline{r^2}(t)$ to a file. It is clear that the expansions at a finite order q grow as t^q at large times, in fact the divergence is really fast and in practice the expansions are useless as soon as $t > 1$. On Fig. .3 we plot the result obtained for four values of α, and compare it with the average activation numbers obtained via numerical simulations of the renewal process parametrized by ψ_c. We observe that the expansions perfectly fits the numerical data for values of the time t smaller than 1.

```
clear;

# define \alpha
a = 0.9;

# define the order of the series expansion
q = 50;

for n = 2:q

  # define the matrix F_n of size n-1
  F = eye(n-1)*0;
  for i = 0:n-2
    for j = 0:n-2
      if (j <= i)
        if (j < n-i-1)
          F(i+1,j+1) = a^(i-j);
          F(i+1,j+1) *= factorial(i+1)/factorial(j+1)/factorial(i-j);
        endif
      endif
    endfor
  endfor

  # define the column vector A_n of size n-1
  A = linspace(a,a,n-1);
  # linspace(u,v,w) is a list of w elements
  # the 1st one being u and the last one v
```

```
  for i = 1:n-1
    for k = 1:i
      A(n-i) = A(n-i)*(a+k);
    endfor
    A(n-i) = (-1)^i*A(n-i);
  endfor

  # define the matrix M_n of size n-1
  M = eye(n-1)*0;
  for i = 1:n-2
    for j = i+1:n-1
      M(i,j) = A(n-j+i);
    endfor
  endfor

  # define the matrix D_n of size n-1
  D = eye(n-1);
  for i = 1:n-1
    # (matrix)' is the transposition operator
    D(i,:) = (M^(i-1)*A')';
  endfor

  # define the coefficients \alpha_n
  alpha(n) = (trace(F*D) + a^n)/factorial(n);

  if (n > 2)
    # define the matrix G_n of size n-2
    G = F;
    # remove the 1st line and then the last column
    G(1,:) = [];
    G(:,n-1) = [];
    # define the column vector A_(n-1) of size n-2
    A2 = A;
    A2(1) = [];
    # define the matrix M_(n-1) of size n-2
    M2 = M;
    M2(n-1,:) = [];
    M2(:,n-1) = [];
    for k = 1:n-2
      G(k,:) *= k;
    endfor

    # define the matrix D_(n-1) of size n-2
    D2 = eye(n-2);
    for i = 1:n-2
      D2(i,:) = (M2^(i-1)*A2')';
    endfor
    # careful with this, \beta_n = alpha(n) + betaa(n)
    betaa(n) = (2*trace(G*D2) + 2*(n-1)*a^n)/factorial(n);
  endif

endfor
```

```
alpha(1) = a;
betaa(2) = a^2;
betaa(1) = 0;

# define the time axis
t = linspace(0,1,100);
for i = 1:q
  rr(i,:)= alpha(i)*t.^i;
  rr2(i,:) = (alpha(i)+betaa(i))*t.^i;
endfor

# define <r>_t
r = sum(rr);

# define <r^2>_t
r2 = sum(rr2);

op = fopen('r_avgTh.dat','w');
for j = 1:100
  fprintf(op,"%e %e %e \n", t(j), r(j), r2(j));
endfor
fclose(op);
```

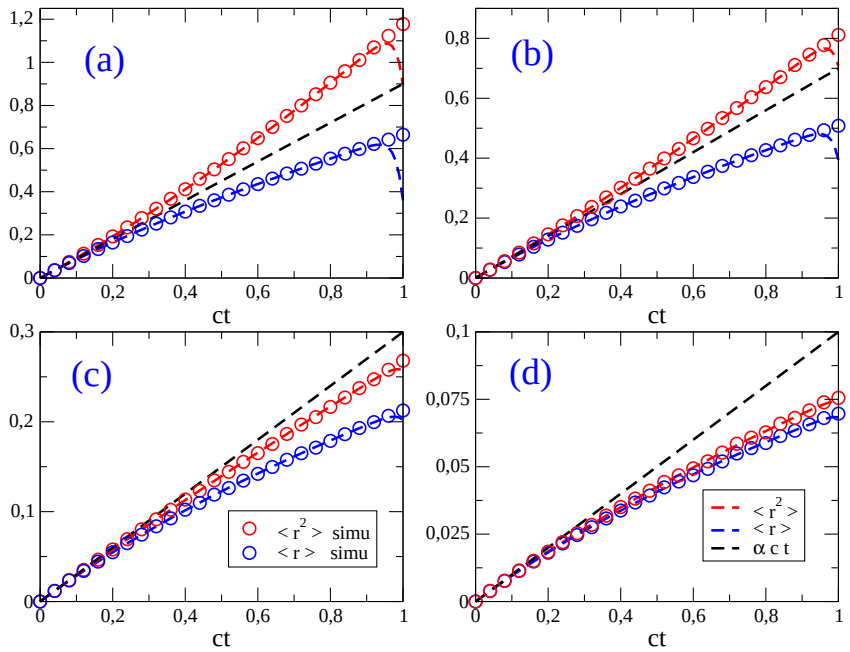

Figure .3.: $\overline{r}_c$ and $\overline{r^2}_c$ as functions of ct for a homogeneous population with waiting time distribution $\psi_c(t) = \alpha\, c\, (ct+1)^{-1-\alpha}$ and different values of α. (a): $\alpha = 0.9$, (b): $\alpha = 0.7$, (c): $\alpha = 0.3$ and (d): $\alpha = 0.1$. The series expansions of $\overline{r}_c$ and $\overline{r^2}_c$ at order $q = 50$, given by Eqs. (.28) and (.34) respectively, are plotted in dashed lines, while the circles represent numerical simulations of the renewal processes defined by ψ_c.

C. Expansion of the steady-state infection prevalence of a SIS process with risk perception on activity driven networks

We want to solve Eq.(6.3) in the stationnary state, defining the following

$$\begin{aligned} \rho &= \sum_a F(a)\rho_a \\ \theta &= \sum_a a\, F(a)\rho_a \end{aligned} \tag{.60}$$

and setting $\mu = 1$ without loss of generality, this equation reads

$$\rho_a = \frac{\lambda(a\rho + \theta)}{1 + \lambda(a\rho + \theta)} \tag{.61}$$

Expanding at second order in ρ and θ, we write

$$\begin{aligned} \rho &= b_1\theta + c_1\rho^2 + d_1\theta^2 + e_1\rho\theta \\ \theta &= b_2\rho + c_2\rho^2 + d_2\theta^2 + e_2\rho\theta \end{aligned} \tag{.62}$$

where the coefficients b_i, c_i, d_i and e_i are functions of λ and the moments $\langle a^n \rangle$ of the activity distribution. Then expressing θ as a function of ρ only, we obtain

$$\begin{aligned} \rho &= \frac{1 - b_1 b_2}{b_1(c_2 + d_2 b_2^2 + e_2 b_2) + c_1 + d_1 b_2^2 + e_1 b_2} \\ \theta &= b_2\rho + c_2\rho^2 + d_2 b_2^2\rho^2 + e_2 b_2 \rho^2 \end{aligned} \tag{.63}$$

In the stationnary state, and at second order, Eq.(6.2) reads

$$\lambda = \lambda_0 \left(1 - \alpha\, \frac{a\rho + \theta}{a + \langle a \rangle}\right) \tag{.64}$$

Then we derive

$$\rho_a = \lambda_0\, a\rho + \lambda_0\, \theta - \lambda_0 \left(\frac{\alpha}{a + \langle a \rangle} + \lambda_0\right)(a\rho + \theta)^2 \tag{.65}$$

and identify the coefficients

$$
\begin{aligned}
b_1 &= \frac{\lambda_0}{1-\lambda_0\langle a\rangle} & b_2 &= \langle a^2\rangle b_1 \\
c_1 &= -\langle a^2 L\rangle b_1 & c_2 &= -\langle a^3 L\rangle b_1 \\
d_1 &= -\langle L\rangle b_1 & d_2 &= -\langle aL\rangle b_1 \\
e_1 &= -2\langle aL\rangle b_1 & e_2 &= -2\langle a^2 L\rangle b_1 \\
L &= \frac{\alpha}{a+\langle a\rangle} + \lambda_0
\end{aligned}
\tag{.66}
$$

The system Eq.(.63) has a non-negative solution if and only if $\langle a^2\rangle b_1^2 - 1 > 0$, from which we obtain the epidemic threshold

$$
\lambda_c = \frac{1}{\langle a\rangle + \sqrt{\langle a^2\rangle}} \tag{.67}
$$

setting $\lambda_0 = \lambda_c(1+\epsilon)$ and expanding at order 1 in ϵ we obtain

$$
\rho = \frac{2\epsilon}{A\alpha + B} \tag{.68}
$$

where

$$
\begin{aligned}
A &= \lambda_c \left\langle \frac{\frac{a^3}{\sqrt{\langle a^2\rangle}} + 3a\sqrt{\langle a^2\rangle} + \langle a^2\rangle + 3a^2}{a+\langle a\rangle} \right\rangle \\
B &= \lambda_c^2 \left(\frac{\langle a^3\rangle}{\sqrt{\langle a^2\rangle}} + 3\langle a\rangle\sqrt{\langle a^2\rangle} + 4\langle a^2\rangle \right)
\end{aligned}
\tag{.69}
$$

D. Details of some computations of the voter-like model on activity driven networks with attractiveness

From the expression of the weights λ_h in Eq. (7.13) we obtain, by multiplying by a and summing over h (in the next equations we write $\sum a\lambda$ and $\sum b\lambda$ as shorthands for $\sum_h a\lambda_h$ and $\sum_h b\lambda_h$, respectively):

$$\sum_h a\lambda_h = p\,\langle\frac{ab}{\Delta_{h,p}}\rangle\,\left[\sum a\lambda\right] + (1-p)\,\langle\frac{a^2}{\Delta_{h,p}}\rangle\,\left[\sum b\lambda\right], \tag{.70}$$

which gives a relation between $\sum a\lambda$ and $\sum b\lambda$

$$\sum b\lambda = \frac{1-p\langle\frac{ab}{\Delta_{h,p}}\rangle}{(1-p)\langle\frac{a^2}{\Delta_{h,p}}\rangle}\sum a\lambda. \tag{.71}$$

The normalization of the weights gives

$$p\,\langle\frac{b}{\Delta_{h,p}}\rangle\,\left[\sum a\lambda\right] + (1-p)\,\langle\frac{a}{\Delta_{h,p}}\rangle\,\left[\sum b\lambda\right] = 1\,. \tag{.72}$$

Combining Eqs. (.71) and (.72) leads to

$$\sum a\lambda = \frac{\langle\frac{a^2}{\Delta_{h,p}}\rangle}{p\langle\frac{b}{\Delta_{h,p}}\rangle\langle\frac{a^2}{\Delta_{h,p}}\rangle + \left(1-p\langle\frac{ab}{\Delta_{h,p}}\rangle\right)\langle\frac{a}{\Delta_{h,p}}\rangle}. \tag{.73}$$

Besides, by definition of $\Delta_{h,p}$ we wrote Eq. (7.29) which, after dividing by $\langle b\rangle$ gives

$$1-p\langle\frac{ab}{\Delta_{h,p}}\rangle = (1-p)\langle\frac{b^2}{\Delta_{h,p}}\rangle\frac{\langle a\rangle}{\langle b\rangle}. \tag{.74}$$

Inserting this into Eqs. (.73) and (.71) one recovers the correct expressions given in Eqs. (7.14) and (7.15).

To derive the expression of the average consensus time, we write, combining Eqs.(7.22), (7.24) and (7.25)

$$\Omega(1-\Omega)\,\frac{\partial^2 T}{\partial\Omega^2}\sum_h \eta_h\,\Delta_{h,p}\left(\frac{\lambda_h}{\eta_h}\right)^2 = -N\langle b\rangle. \tag{.75}$$

We have

$$
\begin{aligned}
\sum_h \eta_h \, \Delta_{h,p} \left(\frac{\lambda_h}{\eta_h}\right)^2 &= \sum_h \eta_h \, \frac{(pb\,[\sum a\lambda] + (1-p)a\,[\sum b\lambda])^2}{\Delta} \\
&= \left[\sum a\lambda\right] \, \left[\sum b\lambda\right] \left(p^2 \langle \frac{b^2}{\Delta_{h,p}} \rangle \frac{\sum a\lambda}{\sum b\lambda} + (1-p)^2 \langle \frac{a^2}{\Delta_{h,p}} \rangle \frac{\sum b\lambda}{\sum a\lambda} + 2p(1-p) \langle \frac{ab}{\Delta_{h,p}} \rangle\right) \\
&= \frac{[\sum a\lambda] \, [\sum b\lambda]}{\langle a \rangle \langle b \rangle} \left(p^2 \langle \frac{a^2}{\Delta_{h,p}} \rangle \langle b \rangle^2 + (1-p)^2 \langle \frac{b^2}{\Delta_{h,p}} \rangle \langle a \rangle^2 + 2p(1-p) \langle \frac{ab}{\Delta_{h,p}} \rangle \langle a \rangle \langle b \rangle\right) \\
&= \frac{[\sum a\lambda] \, [\sum b\lambda]}{\langle a \rangle \langle b \rangle} \left\langle \frac{(\, pa\langle b \rangle + (1-p)\langle a \rangle b\,)^2}{\Delta_{h,p}} \right\rangle \\
&= \left[\sum a\lambda\right] \, \left[\sum b\lambda\right] \qquad (.76)
\end{aligned}
$$

which, inserted in Eq. (.75), finally yields Eq. (7.26).